

THE STOPPING POWER OF VARIOUS  
ELEMENTS FOR PROTONS OF  
MODERATELY LOW ENERGIES

——————————  
ARTHUR BOUNDS CHILTON

1953

Library  
U. S. Naval Postgraduate School  
Monterey, California











THE STOPPING POWER OF VARIOUS ELEMENTS  
FOR PROTONS OF MODERATELY LOW ENERGIES

DISSERTATION

Presented in Partial Fulfillment of the Requirements  
for the Degree Doctor of Philosophy in the  
Graduate School of The Ohio State  
University

By

ARTHUR BOUNDS CHILTON, B.Sc., B.C.E., M.C.E., M.Sc.

The Ohio State University

1953



### ACKNOWLEDGMENTS

The research which this dissertation describes was accomplished through the help and encouragement of many persons and agencies. Thanks are primarily due to Dr. John N. Cooper for his constant interest and encouragement. Gratitude is also expressed for the assistance and cooperation of all others attached to the Van de Graaff Generator Laboratory - Dr. James C. Harris, Graduate Assistants Donald W. Green and James A. Smith, Technicians Ottis Campbell and Ignas Saldukas. Acknowledgments for special services rendered by other individuals or laboratories are included where appropriate in the body of this dissertation.

The help of the Research Foundation, Ohio State University, and of the U. S. Atomic Energy Commission in defraying the expenses incident to the research is appreciated. The writer also wishes to express gratitude to those activities of the U. S. Navy by whose authority he was permitted to undertake this work. Special mention is owing to the U.S. Naval Postgraduate School, which has exercised general supervision over all his academic work, and to the Office of Naval Research, under whose sponsorship such work has been undertaken.



# TABLE OF CONTENTS

	Page
I. Introduction . . . . .	1
A. Definitions and Units . . . . .	3
B. Review of Stopping Power Theory . . . . .	5
1. Classical Fundamentals . . . . .	6
2. Stopping Power - Classical Formulation . . . . .	13
3. Elementary Quantum Considerations in Stopping Power . . . . .	16
4. Strict Quantum-Mechanical Derivation of Stopping Power Formula . . . . .	23
5. Modifications to Theory for Slow Particles Through Heavy Media . . . . .	32
6. Effect of the Physical and Chemical State of the Media on Stopping Power . . . . .	41
7. Capture and Loss of Electrons . . . . .	43
8. Straggling in Stopping Power . . . . .	45
C. Review of Existing Experimental Data . . . . .	46
1. Stopping Power . . . . .	46
2. Straggling . . . . .	47
II. Basic Experimental Technique . . . . .	51
A. Basic Principle . . . . .	51
B. Detailed Analysis . . . . .	53
III. Experimental Details and Preliminary Calculations . . . . .	58
A. Target-Faraday Cage Assembly . . . . .	58
B. Preliminary Measurements on Foils . . . . .	60
C. Design of Magnet Current Regulator . . . . .	68





	Page
D. Technique for Taking and Correcting Yield-Energy Data. . .	71
E. Target Preparation . . . . .	75
F. Analysis of Auxiliary Statistical Variables . . . . .	80
1. Determination of $\Omega_{\text{nat}}$ . . . . .	82
2. Method of Determining $\Omega_{\text{T}}$ . . . . .	84
3. Determination of $\Omega_{\text{S}}$ . . . . .	85
4. Determination of $\Omega_{\text{M}}$ . . . . .	86
G. Analysis of Unshifted Resonance Peaks and Determination of Target Thickness . . . . .	87
H. Energy-Current Calibration . . . . .	93
IV. Experimental Results on Stopping Power . . . . .	101
A. Possible Sources of Systematic Error and Corrections Required . . . . .	101
1. Nuclear Collision Losses . . . . .	101
2. Increase of Path Length by Scattering . . . . .	102
3. Carbonization of Foils . . . . .	102
4. Accurate Computation of Mean Energy of Protons in Medium . . . . .	105
5. Corrections Required for Impurities in the Materials Studied . . . . .	107
6. Possible Errors Due to Air Leakage During Experiment.	113
B. Stopping Power Results - Foils . . . . .	115
1. Determination of Energy of Displaced Peaks, Foils Inserted . . . . .	115
2. Computation of Foil Stopping Power . . . . .	115



3. Discussion of Errors in Experimental Data and Results . . . . .	122
C. Stopping Power Results - Gases . . . . .	125
1. Energy Loss in Window Foils . . . . .	125
2. Energy of Displaced Peaks, Gases and Window Foils Inserted . . . . .	125
3. Determination of the Formula for Atomic Stopping Power of Gases . . . . .	125
4. Computation of Gas Stopping Power . . . . .	134
5. Discussion of Errors in Gas Stopping Power Results . . . . .	134
D. Straggling in Stopping Power . . . . .	146
1. Computation . . . . .	146
2. Discussion of Errors . . . . .	150
V. Summary of Results . . . . .	152
VI. Conclusion - Discussion of Results . . . . .	163
A. Comparison of Present Results with Other Published Results . . . . .	163
1. Stopping Power - Comparison with Theory . . . . .	163
2. Stopping Power - Comparison with Other Experimental Information . . . . .	165
3. Comparison of Results of Straggling Measurements with Theory . . . . .	166
B. Concluding Comments . . . . .	168
Appendix - Design Details of Magnet Voltage Regulator . . . . .	170
References . . . . .	178
Autobiography . . . . .	181



## I. Introduction

The stopping power of a material is defined as the space-rate of loss of energy suffered by a particle of nuclear or atomic dimensions in its passage through the material. Since the time of Thomson and Rutherford the subject has been investigated both theoretically and experimentally in its many complexities, and it early provided a source of tests of atomic structure and mechanics. In recent years the interest of theoretical nuclear physicists in the various facets of the subject has waned, since it is largely a property of the extra-nuclear part of the atom. Nevertheless the subject is still a vital one in the experimental and applied side of nuclear physics. The need for good stopping power formulas and/or data for all types of nuclear particles, over the whole range of energies, and through all types of matter is almost too obvious to mention - e.g., in cosmic ray studies, range determinations, shielding requirements, and so on.

Unfortunately for those who need this information, stopping power formulas provided by theoreticians are in most cases unable to give accurate predictions without the use of semi-empirical constants adjusted to conform to previous experiment. This is due to the physical and mathematical complexities of the subject. By this date theory and experiment are sufficiently advanced that for heavy particles, such as protons or alpha particles, the stopping power can be predicted with accuracy for most types of matter usually encountered, provided the energy of the particles exceeds a few million electron-volts. However if one passes to the energy region lower than this, the predictions become less accurate and even empirical adjustments are





difficult. In such regions experimental data must largely be relied on at present. Such data are still far from complete, even for stopping by basic elements.

For direct measurement of stopping power within this energy region the Van de Graaff generator is well suited, because of the range of accelerating potentials available and because of its ability to produce accelerated particles of precisely defined and accurately measured energies. For this dissertation the writer has elected to report on the experimental results of stopping power of various elements for protons from the Van de Graaff generator at the Ohio State University. Specifically, measurements are herein reported of the stopping power for protons of the metals, copper and nickel, and of the gases, nitrogen, neon, argon, krypton, and xenon. The energy range over which these measurements are taken is from 400 to 1200 kev.

Brief mention is made of the associated problem of "straggling" in stopping power, or the mean square deviation in energy loss per unit thickness of matter for individual protons. This phenomenon is a result of the fact that slowing down of particles is accomplished through random collisions with atoms of the stopping medium and is therefore subject to statistical variations. This factor is less important than that of average stopping power, and both theoretically and experimentally it has been studied less fully. Accurate analysis of straggling is just as difficult in theory as analysis of stopping power itself, and experimentally it is even more difficult, requiring generally a precision of measurement better than stopping power measurement by an order of magnitude. The technique employed by the





writer for determination of stopping does make it possible to determine variations in same, under favorable experimental conditions. It has been found possible to report stopping power straggling for the metallic elements, copper and nickel, although precise accuracy is lacking. Such results are considered as a "by-product" of the major investigation into stopping power itself.

#### A. Definitions and Units.

Stopping power has been defined above; and unless otherwise specified or implied it refers to the average energy loss of a large number of similar particles of the same energy, per unit length of path through the material traversed. It is dependent upon the type of particle, the energy (or velocity) of the particle, and the stopping medium. The concept of stopping power involves a continuous change in particle energy, and yet a specified value of stopping power is valid only for a fixed value of particle energy. This indicates that stopping power must be recognized as a derivative,  $-dE/dx$ , itself a function of energy.

If the stopping medium is composed of a single element, one can use the concept of atomic stopping power, defined as stopping power divided by the number of atoms per unit cube of the stopping material. (This is sometimes called the "stopping cross-section" of the atom.) It may be considered as the average contribution of each atom of the elemental material toward slowing the incident particles. In symbols it is designated as  $\sigma = \frac{1}{N} \left( -\frac{dE}{dx} \right)$ .

Theoretical formulas have been derived in the Gaussian (c.g.s.)



system of units, so that stopping power is given in ergs/cm. For experimental work - both in determination and use of stopping power - energy changes are more usually expressed in electron-volts or similar units, while thicknesses are conveniently expressed in mg/cm<sup>2</sup>. Thus stopping power data from experiment is usually reported in units of kev-cm<sup>2</sup>/mg. The conversion factor between the two system of units is easily seen to be:

$$\text{Stopping power (ergs/cm)} = 1.602 \times 10^{-6} \times \text{Stopping power (kev-cm}^2\text{/mg)} \times \rho, \quad (\text{I-A-1})$$

where

$$\rho = \text{density of medium (g/cm}^3\text{)}.$$

For atomic stopping power the proper c.g.s. units are erg-cm<sup>2</sup>. Experimental conventions make preferable the units ev-cm<sup>2</sup>. The conversion factor between the two systems is obviously:

$$\text{At. stopping power (erg-cm}^2\text{)} = 1.602 \times 10^{-12} \times \text{At. stopping power (ev-cm}^2\text{)}. \quad (\text{I-A-2})$$

The conversion factor from stopping power to atomic stopping power in the c.g.s. system is:

$$\begin{aligned} (\text{At. stopping power})_{\text{cgs}} &= (\text{Stopping power})_{\text{cgs}} / N \\ &= \frac{A}{6.023 \times 10^{23} \times \rho} \times (\text{Stopping power})_{\text{cgs}}, \quad (\text{I-A-3}) \end{aligned}$$

where N is the number of atoms per cubic centimeter of stopping material, and A is the atomic weight of the stopping element.

From the above equations it is easily deduced that in experimental units the conversion factor from stopping power to atomic stopping



power is:

$$(\text{At. stopping power})_{\text{exp.}} = \frac{A}{6.023 \times 10^{17}} \times (\text{Stopping power})_{\text{exp.}} \quad (\text{I-A-4})$$

The concept of stopping power "straggling" is understood most easily by visualizing a statistical distribution of relative frequencies of stopping power losses for individual particles, under identical conditions. If the standard deviation about the mean of this distribution is designated as  $\Omega$ , then  $\Omega^2$  becomes the mean square fluctuation, or the variance; and one best describes the straggling by  $\frac{d}{dx} (\Omega^2)$ . (In finite increments we may consider straggling as  $\Omega^2/\Delta x$ , which is used rather than  $\Omega/\Delta x$  since, as we shall see later, the former is independent of thickness of medium while the latter is not.) This quantity may also be written, as shown by statistical theory (Hoel, 1947), as  $\frac{d}{dx} \left[ \overline{(E^2)} - (\overline{E})^2 \right]$ , where  $E$  in this expression indicates the energy of an individual particle among a large population of similar particles incident on the stopping medium with the same energy.

The units for  $\frac{d}{dx} (\Omega^2)$  are evidently ergs<sup>2</sup>/cm in the a.g.s. system. In experimental work the units employed are kev<sup>2</sup>-cm<sup>2</sup>/mg. The conversion relation between the values of straggling as expressed in these two systems is: -

$$\left[ \frac{d}{dx} (\Omega^2) \right]_{\text{cgs}} = \frac{1.602^2}{10^{15}} \times \text{ } \times \frac{d}{dx} (\Omega^2)_{\text{exp.}} \quad (\text{I-A-5})$$

## B. Review of Stopping Power Theory.

A complete review of stopping power theory would be almost im-





possible and certainly impractical for a report of this nature. It is necessary therefore to present only a brief outline of the theory. Much discussion can be eliminated by concentration only on those aspects bearing on our particular problem. For example, relativity considerations may be ignored, since we are interested only in a range of velocities well below that of light ( $v/c \sim 1/30$ ). Furthermore, we need consider only the stopping of heavy particles such as protons, and primarily by the medium or heavy elements.

In a broad sense there are two approaches to the problem, and each will be summarized in turn.<sup>1</sup> The first, exemplified by the works of N. Bohr and his followers, is classical or semi-classical in spirit. This is advantageous for ease of understanding, mathematical simplicity, and flexibility in application to a wide variety of conditions. The most rigorous formulation of the subject has been achieved, however, by modern wave-mechanical methods, with their mathematical complexities. Such methods may be difficult to appreciate intuitively, but they yield more accurate results in those realms where the basic assumptions are valid.

In presenting the simpler theory we shall follow primarily the excellent treatment given by N. Bohr (1948).

### 1. Classical Fundamentals.

Let us consider the elastic collision between an incident particle (number one) and a second particle which is at rest in the

---

<sup>1</sup> For the sake of clarity and brevity we are not following strictly a historical, or chronological, scheme of presentation. All major contributors to the theory however will be duly acknowledged where their ideas best fit into this summary.





laboratory frame of reference. Figure 1 shows the geometric relationships existing between the velocities in the center-of-mass system.

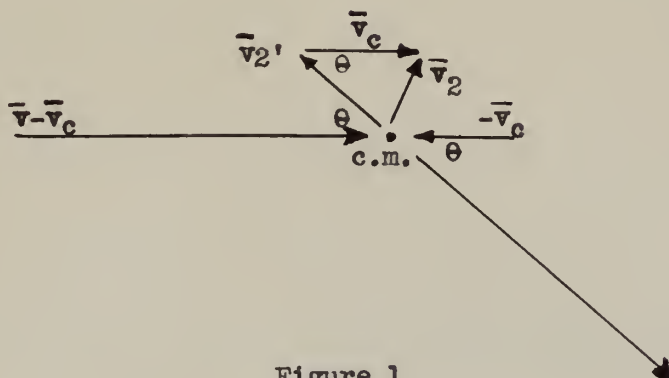


Figure 1.

In this figure,

$\bar{v}$  = velocity of particle 1, laboratory system, before collision;

$\bar{v}_c$  = vel. of center-of-mass, laboratory system, before collision;

$-\bar{v}_c$  = vel. of particle 2, center-of-mass system, before collision;

$\bar{v} - \bar{v}_c$  = vel. of particle 1, center-of-mass system, before collision;

$\theta$  = angle of deviation of each particle in the c.-m. system.

(For direct collision, the particles are always oppositely directed in the center-of-mass system, so that each particle undergoes the same angular deviation in this system.)

Each particle behaves in the center-of-mass system as if it rebounds elastically from the immovable center of mass without loss of energy. Then,

$\bar{v}_2'$  = vel. of particle 2, center-of-mass system, after collision;

and  $|\bar{v}_2'| = |-\bar{v}_c| = \bar{v}_c$  . (I-B-1)

Also,



$$\begin{aligned}\bar{v}_2 &= \text{vel. of particle 2, laboratory system, after collision,} \\ &= \bar{v}_2' + \bar{v}_c .\end{aligned}\quad (\text{I-B-2})$$

We see that  $v_2$  forms the base of an isosceles triangle with vertex angle  $\theta$ . Therefore

$$v_2 = 2 v_c \sin (\theta/2) . \quad (\text{I-B-3})$$

From the definition of center-of-mass it is easily shown that

$$v_c = \frac{m_1}{m_1 + m_2} \cdot v , \quad (\text{I-B-4})$$

where  $m_1$  and  $m_2$  are masses of the two particles. Thus

$$v_2 = 2v \frac{m_1}{m_1 + m_2} \sin (\theta/2) . \quad (\text{I-B-5})$$

Now in the collision particle 2 is given energy at the expense of particle 1 (laboratory coordinates). Let  $T$  be this energy transferred.

$$T = \frac{1}{2} m_2 v_2^2 ; \quad (\text{I-B-6})$$

and from equation (I-B-5),

$$\left. \begin{aligned} T &= \frac{2 m_1^2 m_2}{(m_1 + m_2)^2} v^2 \sin^2(\theta/2) \\ &= \frac{2 m_0^2}{m_2} v^2 \sin^2(\theta/2) , \end{aligned} \right\} \quad (\text{I-B-7})$$

where  $m_0$  is the "reduced mass" and equals  $m_1 m_2 / (m_1 + m_2)$ .

The maximum transfer of energy occurs on direct collision, when  $\theta$  equals  $180^\circ$ . Let  $T_m$  be this amount. Then

$$T_m = \frac{2 m_0^2}{m_2} v^2 ; \quad (\text{I-B-8})$$

and

$$T = T_m \sin^2(\theta/2) . \quad (\text{I-B-9})$$

If the law of attraction or repulsion between the two particles



is Coulombian, one may derive the well known Rutherford scattering formula:

$$d\sigma = \left( \frac{e_1 e_2}{2 m_0 v^2} \right)^2 \cdot \csc^4 (\theta/2) \cdot d\omega , \quad (\text{I-B-10})$$

where

$d\sigma$  = differential probability cross-section that the particle is scattered into solid angle,  $d\omega$ , measured in the center-of-mass coordinate system.

$d\omega$  = total solid angle corresponding to scattering directions between  $\theta$  and  $\theta + d\theta$ ,

$$= 2\pi \sin \theta \, d\theta = 4\pi \sin(\theta/2) \cdot \cos(\theta/2) \cdot d\theta . \quad (\text{I-B-11})$$

$e_1$  = charge of the first particle.

$e_2$  = charge of the second particle.

Substitution of the expression (I-B-11) into equation (I-B-10) gives:

$$d\sigma = 4\pi \left( \frac{e_1 e_2}{2m_0 v^2} \right)^2 \cdot \csc^3(\theta/2) \cdot \cos(\theta/2) \cdot d\theta . \quad (\text{I-B-12})$$

From equation (I-B-7) we obtain by differentiation:

$$dT = T \cos(\theta/2) \cdot \csc(\theta/2) \cdot d\theta . \quad (\text{I-B-13})$$

Then from the last two equations we obtain:

$$\begin{aligned} d\sigma &= \left( \frac{2\pi e_1^2 e_2^2}{m_2 v^2} \right) \frac{dT}{T^2} \\ &= D \frac{dT}{T^2} , \end{aligned} \quad (\text{I-B-14})$$

where D is the quantity within the parentheses.

We may use this result to obtain stopping power relations in a highly idealized case. Let us suppose that an incident particle undergoes a succession of energy-diminishing collisions in traversing a thin layer of matter in a direction normal to the layer.



Let

$\Delta x$  = thickness of layer of matter;

$N'$  = number of particles per unit cube of the stopping medium that absorbs the energy.

It is necessary to assume here that:

(a) The particles of the stopping medium are free particles at rest, interacting with the incident part. through the Coulomb law of force between charged particles.

(b) The energy transfer in an individual collision is small compared with the total energy of the incident particle. This is true provided  $T_m \ll \frac{1}{2} m_1 v^2$ , which according to equation (I-B-8) is true when  $m_0^2/m_1 m_2 \ll \frac{1}{4}$ .

(c) The medium layer is very thin so that  $v$  is essentially constant throughout the progress of the incident particle within the layer.

Assumption (b) indicates that momentum change of the incident particle is small in a single collision, which permits one to state that the particle velocity is almost constant in direction as well as in magnitude.

Now consider that we have made a series of hypothetical experiments in which we were able to follow each particle in an incident beam with common initial characteristics, and further that we could obtain and tabulate the data for each collision each particle undergoes with particles of the stopping material. Divide the possible values of energy loss in a single collision into equal intervals, with  $T_1$  corresponding to the average energy for the  $i^{\text{th}}$  interval and  $\sigma_1$  being the probability that each collision will provide an





energy loss within the interval characterized by  $T_1$ . Since the stopping process is a statistical process because of the randomness of location of particles of the medium in relation to the path of some incident particle, we cannot always get in different trials the same number of collisions characterized by  $T_1$ . Define

$n_1$  = number of collisions characterized by energy loss  $T_1$ ,  
for the case of any one incident particle;

$w_1$  = average number of collisions characterized by  $T_1$ , for  
the total population of incident particles in the beam.

From the given definitions it is evident that

$$w_1 = N' \cdot \Delta x \cdot \sigma_1 \quad . \quad (I-B-15)$$

In a practical case the number of collisions is large and individual "single shot probability" is small. In such cases the probability distribution function for  $n_1$  can be closely approximated by a Poisson distribution formula (Hoel, 1947):

$$P(n_1) = w_1^{n_1} e^{-w_1} / n_1! \quad , \quad (I-B-16)$$

having mean value  $w_1$  as required and having standard deviation equal to  $\sqrt{w_1}$ .

Now if  $\Delta E$  is the change in energy of a particular particle when passing through the given layer of the medium,

$$-\Delta E = \sum_1 T_1 n_1 \quad . \quad (I-B-17)$$

The average value of energy loss is

$$-\overline{\Delta E} = \sum_1 T_1 w_1 \quad ; \quad (I-B-18)$$

and the mean square fluctuation is by definition

$$\Omega^2 = \overline{(\Delta E - \overline{\Delta E})^2}$$



$$\begin{aligned}
&= \sum_1 T_1^2 \overline{(n_1 - w_1)^2} \\
&= \sum_1 T_1^2 (\sqrt{w_1})^2 = \sum_1 T_1^2 w_1 . \quad (\text{I-B-19})
\end{aligned}$$

If we go over to integrals and use equation (I-B-15) we obtain:

$$\overline{\Delta E} = N' \cdot \Delta x \cdot \int_{T_{\min}}^{T_{\max}} T \, d\sigma , \quad (\text{I-B-20})$$

and

$$N^2 = N' \cdot \Delta x \cdot \int_{T_{\min}}^{T_{\max}} T^2 \, d\sigma . \quad (\text{I-B-21})$$

Under the rather idealized conditions assumed we can obtain a formula for stopping power and the statistical variation thereof by substituting equation (I-B-14) in equations (I-B-20) and (I-B-21). In doing so we may make some assumptions based on the particular physical situation we are studying:

- (a) The primary type of particle in the medium responsible for stopping effects is the atomic electron. Nuclear collisions do contribute slightly to stopping power but such contribution is usually small (as will be shown later for our particular case).
- (b) The type of incident particle considered will be heavy, as our work is concerned with protons.

As a result of these assumptions we may make certain modifications in our formulas. If we designate the mass of the electron by  $m$ , then we may replace  $m_2$  by  $m$ . The reduced mass  $m_0$  is also approximately equal to  $m$ . If we designate the charge of the electron by  $e$ , then  $e_1$  becomes  $ze$  and  $e_2$  is simply  $e$ .



We see that the criterion in sub-paragraph (b) on page 10 is quite valid.

If  $N$  is defined as the number of atoms per unit volume of the stopping medium, we may use it instead of  $N'$ , provided we also sum over all electrons in the atom. Thus  $N'$  is replaced by  $N$  and a summation sign over  $s$ , where  $s$  is the index for each electron of the atom effective in the stopping phenomenon. If there is no reason to separate the contributions of various atomic electrons, or if their properties can be characterized by overall average values, then  $N'$  can be replaced by  $NZ$ , where  $Z$  is the atomic number of the element constituting the stopping medium.

We obtain then for stopping power:

$$\left. \begin{aligned} -\frac{dE}{dx} &= D \cdot N \sum_s \ln \frac{T_{\max}}{T_{\min}} \\ &= \frac{2\pi z^2 e^4 N}{m v^2} \sum_s \ln \frac{T_{\max}}{T_{\min}} \end{aligned} \right\} \quad (I-B-22)$$

For stopping power straggling we obtain:

$$\begin{aligned} \frac{d}{dx} (\Omega^2) &= D N Z (T_{\max} - T_{\min}) \\ &\cong D N Z T_{\max}, \end{aligned} \quad (I-B-23)$$

provided (as is usual)  $T_{\max} \gg T_{\min}$ , and  $T_{\max}$  is the same for all atomic electrons.

## 2. Stopping Power - Classical Formulation.

Inherent in the above analysis is the assumption that the electron behaves as a free particle, whereas it is actually bound to the atom. Nevertheless under many circumstances this assumption may be quite reasonable. For the present discussion let us assume that the particle





velocity,  $v$ , is greater than the "orbital velocity" of the electrons. (The classical approach is essentially the same whether the electron is considered as bound by elastic or Coulomb forces to the atom.) If  $u_s$  is the orbital velocity of the  $s^{\text{th}}$  electron, and  $I_s$  its ionization energy, then

$$I_s \approx \frac{1}{2} m u_s^2 \quad . \quad (\text{I-B-24})$$

It is possible to divide the stopping power into two parts -

(a) that portion due to close collisions of the particle with atoms, and (b) that portion due to more distant collisions. These must be considered separately.

(a) Close collisions are those for which  $T > I_s$ . If  $T_{\text{max}} \gg I_s$ , then for most close collisions, the ionization energy is so much smaller than  $T$  that it may be disregarded. This makes reasonable the assumption that for close collisions the electron may be considered as free. Under such circumstances it is clear that in a direct collision, giving  $T_{\text{max}}$ , the electron is ejected with a velocity practically equal to  $2v$ , so that

$$T_{\text{max}} = 2 m v^2 \quad (\text{I-B-25})$$

We may note that our original assumption that  $v > u_s$  leads directly to the conclusion that  $2mv^2 \gg \frac{1}{2}mu_s^2$ , or  $T_{\text{max}} \gg I_s$  - thus confirming this assumption.

$T_{\text{min}}$  for these collisions is of course  $I_s$ . Then equation (I-B-22) leads to

$$\left[ -\frac{dE}{dx} \right]_a = D N \sum_s \ln \frac{2 m v^2}{I_s} \quad . \quad (\text{I-B-26})$$

(b) For more distant collisions the energy transferred by classical





collisions would be smaller than the ionization energy. Classical models consider the electron as an oscillator (real or virtual) which can absorb any amount of energy, however small, when set into vibration by a sudden impulse from a changing force field, such as would be provided by a passing charged particle. The fact that  $v$  is greater than  $u_s$  indicates that the oscillator has moved from its equilibrium position only slightly by the time the particle has passed. Thus the "restoring force" has not been mobilized to any extent during the collision time. Once more therefore the electron may be considered as undergoing a free collision, under a situation however which permits energy absorption without ejection from the atom.

The value of  $T_{\max}$  used in this region of stopping is obviously the value of  $T_{\min}$  used in the previous case; to wit,  $I_s$ .

The value of  $T_{\min}$  cannot be zero, since this would give an infinite answer for stopping power. It has been deemed necessary to presume the existence of an "adiabatic limit" to the distance from the atom to the particle path. It is presumed that if a particle passes at a distance greater than this limit, the electric field is applied and released so slowly that the electron is eased out of and back into position without being left in an oscillatory (excited) state.

The duration of the impulse from the particle field is on the order of  $d_s/v$ , where  $d_s$  is the adiabatic limit corresponding to the  $s^{\text{th}}$  electron. If this duration is less than  $1/\omega_s$ , where  $\omega_s$  is the oscillatory frequency, then the impulse is faster than the ability of the electron to absorb and return it in adiabatic fashion.



Thus we make

$$d_s = v / \omega_s . \quad (\text{I-B-27})$$

Then  $T_{\min}$  will be the value of energy transfer for collisions at this distance. It can be shown that for such distant collisions between free particles (N. Bohr, 1948, Eq. 1.1.10):

$$T_{d_s} \approx \frac{2 z^2 e^4}{m v^2} \cdot \frac{1}{d_s^2} . \quad (\text{I-B-28})$$

We see then with the use of equation (I-B-27) that

$$T_{\min} = \frac{2 z^2 e^4 \omega_s^2}{m v^4} . \quad (\text{I-B-29})$$

Equation (I-B-22) leads to:

$$\left[ - \frac{dE}{dx} \right]_b = D N \sum_s \ln \frac{I_s m v^4}{2 z^2 e^4 \omega_s^2} , \quad (\text{I-B-30})$$

The total stopping power is given by adding the results of equations (I-B-26) and (I-B-30):

$$- \frac{dE}{dx} = 2 D N \sum_s \ln \frac{k m v^3}{z e^2 \omega_s} , \quad (\text{I-B-31})$$

This is the classical formula proposed by N. Bohr (1913) . It should be noted that the constant  $k$  has been introduced arbitrarily into the formula. Insofar as the above considerations apply the value of  $k$  is unity. Bohr's more rigorous approach gave to  $k$  a value of 1.123 .

### 3. Elementary Quantum Considerations in Stopping Power.

Unfortunately Bohr's formula gave values which were not in very good agreement with the experimental data on alpha particle stopping which were available at that time. Early attempts to improve the formula were unsuccessful.



The older quantum theory of atomic structure which Bohr developed at about this same time established that the bound energy states of the atomic electrons are discrete. This threw doubt upon the classical oscillator concept which permits the electron to absorb any amount of energy (within the restrictions of the adiabatic limit) and leads to formula (I-B-30). Henderson (1922a) suggested that only close, ionizing collisions should be considered, which led to a formula equivalent to equation (I-B-26) for the complete stopping power. This scheme likewise failed for alpha particles, but it is interesting to note that it gives answers equal to just about one-half of the experimental values (Fowler, 1923).

With our present comprehension of the limitations of classical mechanics at atomic distances, it is not difficult to deduce wherein formula (I-B-31) fails. We must accept the quantum requirement that energy transfer in a collision must be at least as large as  $I_s$  for the  $s^{\text{th}}$  electron. (For simplicity, we disregard excitation possibilities.) Thus classical theory can be expected to hold only if  $T_{\text{min}}$ , as given by equation (I-B-29), is greater than  $I_s$ . This criterion can be transformed by use of the relation

$$\omega_s \cong I_s / \hbar \quad (\text{I-B-32})$$

and the equation (I-B-24) into the form

$$\left( \frac{u_s}{v^2} \cdot \frac{z e^2}{\hbar} \right)^2 > 1 \quad (\text{I-B-33})$$

Now if we define  $v_0$  as the velocity of the electron in the ground state of the hydrogen atom, we know that

$$v_0 = e^2 / \hbar = 0.219 \times 10^9 \text{ cm/sec} . \quad (\text{I-B-34})$$





By substitution in equation (I-B-33) and taking the square root, the criterion becomes:

$$z v_0 / v > v / u_g . \quad (\text{I-B-35})$$

Our original assumption was that  $v > u_g$ , so that all criteria for applicability of the classical formula can be expressed as:

$$\frac{z v_0}{v} > \frac{v}{u_g} > 1 . \quad (\text{I-B-36})$$

Bohr (1948) showed that this criterion is a little stricter than necessary, and that correct results can be expected from the classical formula for values of  $z v_0 / v$  down to about unity .

Unfortunately, with respect to protons or alpha particles, the whole stopping power theory herein derived fails when  $z v_0 / v$  is appreciably greater than unity, because the particles tend to lose their charge by electron capture under such circumstances (Bohr, 1948; also see Section 7, below). Thus the failure of the classical equation for such particles is obvious.

For analysis of stopping power when  $v > z v_0$  (or for protons  $v > v_0$ ), we must once again divide the effect into two parts.

(a) Consider the  $s^{\text{th}}$  electron, for which equations (I-B-24) and (I-B-32) are still valid. This electron cannot be precisely located, but has a position which is smeared out over a distance having order of magnitude  $a_g$ , where

$$a_g = \hbar / m u_g . \quad (\text{I-B-37})$$

$a_g$  is fairly comparable to atomic dimensions. We first consider the contribution to stopping power of those collisions where the minimum approach distance of the incident particle is less than  $a_g$ , which





means that this portion is comparable to part (a) of the classical approach.

For those fast electrons of the stopping material, in case of which  $u_s \geq v$ , we note that

$$\frac{h}{m u_s} \leq \frac{h}{m v} \approx \frac{h}{m_0 v},$$

or  $a_s \leq \lambda$ , where  $\lambda$  is the de Broglie wave-length of the reduced particle. ( $\lambda$  equals  $\lambda/2\pi$ , just as  $h$  equals  $h/2\pi$ .)

Since in this discussion the approach distance is less than  $a_s$ , it is always less than  $\lambda$ ; and we no longer have a well defined collision in the classical sense. Such electrons therefore have little stopping effect.

For electrons in the case of which  $v \gg u_s$  (giving  $\lambda \ll a_s$ ) we have a situation which still permits a classical approach within certain limits.

When the incident particle penetrates the  $s^{\text{th}}$  electronic cloud of the atom (that is, roughly, within the distance  $a_s$ ) the collision may be a direct one, giving  $T_m = 2 m v^2$ . However, many collisions will not be quite direct. The least amount of energy able to be transferred within this region is indicated by the uncertainty principle. Since we are considering only those collisions where approach is closer than  $a_s$ , our uncertainty in electron position cannot exceed this amount. Then equation (I-B-37) indicates that uncertainty in momentum cannot be less than  $m u_s$ . This in turn means that uncertainty in energy is not less than  $\frac{1}{2} m u_s^2$  ( $\cong I_s$ ). Thus we can use the classical formulas with  $T_{\min} = I_s$ . (We are assured that  $T_m > I_s$ ,



just as in part (a) of the purely classical approach.)

We thus obtain for stopping power in this region a formula which is the same as (I-B-26):

$$\left[ -\frac{dE}{dx} \right]_a = D \cdot N \sum_s \ln \frac{2 m v^2}{I_s} \quad (\text{I-B-38})$$

Collisions in this category are called "free collisions" since most of them provide energy transfers greatly exceeding the binding energy of the electron, permitting it to be considered as free.

(b) For collision approach distances equal to  $a_s$ , one can find the energy transferred by a formula similar to equation (I-B-28):

$$\begin{aligned} T_{a_s} &= \frac{2 z^2 e^4}{m v^2} \cdot \frac{1}{a_s^2} ; \\ &= \left( \frac{2 z v_0}{v} \right)^2 I_s , \end{aligned} \quad (\text{I-B-39})$$

obtained with the assistance of equations (I-B-24) and (I-B-37).

This indicates that, for heavy particles with velocities well above  $v_0$ ,  $T_{a_s} < I_s$ . Thus, if we take a classical point of view, few, if any, collisions where the particle passes outside the atom can cause ionization. It is this fact which led to the difficulties of Henderson (1922) previously mentioned, and such difficulties were unresolved until modern wave-mechanics established the possibility of energy transfer through the "resonance" process.

Previous to this, however, Fermi (1924) had espoused an idea which was to be fruitful. He proposed that the perturbing force exerted by the particle on the atom could be analyzed as a function of time into Fourier components, and the effect of each component on the atoms could be compared to the effect of electromagnetic radiation



of the same wave-length. This analogy between particle collision theory and electromagnetic absorption theory may not be valid for close collisions, but for distant collisions where the particle field is almost constant over the whole atom the analogy seems promising. Even the idea of the "adiabatic limit" can be carried over, since at that remote distance the perturbing field no longer contains oscillatory components of appreciable magnitude which can effect any sort of resonance interaction with the atomic electrons.

It is well known today that the classical theory of electromagnetic absorption gives results almost the same as those obtained by a strict quantum approach and confirmed by experiment (Compton, 1919; for general discussion see Compton and Allison, 1935). One may presume then that for distant collisions we may obtain a correct result by continuing the classical approach. This gives us then, from equation (I-B-22):

$$\begin{aligned}
 \left[ -\frac{dE}{dx} \right]_b &= D \cdot N \sum_s \ln \frac{T_{a_s}}{T_{d_s}} \\
 &= D \cdot N \sum_s \ln \left( \frac{d_s}{a_s} \right)^2, \text{ by equations (I-B-28) and} \\
 \text{(I-B-39);} & \\
 &= D \cdot N \sum_s \ln \frac{2 m v^2}{I_s}, \quad \text{(I-B-40)}
 \end{aligned}$$

obtained with the use of equations (I-B-24), (I-B-27), (I-B-32), and (I-B-37).

Collisions leading to this component of stopping power are called "resonance collisions". Just as in the case for free collisions, those electrons for which  $u_s > v$  are to be ignored, as their con-





tribution according to the formula is quite small. In fact it can be seen that the formula even provides a negative (and completely unphysical) result when  $I_s > 2 m v^2$ .

In general, then, the formulation for total stopping power is simply:

$$-\frac{dE}{dx} = 2 D \cdot N \sum_s \ln \frac{2 m v^2}{I_s}, \quad (\text{I-B-41})$$

being the sum of contributions given in equations (I-B-38) and (I-B-40).

One refinement may be inserted here, for which we shall give only a qualitative justification. Hitherto the interaction of the atomic electrons has been ignored, but because of the screening effects of the electrons on one another they cannot be considered as independent oscillators. It is proper to weight the contribution of each electron by a factor  $f_s$ , called the "oscillator strength" of the  $s^{\text{th}}$  electron. The value of each  $f_s$  is still on the order of unity, and it has been shown (Kuhn, 1925; Thomas, 1925; and many others) that

$$\sum_s f_s = Z \quad (\text{I-B-42})$$

Thus we see that equation (I-B-41) is still approximately correct, but more precise answers would be given by:

$$\begin{aligned} -\frac{dE}{dx} &= 2 D N \sum_s f_s \ln \frac{2 m v^2}{I_s} \\ &= \frac{4 \pi z^2 e^4}{m v^2} N \sum_s f_s \ln \frac{2 m v^2}{I_s}. \end{aligned} \quad (\text{I-B-43})$$

Except for a slight modification of the term  $I_s$ , this formula checks with that found by Bethe (1930), using a rather strict quantum-mechanical approach, similar to that given in the next section.





We should note here that Bloch (1933) by another rigorous quantum-mechanical approach obtained a general formula which contained Bohr's classical equation (I-B-31) and Bethe's equation (I-B-43) as limiting cases, according to whether  $2zv_0/v$  is much greater or much less than unity. (He retained the qualification that  $v > u_g$  for all electrons.) As we have seen, the conditions we are interested in are those which put us definitely in the quantum region of applicability, so that the refinements of Bloch's formula need not be considered.

#### 4. Strict Quantum-Mechanical Derivation of Stopping Power Formula.

The derivation of stopping power formula using quantum mechanics may use any of several different approaches. The one outlined here is equivalent to that given by Bethe (1930, 1933).

The system to be considered consists of an atom and a moving charged particle within a large cube of dimension  $L$ . The interaction between the atom and the moving particle is to be considered as a time-dependent perturbation. Before the interaction occurs, the particle and atom are completely independent, with the former having the wave function for a free particle. The wave-function for the initial state of the system can be written therefore as:

$$U_0 = \frac{1}{L^{3/2}} \exp \left( \frac{i}{\hbar} \underline{p}_0 \cdot \underline{R} \right) \psi_0(\underline{r}_j) , \quad (\text{I-B-44})$$

where

$\underline{p}_0$  = the initial momentum of the "reduced" particle, with respect to the center-of-mass of the system,  $= M \underline{v}$ ;

$M$  = the reduced mass of the particle-atom system

$$= \frac{M_1 M_a}{M_1 + M_a} ;$$



$\underline{R}$  = the position vector of the particle, referred to the atomic nucleus;

$\underline{r}_j$  = the position vector of the  $j^{\text{th}}$  electron, referred to the atomic nucleus;

$\psi_0(\underline{r}_j)$  = the wave function of the unperturbed atom in its ground state.

We will concern ourselves with the probability of transition of this system to a final state in which the atom is left in a certain state (excited) characterized by the subscript  $n$  (this  $n^{\text{th}}$  state of the atom may be one in which the electrons are still bound or may be in that continuum of states where one of the electrons is emitted from the atom), and the particle is moving in another direction with momentum  $\underline{p}$ . After the collision is essentially completed, the wave-function of the system is again that of atom and free particle without further interaction:

$$U_n = \frac{1}{L^{3/2}} \exp \left( \frac{1}{\hbar} \underline{p} \cdot \underline{R} \right) \cdot \psi_n(\underline{r}_j) \quad (\text{I-B-45})$$

Let us use the well known formula for first order transition probabilities (Schiff, 1949, p. 193; Landé, 1951, p. 172) :

$$W = \frac{2\pi}{\hbar} \rho_E \cdot |H'_{on}|^2, \quad (\text{I-B-46})$$

where

$W$  = the number of particles per unit time scattered into a differential element of solid angle (to be precisely described below) with final momentum  $\underline{p}$ , presuming that incident particles arrive at such a rate that the requirement of one incident particle per cube of



dimension  $L$  is maintained;

$\rho_E$  = the density of final energy states of the system (since the atom is left in a definite energy state, the final density of states of the system must be obtained by consideration of density of states available to the scattered particle having momentum  $p$  ; the density is further curtailed by the fact that we must consider only possible directions of the final momentum vector contained within the element of solid angle specified in the definition of  $W$ ) ;

$H'_{on} = \int \bar{U}_0 H' U_n d\tau$  , where the integration is carried out over all space coordinates of all particles in the system.

To find  $\rho_E$  , we note that the number of momentum states available to a free particle definitely contained in a cube of dimension  $L$ , with momentum within the increments  $dp_x$ ,  $dp_y$ , and  $dp_z$  is  $(L^3/h^3) dp_x dp_y dp_z$  . This is equally applicable to any element in momentum space, so that if we are interested in the number of states of the particle with an absolute value of momentum between  $p$  and  $p + dp$  , the number of momentum states available is  $(L/h)^3 p^2 dp$  per unit solid angle. Our solid angle shall be restricted by considering only those collisions wherein the scattering angle in the center-of-mass system is between  $\theta$  and  $\theta + d\theta$  , so that the solid angle is  $2\pi \sin \theta \cdot d\theta$  .

The number of energy states in the energy interval  $dE_t$  is the same as the number of momentum states in the momentum interval  $dp$  ,





provided the intervals correspond. Thus

$$\rho_E dE_t = (L/h)^3 p^2 dp (2\pi \sin \theta \cdot d\theta) . \quad (I-B-47)$$

The relation between  $dE_t$  and  $dp$  can be obtained from the expression for total final energy of the system:

$$E_t = \frac{p^2}{2M} + E_n (\text{atom}) ; \quad (I-B-48)$$

and

$$\frac{dE_t}{dp} = \frac{p}{M} . \quad (I-B-49)$$

Therefore,

$$\rho_E = \frac{2\pi M L^3 p}{h^3} \sin \theta \, d\theta . \quad (I-B-50)$$

Substitution of equation (I-B-50) into equation (I-B-46) gives:

$$W = \frac{M L^3}{2\pi h^4} p \sin \theta \, d\theta \left| H'_{on} \right|^2 . \quad (I-B-51)$$

Let us now define  $d\Phi_n(\theta)$  as the differential scattering cross-section with angle between  $\theta$  and  $\theta + d\theta$ , for one particle incident per second upon one square centimeter, and leaving the atom in the  $n^{\text{th}}$  excited state. This differs from  $W$  in that we now have  $1/v$  particles per cubic centimeter whereas before we had  $1/L^3$  particles per cubic centimeter. Then

$$\begin{aligned} d\Phi_n(\theta) &= (L^3/v) W = \frac{L^3 M}{p_0} W \\ &= \frac{M^2 L^6}{2\pi h^4} \cdot \frac{p}{p_0} \sin \theta \, d\theta \left| H'_{on} \right|^2 . \end{aligned} \quad (I-B-52)$$

This result is the same as that obtained through use of the Born approximation, to which this approach is equivalent; and therefore for its validity it depends upon those criteria which make the Born





approximation valid. (Schiff, 1949)

Let us reduce  $H'_{on}$ . The perturbing portion of the Hamiltonian is the interaction potential energy between the particle and the atom:

$$H' = z e^2 \left[ \frac{Z}{|\underline{R}|} - \sum_{j=1}^Z \frac{1}{|\underline{R} - \underline{r}_j|} \right] \quad (I-B-53)$$

The first term in the bracket can be neglected, as it gives a result for elastic scattering (corresponding to what Bohr calls nuclear scattering) which may be ignored for protons or alpha particles insofar as it affects energy loss.

It can be shown (Bethe, 1930) that by integration over the space coordinates of the particle,  $H'_{on}$  can be reduced to the following form:

$$H'_{on} = \frac{z e^2}{L^3} \frac{4 \pi \hbar^2}{|\underline{p}_0 - \underline{p}|^2} \cdot \epsilon_n \quad (I-B-54)$$

where

$$\epsilon_n = - \int \sum_j \frac{\exp \left( \frac{i}{\hbar} |\underline{p}_0 - \underline{p}| \cdot \underline{r}_j \right)}{|\underline{p}_0 - \underline{p}|} \bar{\Psi}_0 \cdot \Psi_n d\tau_j \quad (I-B-55)$$

Substitution of the above expression into equation (I-B-52) gives:

$$d\Phi_n(\theta) = \frac{8 \pi \hbar^2}{|\underline{p}_0 - \underline{p}|^4} (z e^2)^2 \cdot \frac{p}{p_0} \sin \theta \cdot d\theta \cdot |\epsilon_n|^2 \quad (I-B-56)$$

Define a new parameter:

$$\underline{q} = \underline{p}_0 - \underline{p}$$

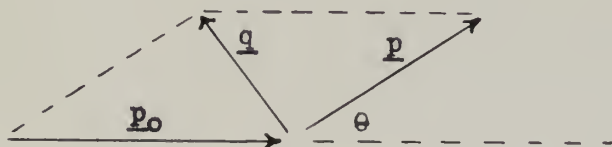


Figure 2



From the figure we see that

$$q^2 = p^2 + p_0^2 - 2 p p_0 \cos \theta . \quad (\text{I-B-57})$$

For a given  $p_0$  and  $p$ ,  $q$  is a function of  $\theta$  only. By differentiation we can derive that:

$$\sin \theta \, d\theta = \frac{q \, dq}{p \, p_0} . \quad (\text{I-B-58})$$

Then (I-B-56) can be written:

$$d\Phi_n(q) = \frac{8\pi z^2 e^4}{q^3 v^2} \, dq \, |\epsilon_n|^2 . \quad (\text{I-B-59})$$

This expression can be written more simply and in a form permitting easy comparison with the classical approach given above, if we let:

$$Q = \frac{|p_0 - p|^2}{2m} = \frac{q^2}{2m} . \quad (\text{I-B-60})$$

Introduction of  $Q$  in equation (I-B-59) to replace  $q$  as parameter gives:

$$d\Phi_n(Q) = \frac{2\pi z^2 e^4}{m v^2} \cdot \frac{dQ}{Q^2} \cdot |\epsilon_n|^2 . \quad (\text{I-B-61})$$

We recognize this as being in correspondence with equation (I-B-14) obtained by strictly classical means, provided we relate  $Q$  to  $T$  and provided  $|\epsilon_n|^2$  is approximately unity for a one-electron atom. It is easily shown that  $Q$ , from its definition, is the energy the secondary electron would receive from the collision provided it was not bound to the atom.

To obtain the total probability of a transition which leaves the atom in the  $n^{\text{th}}$  excited state, we must integrate over all possible values of  $Q$  :



$$\Phi_n = D \cdot \int_{Q_{\min}}^{Q_{\max}} \frac{dQ}{Q^2} \cdot |\epsilon_n|^2 \quad (I-B-62)$$

Let us define  $E_0$  as the energy of the atom in its ground state, and remember that  $N$  equals the number of atoms per cubic centimeter of the stopping material. The total energy loss of the particle per atom (atomic stopping power) is the average energy gain per atom, obtained by multiplying  $\Phi_n$  by  $(E_n - E_0)$  and then summing (including integrating in the continuum of energy states) over all values of  $n$  available for excitation. If we multiply by  $N$ , we then get the total stopping power:

$$-\frac{dE}{dx} = D \cdot N \sum_n (E_n - E_0) \int_{Q_{\min}}^{Q_{\max}} \frac{dQ}{Q^2} |\epsilon_n|^2 \quad (I-B-63)$$

For high values of energy transfer, the ionization energy can be ignored; and as we have previously seen,  $Q \cong T$ . Then for  $Q_{\max}$  we may use  $T_{\max} \cong 2 m v^2$ , by equation (I-B-25). (This is not accurate for low values of  $n$  since the binding energy of the electron has too strong an influence to be ignored in such cases. Under normal circumstances these low levels give only a very minor contribution to stopping power, so that the approximation for  $Q_{\max}$  gives a negligible error overall.)

For  $Q_{\min}$ , we can easily derive an expression from (I-B-60) :

$$\begin{aligned} Q_{\min} &= \frac{1}{2 m} (p_0 - p)^2 \\ &= \frac{M}{m} \cdot \frac{(E_n - E_0)^2}{4 E} \end{aligned} \quad (I-B-64)$$

Further development would be facilitated by reversal of the



order of summation and integration. As the equation stands this is not possible since  $Q_{\min}$  is dependent on the particular value of the quantum number  $n$ . However let us split the integration into two parts - with the middle limit,  $Q_0$ , being independent of  $n$ . The only other restriction on  $Q_0$  is that it be less than the average ionization potential of the atomic electrons concerned in the stopping.

Let us determine first of all the stopping power formula, considering hydrogen as the stopping medium. If  $Ry$  is defined as the ionization energy of the hydrogen atom (13.6 ev), we can use

$$Q_0 = (Ry)^2 / 2mv^2 \quad (I-B-65)$$

Then we obtain:

$$-\frac{dE}{dx} = D \cdot N \cdot \left\{ \int_{Q_0}^{Q_{\max}} \frac{dQ}{Q^2} \sum_n (E_n - E_0) |\epsilon_n|^2 + \sum_n (E_n - E_0) \int_{Q_{\min}}^{Q_0} \frac{dQ}{Q^2} |\epsilon_n|^2 \right\} \quad (I-B-66)$$

In the evaluation of the first integral, we can use a theorem proved by Bethe (1930), which indicates that  $\sum_n (E_n - E_0) |\epsilon_n|^2 = Q$ .

Evaluation of the second integral can be simplified since  $Q_0$  and  $Q_{\min}$  are both much less than  $Ry$ . This indicates that  $Q$  is very small; consequently  $p_0 - p$  is small and approximately perpendicular to the path of the incident particle. The situation becomes closely equivalent to the case of energy absorption from electromagnetic waves. In such cases the square of the matrix element  $\epsilon_n$  can be shown to equal the optical oscillator strength for the transition from ground





to  $n^{\text{th}}$  excited state of the atom. Bethe (1930; 1933) uses this simplifying fact and carries out a complete numerical solution for the stopping power of hydrogen. In doing so he uses the well known wave functions for hydrogen - expressed in polar spherical coordinates for the discrete levels, and in parabolic coordinates for those levels in the continuum above. He obtains:

$$\sum_n (E_n - E_0) \int_{Q_{\min}}^{Q_0} \frac{dQ}{Q^2} |\epsilon_n|^2 = -0.098 \quad (\text{I-B-66})$$

Then,

$$\begin{aligned} \left[ -\frac{dE}{dx} \right]_{\text{Hydrogen}} &= D \cdot N \left[ \ln \frac{Q_{\max}}{Q_0} - 0.098 \right] \\ &= \frac{4\pi z^2 e^4 N}{m v^2} \ln \frac{2 m v^2}{1.103 \text{ Ry}} \quad (\text{I-B-67}) \end{aligned}$$

This formula is fairly accurate and is confirmed approximately by experimental work (Mano, 1934). It should be noted that in its derivation it has been necessary to do the same thing as was done in sub-sections 2 and 3 above - that is, to divide the stopping effect into two parts, that involving close collisions where the binding energy of the electron is negligible, and that involving distant collisions where analogy to electromagnetic dispersion and absorption theory is utilized.

For heavier elements the situation is a little more complex. Bethe (1930) shows that for each electron of the stopping material, the above formula is valid, provided that the factor 1.103 Ry is replaced by a term  $I'_s$ , which is somewhat larger than the ionization energy of the electron. Further, in summing the effect of each



electron, it must be weighted by its oscillator strength.

The determination of  $I'_s$  is rather complex, as its precise value depends upon a knowledge of the wave-functions for the atom concerned.

The formula for complex atoms may be stated as follows:

$$-\frac{dE}{dx} = \frac{4\pi z^2 e^4 N}{m v^2} \sum_s f_s \ln \frac{2 m v^2}{I'_s}, \quad (\text{I-B-68})$$

$$= \frac{4\pi z^2 e^4 N}{m v^2} Z \ln \frac{2 m v^2}{I_{av}}, \quad (\text{I-B-69})$$

where  $I_{av}$ , called the "average excitation energy," is theoretically defined by:

$$Z \ln I_{av} = \sum_s f_s \ln I'_s. \quad (\text{I-B-70})$$

Formula (I-B-68) is of course identical with (I-B-43) above, except that  $I'_s$  is probably a little larger than  $I_s$ , the true ionization energy. In practice it is necessary to select empirically the value of  $I_{av}$  or the values of one or more  $I'_s$  to make the formula agree with experimental data.

##### 5. Modifications to Theory for Slow Particles Through Heavy Media.

Most of the above theory was developed on the basis that the charged particle has a velocity faster than the "orbital velocity" of each of the atomic electrons in the stopping medium. That the criterion fails for protons having energies in the region we are studying is easy to show. If we consider the velocity of an atomic electron given by equation (I-B-24), then the energy of a proton having the same velocity as an atomic electron of ionization energy  $I_s$  is given by  $(M/m)I_s$ . The criterion for validity of the unmodified equation for stopping power becomes:



$E \gg (M/m)I_s$  for every electron of the atom, where  $E$  is the actual proton energy.

From tables of ionization energies (Siegbahn, 1931), it is easily computed that the criterion fails:

For  ${}^7\text{N}$ , K electrons, when  $E \gtrsim 0.72$  Mev;

For  ${}^8\text{O}$ , K electrons, when  $E \gtrsim 1.0$  Mev;

For  ${}^{10}\text{Ne}$ , K electrons, when  $E \gtrsim 1.6$  Mev;

For  ${}^{18}\text{A}$ , K electrons, when  $E \gtrsim 5.8$  Mev;

For  ${}^{18}\text{A}$ , K and L electrons, when  $E \gtrsim 0.35$  Mev;

For  ${}^{28}\text{Ni}$ , K and L electrons, when  $E \gtrsim 1.5$  Mev;

For  ${}^{36}\text{Kr}$ , K, L, and M electrons, when  $E \gtrsim 0.48$  Mev;

For  ${}^{54}\text{Xe}$ , K, L, and M electrons, when  $E \gtrsim 1.5$  Mev.

What does one do if the criterion fails? One approximation (Livingston and Bethe, 1937) involves the assumption that all electrons for which  $E > (M/m)I_s$  are fully effective in stopping, and the other electrons do not contribute at all. This means that formula (I-B-69) is usable provided  $Z'$  is used in place of  $Z$ , where

$$Z' = \sum_n f_n, \quad (\text{I-B-71})$$

the summation being taken only over those electrons slower than the incident particle.  $I_{av}$  is also different in such cases, since only those outer electrons conforming to the criterion are used in the averaging.

This method gives a curve of proper shape but requires experimental values at various energies to provide precise accuracy. Furthermore, unless  $I_{av}$  is readjusted accordingly, discontinuities are likely





to appear in the curve at the points where  $E = (M/m)I_s$ , since  $Z'$  changes at these points.

Bohr (1948), who was less interested in precise results than in general trends, evaded this difficulty. He recognized in his analysis which led to the equation called herein equation (I-B-41) that those electrons for which  $u_s > v$  should be ignored. To determine those electrons which are effective in the stopping process, he used a formula based on the Thomas-Fermi statistical model of the atom (Thomas, 1927; Fermi, 1928):

$$\begin{aligned} n(u_s) &= \text{the number of electrons in the atom with velocity} \\ &\quad \text{smaller than } u_s ; \\ &\approx Z^{1/3} u_s / v_0 . \end{aligned} \quad (\text{I-B-72})$$

Equation (I-B-41) is modified by integrating over  $dn(u_s)$  instead of summing over  $s$  :

$$-\frac{dE}{dx} = 2 D N \int_0^{2v} \ln \frac{2 m v^2}{\frac{1}{2} m u_s^2 (= I_s)} dn(u_s) . \quad (\text{I-B-73})$$

The upper limit is that value for which the logarithm goes to zero.

Simplification and integration then gives:

$$\left. \begin{aligned} -\frac{dE}{dx} &= 8 D N Z^{1/3} (v/v_0) \\ &= \frac{16 \pi z^2 e^4 N}{m v_0} \cdot \frac{Z^{1/3}}{v} \end{aligned} \right\} \quad (\text{I-B-74})$$

Bohr states that the formula he uses for  $n(u_s)$ , is not very accurate if  $u_s$  represents the velocity of the very outer or very inner electrons. Thus formula (I-B-74) may be expected to be most valid for those particle velocities which are comparable to electron velocities in the intermediate shells.

Neufeld (1950) attempted to improve Bohr's approach so as to



provide answers more accurate than that given above. He went back to the basic formulation wherein stopping effects are separated into two parts - the contribution from "free collisions" and that from "resonance collisions". For the latter he used a more elaborate formula which had first been proposed by Fermi (1940). This formula is noteworthy since it provides positive contributions from every electron, regardless of velocity. Furthermore it is convergent if all distant collisions are included, even out to a collision distance of infinity. This obviates the need for the "adiabatic limit" concept.

Neufeld's approach is tedious and requires a separate set of calculations for each type of stopping element. His calculated values for a few metals seem to be about 10% less than the best experimental results available at the moment. The advantage of his approach is that it requires no previous experimental work to determine the parameters.

We have reserved till last the discussion of a more exact treatment of this problem, which was initiated by Livingston and Bethe (1937). As a prelude to this contribution, it should be noted that shortly after Bethe (1930) gave his stopping power formula, Mott (1931) and Henneberg (1933) showed that the Born method of treating collision problems could be applied with validity to collisions of heavy particles with heavy atoms having electronic velocities faster than the particle velocity. This is true for atoms of high atomic number, since the perturbing potential of the incident particle is small compared to the binding potential for the fast, inner electrons.



(See also Mott and Massey, 1949.) This fact gives one faith in the use of previously derived formulas even when the original criterion that  $v > u_s$  is not completely adhered to.

Suppose one wishes to obtain results which are valid for particle velocities down to the order of magnitude of the velocity of the K-shell electrons, or somewhat lower. An exact solution of the contribution of the K electrons is obviously much better than an assumption requiring either full contribution or zero contribution of the K electrons to the stopping effect. We may note that fairly simple wave-functions are available for use here, since even in a complex atom the innermost electrons obey wave-functions which are almost hydrogen-like. The formula used by Livingston and Bethe is thus simply a modification of the equation used by Bethe to derive the stopping power of hydrogen (equation I-B-63):

$$\left[ - \frac{dE}{dx} \right]_K = \frac{4 \pi z^2 e^4}{m v^2} N \cdot B_K, \quad (\text{I-B-75})$$

where

$$B_K = \int_0^\infty E' dE' \int_{Q_{\min}}^\infty \frac{dQ}{Q^2} \cdot |\mathcal{E}|^2. \quad (\text{I-B-76})$$

In this formula one integrates instead of summing over the various energy changes, since most of the discrete levels well below the continuum can be considered as filled. The scale of the values of energy and  $Q$  are changed to put all calculations on a uniform basis for different values of  $Z$ :

$$E' = \frac{E_n - E_0}{Z_{\text{eff}}^2 \cdot Ry}, \quad (\text{I-B-77})$$





where  $Z_{\text{eff}}$  = effective nuclear charge as felt by the K electrons,  
 $= Z - (\text{inner screening constant})$  (Slater, 1930)

$$\phi = \frac{I_K}{Z_{\text{eff}}^2 \cdot Ry} ; \quad (\text{I-B-78})$$

$$Q = \frac{1}{Z_{\text{eff}}^2 \cdot Ry} \cdot \frac{(p_0 - p)^2}{2m} ; \quad (\text{I-B-79})$$

$$\eta = \frac{\frac{1}{2} m v^2}{Z_{\text{eff}}^2 \cdot Ry} = \frac{E m}{M} \frac{1}{Z_{\text{eff}}^2 \cdot Ry} ; \quad (\text{I-B-80})$$

$$Q_{\text{min}} = E^2 / 4 \eta , \quad (\text{I-B-81})$$

which is actually the same as equation (I-B-64).

$\phi$  is the lower limit of  $E'$ , inasmuch as we consider transitions to the discrete levels as impossible by reason of their being filled. Infinity is permitted as upper limit for  $Q$ , since the computations of the matrix element make the probabilities exceedingly small for any contributions by values of  $Q$  above  $2mv^2$ .

Livingston and Bethe have evaluated this formula for  $B_K$  by numerical integration. For  $\phi$  equal to 0.7, which is approximately correct for values of  $Z$  from 6 to 13, they have plotted  $B_K$  against  $\eta$  as argument.  $B_K$  can also be expressed as:

$$B_K(\phi = 0.7, \eta) = 1.81 \ln 3.63 \eta - C_K(\eta) , \quad (\text{I-B-82})^1$$

where  $C_K$  is a corrective term to the basic formula (I-B-68 or I-B-69) which approaches zero as particle energy (or  $\eta$ ) increases.

Curves for  $C_K$  are also given by Livingston and Bethe.

<sup>1</sup> It is easy to show that the factor 1.81 is approximately the sum of the oscillator strengths of the two K electrons, while

$$3.63 \eta = \frac{2 m v^2}{1.103 Z_{\text{eff}}^2 \cdot Ry} .$$





They have also given a curve for atomic stopping power of air for protons, data from which is tabulated in Table I, over the energy range in which we are interested.

This formulation of K electron stopping power has been extended by Brown (1950) and Walske (1952) to values of  $\phi$  higher than 0.7, which in effect extends the theory to heavier atoms. They have made the computations and supplied graphical results for  $B_K(\phi, \eta)$  and  $C_K(\phi, \eta)$ .

It is pertinent to ask about the corrections required for L, M, and higher electrons as the velocity of the incident particle approaches their orbital velocities. This is particularly important, as we have seen, for the heavier elements. The exact analysis for stopping power of electrons in these shells is well nigh impossible to carry out because of the complexity and lack of knowledge of the wave-functions at these shells.

Hirschfelder and Magee (1948) generalized the foregoing method to apply to shells higher than the K shell. They utilized the original curves provided by Livingston and Bethe since those of Brown or Walske were not available at that time. In effect they noted that the stopping number B, where

$$B = Z \ln \frac{2 m v^2}{I_{av}} - C_K - (\text{higher shell corrections}), \quad (\text{I-B-83})$$

can be expressed as:

$$B = \sum_i q_i f_i b_i, \quad (\text{I-B-84})$$

where

$$q_i = \text{number of electrons in the } i^{\text{th}} \text{ shell};$$



$f_1$  = effective oscillator strength of an electron of the  $i^{\text{th}}$  shell;

$b_1$  = the essential variable for the  $i^{\text{th}}$  shell, depending upon  $\eta$ .

For the K shell it is seen from equation (I-B-82) that

$$b_K = \frac{B_K(\eta)}{1.81} = \ln(3.63 \eta) - \frac{C_K}{1.81}, \quad (\text{I-B-85})$$

and, as before,

$$\eta = \frac{E}{(M/m) I''_K}, \quad (\text{I-B-86})$$

with

$$I''_K = Z_{\text{eff}}^2 \cdot R_y \quad (\text{I-B-87})$$

The generalization was made in the assumption that, in form,

$b_1$  is the same as  $b_K$  for all values of  $i$ . It is only necessary to use a different value of  $I''_i$  (the ionization energy without external screening for the shell considered) in computing the argument  $\eta$  with which to use the curves for  $B_K$ . For all but the outer shell, the value of  $I''$  was taken to be:

$$I''_i = \frac{Z_{\text{eff}}^2 \cdot R_y}{n_i^2}, \quad (\text{I-B-88})$$

with  $n_i$  being the effective principal quantum number of the  $i^{\text{th}}$  shell.

It is hardly necessary to point out that such a procedure is approximate - primarily because of the marked deviation of the wavefunctions of the middle shells from a hydrogen-like character. The originators of this approach hoped to predict the trends rather closely however; and the semi-empirical character of Bethe's original formulation was retained by adjusting the value of  $I''$  for the outer



Table I.

Semi-empirical Calculations of Atomic Stopping Power

Air - Livingston and Bethe (1937)  
 Argon- Hirschfelder and Magee (1948)  
 Xenon- Hirschfelder and Magee (1948)

E (Mev)	$\sigma$ ( $10^{-15}$ ev-cm <sup>2</sup> )		
	Air	Argon	Xenon
0.3	12.93	20.834	35.5828
0.4	10.63	17.601	30.6465
0.5	8.86	15.432	27.2376
0.6	7.70	13.833	24.7589
0.7	6.90	12.604	22.7846
0.8	6.30	11.610	21.1880
0.9	5.81	10.792	19.8589
1.0	5.45	10.108	18.7458
1.1	5.11	9.522	17.7874
1.2	4.80	9.011	16.9314
1.3	4.53	8.563	16.1795
1.4	4.29	8.160	15.5181
1.5	4.07	7.807	14.9227





shell of electrons as necessary to conform to experimental values of range in the media (gaseous) selected for study.<sup>1</sup>

The studies of Hirschfelder and Magee were applied to two gases of particular interest here - argon and xenon. The computed results for atomic stopping power of these two gases for protons are tabulated in Table I, over the range of energies in which we are interested.

#### 6. Effect of the Physical and Chemical State of Media on Stopping Power.

In all of the theory presented previously the atom which absorbs the energy has been considered to be in a free state, such as a monatomic gas. Any sort of chemical combination or condensation of the medium into a liquid or solid state might be expected to shift the energy levels, at least of the electrons in the outer shells, and thus affect the stopping power by changing the value of  $I_{av}$ , the average excitation energy.

As far as chemical combination in gases is concerned, the effect, if present, must be quite small. If the atoms act independently, the stopping power per molecule should be a simple sum of the atomic stopping powers of the individual atoms. This rule seems valid in gases though not always in liquids and solids. (See the excellent reviews of this aspect of stopping power given by Geiger (1927) and Taylor (1952).) We are concerned with the stopping power of compounds in two respects. First, some of the impurities found in the gases are compounded of more than one element; second, one of the primary gases studied in this research (nitrogen) occurs in a diatomic

---

<sup>1</sup> The relation between range and stopping power is easily seen to be

$$R(E_0) = \int_0^{E_0} \frac{dE}{-(dE/dx)} \quad . \quad (I-B-89)$$



state.

Theory hints that more appreciable effects might be forthcoming if the stopping medium is in a condensed state, because of the influence of the many adjacent atoms on the outer electron energy levels. Some early experiments seemed to indicate a consistent difference between the stopping of alpha particles by elemental solids and gases (Briggs, 1927; Geiger, 1927). These seeming differences were later shown to be due to experimental factors (Livingston and Bethe, 1937). Experimental data - not entirely in agreement among themselves - still accumulate however to indicate that special effects may be present in certain cases (Taylor, 1952).

Both theory and experiment have shown marked effects in condensed substances at relativistic velocities of incident particles, but we are not interested in that energy region.

Theoreticians have given special attention to stopping by metals. The outer electrons in metals are practically free and their behavior is radically different from those electrons bound to individual atoms. As early as 1933, von Weisacker (1933) derived a formula which strongly related stopping power to conductivity. His theory was shown by subsequent experiment (Gerritsen, 1946) to make incorrect predictions, and Kramers (1947) proved theoretically that special conduction effects were practically cancelled by polarization effects. A. Bohr (1948) and Pines (1952) published further estimates of small reductions in stopping power by free valence electrons for incident particles of moderate velocity. These corrective factors are not large, however, and for heavier elements wherein the proportion of conduction elec-



trons is small the corrections predicted are quite negligible. This is confirmed experimentally by Heller and Tendam (1951), who found that for  $Z \geq 13$  no consistent differences between stopping power of metals and semi-conductors are found except the expected variations with atomic number. (Note should be made that such results were obtained only for particle velocities in excess of the velocity of 1 Mev protons.) The only experimental confirmation of special effects due to conduction properties of metals is the work of Madsen and Venkateswarlu (1948a) on stopping by beryllium for protons in the energy region from 500 to 1500 kev. The effect is expressed as an abnormally large value of  $I_{av}$  for beryllium to be used in the stopping power equation.

A. Bohr further indicated possible polarization effects may affect stopping power for condensed media even when non-conducting. Halpern and Hall (1948) also suggested the possibility that the more loosely bound electrons in condensed media may have different oscillator frequencies associated with them than they would have in the gaseous state. The special effects predicted are still small except in those cases where the outer electrons constitute a large proportion of all electrons effective in stopping.

## 7. Capture and Loss of Electrons.

In 1922, Henderson (1922b) observed that a beam of alpha particles contains a portion of singly charged particles, which portion increases with decreasing beam velocity. Since that time experiment and theory have confirmed that for all charged particles there is a pronounced tendency at low velocities for the particle to change its charge by





capture and loss of electrons. It is desirable to consider the phenomenon briefly in respect to stopping power of protons, since the stopping power theory presented above depends on the retention of positive charge by the proton.

Theory (Bohr, 1948) has given an approximate answer to the cross-section for capture of an electron by a proton, giving neutral hydrogen; and also a formula is provided for the cross-section for loss of this electron by the neutral hydrogen in flight. A proton undergoes in its passage through matter a succession of neutralizing and re-ionizing events, so that the proportion of its flight which occurs in the charged state may be obtained by taking the ratio of cross-sections.

Let  $y$  = the proportion of flight as neutral hydrogen;

$$y = \frac{\sigma_c}{\sigma_c + \sigma_1} \quad , \quad (I-B-90)$$

where

$\sigma_c$  = the electron capture cross-section ;

$\sigma_1$  = the electron loss cross-section .

If  $\sigma_1 \gg \sigma_c$  , then

$$y \approx \sigma_c / \sigma_1 \quad . \quad (I-B-91)$$

According to Bohr (1948) ,

$$\sigma_c = 4 \pi a_0^2 z^5 Z^{1/3} (v_0/v)^6 ; \quad (I-B-92)$$

$$\sigma_1 = \pi a_0^2 z^{-1} Z^{2/3} (v_0/v) \quad . \quad (I-B-93)$$

Since  $z$  equals unity,

$$y = 4 Z^{-1/3} (v_0/v)^5 \quad . \quad (I-B-94)$$

Now in our experimental work the lowest value of  $v$  is  $0.81 \times 10^9$  cm/sec (corresponding to an energy of 340 kev), the lowest value of  $Z$





is 7, and the value of  $v_0$  is  $0.219 \times 10^9$  cm/sec, so that  $y_{\max}$  equals 0.0031. Thus  $y$  is so low and decreases so rapidly as particle velocity increases that we may ignore entirely the possibility of electron capture.

A confirmatory note should be added. T. Hall (see Warshaw, 1949) has found that experimental results are in substantial agreement with Bohr's theory used above.

### B. Straggling in Stopping Power.

Bohr's equation for straggling in stopping power is given by substituting equation (I-B-25) into equation (I-B-23):

$$\frac{d}{dx}(\Omega^2) = 4\pi z^2 e^4 N Z. \quad (\text{I-B-95})$$

This equation is valid for fast incident particles. For slower particles, such that some atomic electrons are no longer slow compared to the particle velocity, Bohr returns to the Thomas-Fermi model and uses only those electrons slower than  $2v$ . That is,  $Z$  is replaced by  $Z'$ , where

$$Z' = Z^{1/3} (2v/v_0), \quad (\text{I-B-26})$$

as determined from equation (I-B-72).

Livingston and Bethe (1937) outline an approach to this problem which parallels the analysis of Bohr, previously given, in much the same way that Bethe's derivation of stopping power formula is analogous to Bohr's classical approach. They obtain:

$$\frac{d}{dx}(\Omega^2) = 4\pi z^2 e^4 N \left[ Z' + \sum_n \kappa_n \frac{I'_n Z_n}{m v^2} \ln \frac{2 m v^2}{I'_n} \right], \quad (\text{I-B-97})$$

where  $Z'$  is defined as in equation (I-B-71);  $\kappa_n$  is a numerical



factor usually equal to about  $4/3$  ;  $Z_n$  is the number of electrons in the  $n^{\text{th}}$  shell; and  $I_n'$  is the average excitation energy of the  $n^{\text{th}}$  shell, as usual.

This formula is somewhat difficult to use, as the values of  $I_n'$  can only be estimated. Furthermore the value of  $K_n$  given is only approximate and its true value is difficult to determine.

The extra factor in the bracket is the essential correction to Bohr's formula, and actually seems to be not so much a true quantum correction, as a term to take into account the motion of the orbital electrons. (The factor  $I_n'$  in the numerator is actually only an approximation for the kinetic energy of the electron.) Bohr's theory, it must be remembered, assumes that the electrons are motionless before collision. Averaged over all particle-electron collisions, this is approximately true, so that the stopping power relation is not affected by such an assumption; but energy transfer variations in individual collision cases are enlarged because of this electron motion, so that the straggling is increased.

### C. Review of Existing Experimental Data.

#### 1. Stopping Power.

To review all experimental data which has ever been published on stopping power would be very tedious and quite unnecessary. At the opposite extreme, to list available experimental results only if they cover precisely the same set of conditions and materials which we are studying would be rather simple - there is very little to date.

It is profitable to take a middle course - to list not only that data which may duplicate our own, but also to list data in either one



of the following categories:

(a) stopping power for protons of the materials we are studying in energy regions to either side of the regions we are concerned with (400 - 1100 kev);

(b) stopping power for protons of other elements, in the energy region which coincides with ours.

In this way we may synthesize our results with others into the overall stopping power scheme.

Table II.

Experimentally Determined Values of  
Average Excitation Energy ( $I_{av}$ ).

Element	Z	Z' (if used)	$I_{av}$ (ev)	Particle and velocity or energy	Reference
$\frac{1}{2}N_2$	7		81	*	Mano, 1934
Ne	10		132	*	" "
A	18		195	*	" "
Ni	28		325	*	" "
Cu	29		320	*	" "
			279	300 Mev prot.	Bakker & Segré, 1951
			307	240 " "	Mather & Segré, 1951
			375	70 " "	Bloembergen & van
			365	100 " "	Heerden, 1951
		27.4	293	2 " "	Liv. & Bethe, 1937
Kr	36		390	*	Mano, 1934
Xe	54		530	*	" "

\* Alpha particles from natural radioactive elements (6 - 11 Mev), which corresponds to protons having velocities equivalent to 1.5 - 2.8 Mev of energy.





Let us first list all data available for energies higher than the range studied herein. This is best summarized by indicating the value of  $I_{av}$  found necessary to make Bethe's formula (equation I-B-69) check with experiment (see Table II, above).

On the low energy side of the energy spectrum, some data is available relating to the materials in which we are interested. A certain amount of work has been done by the "Kevatron" group at Chicago. Wilcox (1948) published results at low proton energies for aluminum and gold, but his results have been superseded by better data. Warshaw (1949) has published data for protons of energies from 40 to 360 kev for aluminum, copper, silver, and gold. He extrapolated his curves up to several Mev, where the theoretical formula of Bethe would be expected to be valid.

Work for gases has been reported recently both from the University of Chicago and the California Institute of Technology. From the latter institution Dunbar, et al. (1952) have reported on stopping power of some gases for protons of energies from 25 to 600 kev. Additional data has been recently provided by this group of workers<sup>1</sup> which means that most of the simple gases, including all those we are reporting on herein, have been covered for protons up to 600 kev of energy. Their curves are reproduced in Figure 13, to show the match with our data. Weyl (1953) at Chicago has provided data for stopping power of various light gases, including argon, for protons of energies from 50 to 500 kev. His data is consistent with that from

---

<sup>1</sup> Up-to-date information from the Cal.Tech. laboratory has been kindly transmitted by Prof. W. Whaling (personal communication). This is expected to be published later under authorship of Dunbar et al.



the California Institute of Technology and is therefore not plotted.<sup>1</sup>

Stopping data providing a complete coverage of the particular region of interest to us has been provided by only a few workers. Madsen and Venkateswarlu (1948a), being the first to employ the experimental technique we employ with the Van de Graaff generator, published results for beryllium stopping of protons with energies from 500 to 1500 kev. Using Bethe's formula, and including the correction term  $C_K$ , they found the data to be consistent with a value of  $I_{av}$  of  $64 \pm 5$  ev.

Using the same technique Huus and Madsen (1949) obtained a little data in this region for gold. Madsen has also recently submitted some data for copper.<sup>2</sup> His results for the latter element are not consistent with other experimental work, which is possibly due to difficulties in obtaining foils of consistent thickness.

The greatest amount of work in this region is provided by Kahn (1953), who has obtained curves for protons of energies from 400 kev to 2.0 Mev for beryllium, aluminum, copper, and gold. Figure 12 contains his results, which agrees with the earlier data on beryllium and gold mentioned above.

## 2. Straggling.

Very little previous experimental work has been published on straggling in stopping power in the energy region of interest to us. The reason is easily seen. Even the techniques for stopping power

---

<sup>1</sup> Detailed information on the work at Chicago, as well as other information available to him, has been kindly provided by Prof. S. K. Allison (personal communication).

<sup>2</sup> We acknowledge appreciatively a personal communication from Dr. Madsen, giving detailed information on all his work to date.



determination in this energy region are somewhat crude, and experimental variations sometimes wide. It can be appreciated that the theoretically valid deviations in stopping power can be easily masked by the same factors which cause inaccuracies in stopping power experiments.

The only experimental work published on straggling is by Madsen and Venkateswarlu (1948b), who were able to analyze the results of their stopping power data (1948a) to give straggling in addition to mean stopping power. Results are for beryllium, with proton energies from 400 to 1200 kev. The results vary widely, but seem on the average to be in reasonable agreement with the theory of Bohr (1948), given herein as equation (I-B-95). The value of  $\Omega/(\Delta x)^{\frac{1}{2}}$  was found to average 8.99 kev-cm/mg <sup>$\frac{1}{2}$</sup> , with individual readings ranging from 6.9 to 10.4 . In these units, the theoretical prediction is 8.3 .





## II. Basic Experimental Technique.

### A. Basic Principle.

If a beam of monoenergetic protons impinges upon a target of a certain material, a nuclear reaction may be induced which produces quanta or particles as a result. The investigation of proton-gamma reactions requires the determination of the number of gamma photons produced (and detected) per designated number of protons incident on the target material. For a given target, such a figure, which we may call the yield, is a function of the energy of the incident proton. By varying the proton energy in small increments and measuring the yield at each step, one can accumulate data on yield versus proton energy. For many light isotopes as targets, a plot of these results in the Van de Graaff energy region (a few hundred kev up to several Mev) gives a type of curve which is low and slowly rising, on which is superposed a number of "resonance peaks" whose height, width, and position in the energy spectrum are characteristic of the isotope(s) involved.

Now if a given thickness of matter is interposed in the path of the beam after it leaves the accelerator but before it hits the target, the protons are slowed by amounts, the average of which is determined by the average energy loss of the protons in the interposed material. Then to duplicate a "peak" in a yield-versus-proton energy experiment, the protons obviously must be given an initial energy greater than that characteristic of the target material by just the amount of energy loss in the interposed material.





If, in such an experiment, one measures proton energy before the beam strikes the interposed stopping material, a yield-energy curve may be constructed, called hereafter a shifted or displaced spectrum. The peak-to-peak correspondence with the undeviated spectrum is easily established by inspection.

The undeviated peak energy values may be determined by experiments without stopping media interposed or, if already well established, they may be determined from the literature. One then can subtract the energy values for the corresponding peaks in the deviated and undeviated spectrum to obtain energy loss  $\Delta E$  in the material. Dividing by the path length of the protons in the medium gives  $\Delta E/\Delta x$ . The theorem of mean value indicates that this value, which depends on the energy of the beam as it enters and as it leaves the medium, is the same as the value of  $dE/dx$  for some value of  $E$  between the incident and exit beam energy. This mean value of  $E$  is not difficult to determine when  $\Delta E$  is small compared to  $E$ .

It is found that the peaks in the displaced spectrum are broader than those in the basic, unshifted spectrum. This is caused by individual proton variation, or straggling, in stopping power. That is, when deviations in energy loss are possible for individual protons passing through matter, then beams of average energy appreciably different from the proper displaced peak value will still contain protons of the proper energy to excite the target atoms in the resonance region.

The technique briefly outlined above was first used by Madsen and Venkateswarlu (1948a,b). A more detailed analysis is now presented,



showing the corrections necessary to get a true answer from experimental results.

### B. Detailed Analysis.

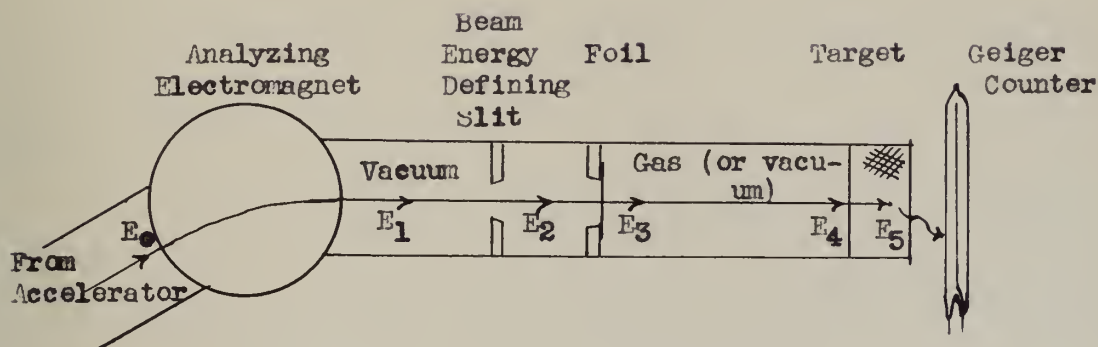


Figure 3

Figure 3 is a schematic diagram of the apparatus for measurement of stopping power, with the voltages specified for a proton from the moment it leaves the accelerator section until it enters the target nucleus to release a photon to be counted. In this figure,

- $E_0$  = energy of a photon-producing proton as it leaves the accelerator;
- $E_1$  = energy of the photon-producing proton after passing through the analyzing field;
- $E_2$  = energy of the photon-producing proton after passing the defining slit and as it enters the foil;
- $E_3$  = energy of the photon-producing proton as it leaves the foil and enters the gas space;
- $E_4$  = energy of the photon-producing proton as it leaves the gas space and enters the target material;



$E_5$  = energy of the photon-producing proton as it enters the nucleus to produce the reaction.

We note that if the gas chamber is evacuated,  $E_3 = E_4$ .

In order to find the energy  $E_0$  of a gamma-producing proton as it comes from the accelerator, it is possible to start with  $E_5$  and successively add to it the energy losses suffered in all parts of the system between  $E_5$  and  $E_0$ . Thus

$$E_0 = E_5 + |\Delta E_T| + |\Delta E_G| + |\Delta E_F| + |\Delta E_S| + |\Delta E_M|, \quad (\text{II-B-1})$$

where

$\Delta E_T$  = the energy change of the proton in passing through a certain amount of the target material;

$\Delta E_G$  = the energy change of the proton in passing through the gas;

$\Delta E_F$  = the energy change of the proton in passing through the foil;

$\Delta E_S$  = the energy change of the proton in passing through the defining slit, or as a result of the regulatory action of the defining slit;

$\Delta E_M$  = the energy change of the proton in passing through the magnet, or as a result of any miscellaneous effect in the system.

What we are particularly concerned with, however, are the relationships among the distributions in energy of the probability of detecting a gamma photon for each proton accepted from the accelerator. These distribution functions depend not only upon proton energy, but also upon the position in the apparatus where the energy is specified,





so that we conclude that there is a probability distribution for each of the variables in equation (II-B-1).

The statistical variables of interest are the mean and the variance (square of the standard deviation) of the distributions. For the mean value:

$$\overline{E}_0 = \overline{E}_5 + |\overline{\Delta E}_T| + |\overline{\Delta E}_G| + |\overline{\Delta E}_F| + |\overline{\Delta E}_S| + |\overline{\Delta E}_M| ; \quad (\text{II-B-2})$$

and for the variances, the following formula is valid (Hoel, 1947) :

$$\Omega_0^2 = \Omega_5^2 + \Omega_T^2 + \Omega_G^2 + \Omega_S^2 + \Omega_F^2 + \Omega_M^2 , \quad (\text{II-B-3})$$

where the subscripts refer to the same portion of the apparatus as in equation (II-B-1). The precise values of some of these statistical variables will be determined later, but others can be simplified in such an obvious way that we may conveniently do so at this point.

We assume that the resonance peaks are so widely separated that they do not interfere with one another, and thus the statistical analysis may be carried out on each peak alone. Furthermore, the frequency distribution is considered sufficiently symmetrical that the maximum value can be taken as the mean value without appreciable error. To simplify the notation let us assume, unless otherwise stated, that when we refer to energy henceforth, we mean the mean value of the energy of the whole proton beam, without the necessity of placement of a bar over the symbol.

$E_0$  becomes the average beam energy from the accelerator giving the resonance maximum.  $E_5$  is the value of proton energy as it enters the target nucleus to give the resonance maximum, and we will therefore re-designate it as  $E_{nat}$ .  $\Delta E_T$  is the average value of energy loss of



protons in the target material, and is therefore  $\frac{1}{2}T$ , where  $T$  is the target thickness expressed as the average energy loss for protons passing through the target. If we assume that the effect on individual protons by the slit and the magnet are as likely to be in a positive as a negative direction (see discussion below) then  $\Delta E_S$  and  $\Delta E_M$  are zero.

$\Omega_0$  is the standard deviation of the yield curve about the resonance maximum point, and is determined from the experimental data; whereas  $\Omega_5$  is the standard deviation of the natural, or theoretical, curve and will be called  $\Omega_{nat}$  henceforth.  $\Omega_G$  and  $\Omega_F$  measure the straggling effect in energy loss in the gas and foil respectively. The deviations caused by the slit and magnet may be explained somewhat:

- (a) The slit is of finite width, and the voltage regulation system of the Van de Graaff generator (Smith, 1952) is such as to keep the proton beam between the sides of the slit. Then the maximum swing in beam voltage is on the order of the amount required to swing the beam from one side of the slit to the other. If the value of average beam voltage is measured with the beam centered in the slit, the deviations are equally likely to be plus or minus.
- (b) We may expect other miscellaneous variations of a presumed random nature: inhomogeneities in the magnetic field, variations in the vertical and horizontal position of the principal axis of the focused beam, slight variations in the electromagnetic field current, and miscellaneous variations of a human or instrumental nature. These are conveniently grouped together with the subscript  $M$ .

Using the modifications given above we can now re-write equations



(II-B-2) and (II-B-3). Let us first do so for an experimental curve without any stopping media at all:

$$E_o = E_{nat} + \frac{1}{2}T ; \quad (II-B-4)$$

$$\text{and } \Omega_o^2 = \Omega_{nat}^2 + \Omega_T^2 + \Omega_S^2 + \Omega_M^2 . \quad (II-B-5)$$

Then we can write the equations valid for experimental curves where stopping media are interposed in the beam. In doing so those values which are the same for the corresponding peak without media interposed are left unprimed, values which are shifted are primed:

$$E'_o = E_{nat} + \frac{1}{2}T + |\Delta E_G| + |\Delta E_F| ; \quad (II-B-6)$$

$$\text{and } \Omega_o'^2 = \Omega_{nat}^2 + \Omega_T^2 + \Omega^2 + \Omega_S'^2 + \Omega_M'^2 \quad (II-B-7)$$

In the latter formula,  $\Omega^2$  signifies the sum of the variations in energy loss through both foil and gas. In practice it will denote only the variation for the foil, inasmuch as we have obtained no results in cases where both gas and foil are used.

Subtracting equations (II-B-4) from (II-B-6), and (II-B-5) from (II-B-7) gives the basic equations which permit determination of stopping power and straggling from experimental results for the resonance peaks:

Without gas,

$$\Delta E_F = E'_o - E_o ; \quad (II-B-8)$$

with gas and foil,

$$\Delta E_G = E'_o - E_o - \Delta E_F ; \quad (II-B-9)$$

and without gas,

$$\Omega^2 = (\Omega_o'^2 - \Omega_o^2) - (\Omega_S'^2 - \Omega_S^2) - (\Omega_M'^2 - \Omega_M^2) . \quad (II-B-10)$$

That the primed and unprimed values of  $\Omega_S$  and  $\Omega_M$  do not always cancel may be understood from the discussion in sections III.F.3 and 4.





### III. Experimental Details and Preliminary Calculations.

The principle of operation of the Van de Graaff type of generator-accelerator is too well known to require any explanation here. A description of the particular one at the Ohio State University and its associated auxiliary equipment may be found elsewhere (Grove, 1947; Cooper, 1949; Grove, 1950; Taylor, 1952; Smith, 1952). Certain improvements and modifications were required in order to fit the machine to the purpose of the present research. They will be described in the sections immediately following.

#### A. Target-Faraday Cage Assembly.

In order that the protons may be collected and counted, the target on which the protons impinge is mounted on an assembly called a "Faraday cage." This is insulated electrically from the rest of the accelerator, so that the collected positive charge can drain to ground through an "integrator" which measures this charge.

It was necessary to provide a mechanism for introducing a foil into the proton beam; also a gas-holding chamber was required with a thin foil-covered window so that protons could be introduced to traverse the gas. For this purpose a type of valve box<sup>1</sup> was modified to perform all the functions of target holder, Faraday cage, gas holder, and foil retainer. This assembly is depicted in Figure 4, and is almost self-explanatory.

The system may operate with the valve down for basic calibration runs. If stopping power of a foil is to be investigated, the foil

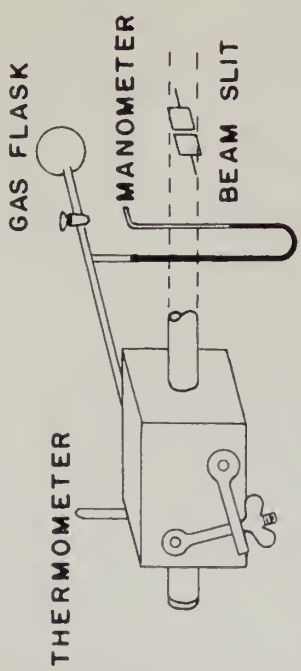
---

<sup>1</sup> This box was originally made after a type used on the University of Wisconsin Van de Graaff generator ~~and~~ the pattern for which was generously provided by Prof. R. G. Herb .

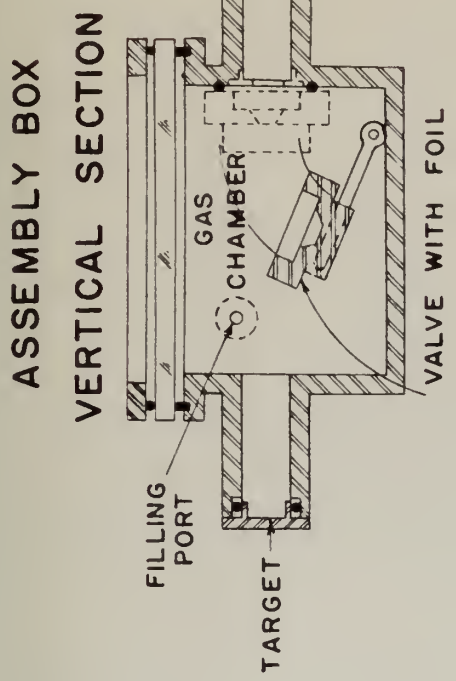




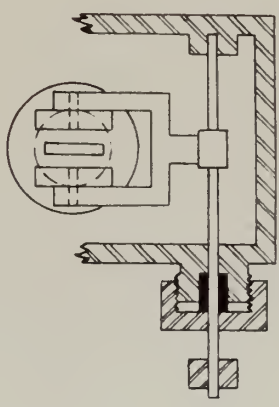
# TARGET, FOIL, AND GAS FILL- ING ASSEMBLY



SKETCH OF COMPLETE  
ASSEMBLY



ASSEMBLY BOX  
VERTICAL SECTION



FOIL COVERED VALVE  
FRONT VIEW

Fig. 4



is attached (with the use of clear glyptal) across the slit in the valve, which is then raised into a vertical position. In this position the system is aligned so that protons passing first through the beam defining slit strike the foil at approximately the middle of the valve slit.

If stopping power of a gas is required, the foil across the valve slit is made gas-tight by painting with glyptal around all the foil edges. The system is placed on the vacuum system and the valve is raised and clamped against the valve seat to gas-tightness. (The valve may be manipulated from the outside by a shaft through a Wilson seal.) Gas may then be introduced to the desired pressure, and the experiment performed. This technique interposes both a foil and the gas in the path of the beam at the same time, so that in determining the stopping power of the gas the energy loss in the foil must be known and allowed for.

#### B. Preliminary Measurements on Foils.

The foils used were of copper and nickel, of nominal thickness between 0.03 mil and 0.1 mil. This amounts to a surface density of from 0.6 to 2 mg/cm<sup>2</sup>. This is somewhat thicker than is usually used for stopping power experiments; but in selecting such foils the greatest importance was placed on consistency in thickness - the lack of which has often plagued experimenters who used thinner foils. Furthermore certain fixed errors, such as that caused by carbon accumulation on the foil, are less percentagewise when thicker foils are used. (See Section IV.A, below.)

The foils were obtained from the Chromium Corporation of



America, Waterbury, Conn., who prepared them by electrolysis.<sup>1</sup>

They were guaranteed by the company to have an average thickness within 10% of the nominal thickness, and to have a spot-to-spot variation in thickness of less than 5%. The foils used were judiciously selected to obtain the best consistency possible; and a technique was developed to check thickness variations to within about 1%.

This technique depends on the range-straggling of alpha particles. The apparatus is quite simple and is illustrated in Figure 5. The principle of operation is explained by following the procedure outlined below.

With the foil removed, data is taken of counting rate as a function of height of the movable platform from the fixed surface. This gives a curve similar to curve (a), Figure 6. The steepness of rise of the curve is determined by the range-straggling of the alpha particles and is important in determination of the sensitivity of measurement of the relative foil thickness. Now if the experiment is repeated with the foil interposed over the 1/32" hole, a curve of similar shape, but displaced by amount  $A$ , is able to be determined. This distance  $A$  is the air-equivalent of the foil for alpha particle stopping.

If we set the apparatus at height  $H$ , to give an operating point on a reasonably linear part of the steep portion of the curve, we may then take readings with various portions of the foil positioned over the hole. If the counting rate changes by amount  $\Delta c$ , then this

---

<sup>1</sup> Information on these foils was kindly provided by Mr. M. M. Sternfels, Chemical Engineer for the Chromium Corp.





# APPARATUS FOR CHECKING THICKNESS VARIATION IN THIN FOILS

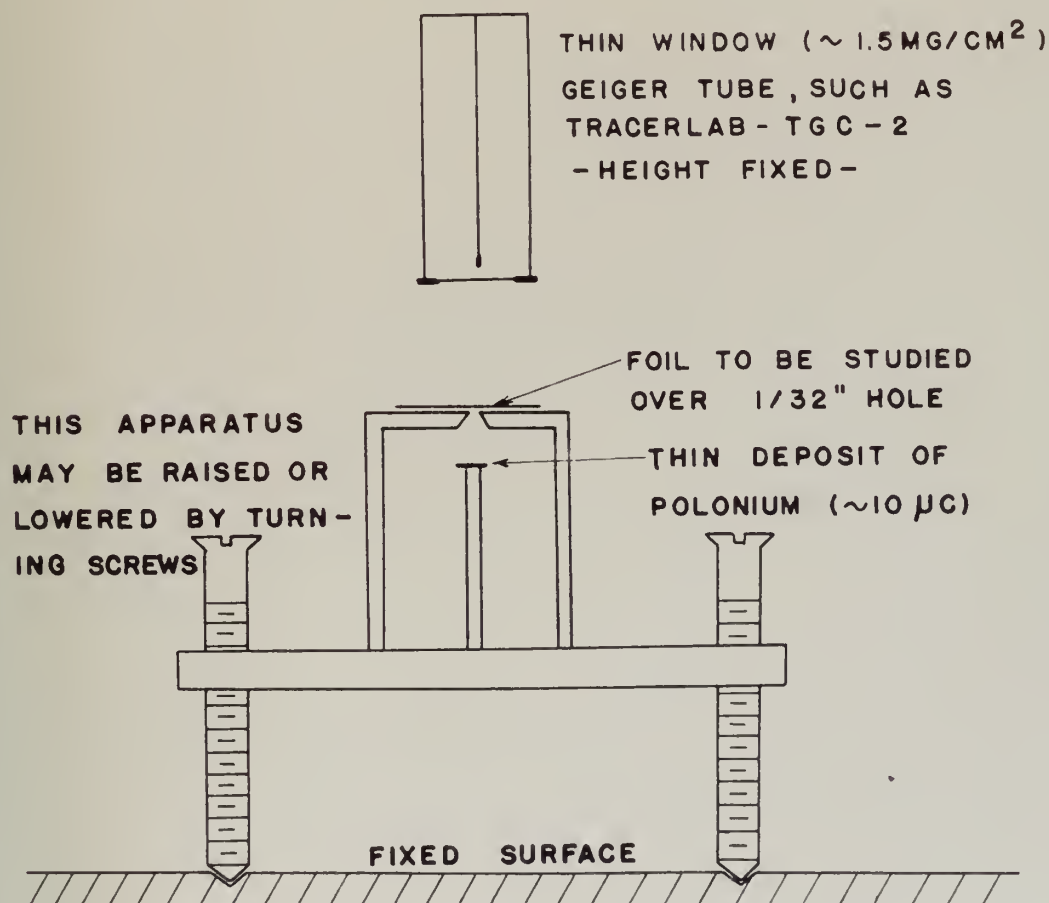


Fig. 5



# CALIBRATION CURVES

FOR CHECKING VARIATIONS IN  
FOIL THICKNESS

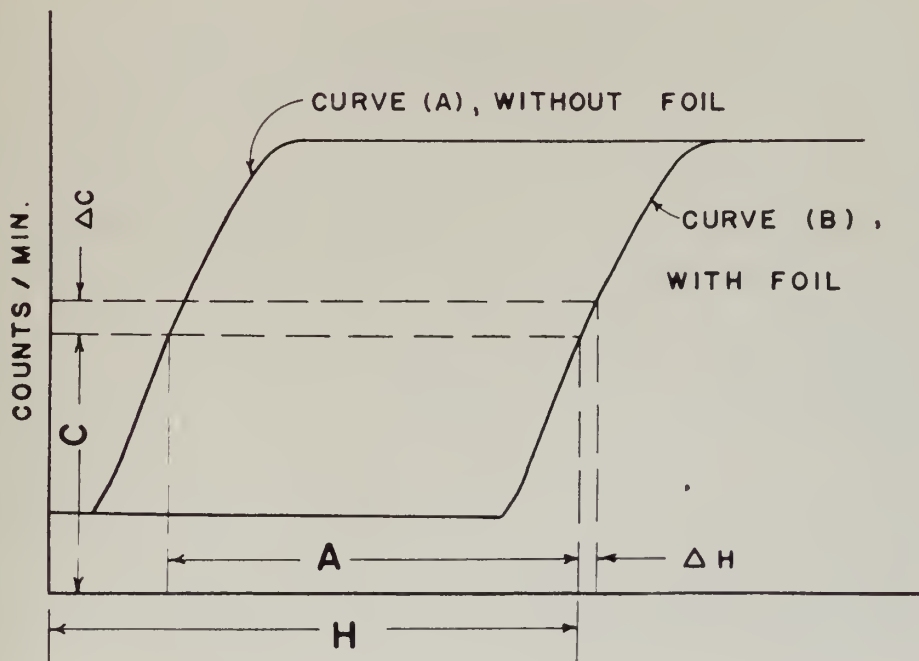


FIG. 6



indicated a change in air-equivalent of  $\Delta h$  . The value of  $\Delta h/A$  indicates the fractional variation in thickness from the original spot to the new spot studied. If a large number of spots on the foil are studied thus, we can determine the mean value of  $H$  by knowing the overall average counting rate. The statistical variation in thickness is easily computed as the average root-mean-square of  $\Delta h/A$  . Such a variation corresponds to a counting variation (fractional) of  $\Delta c/C$  . To translate a counting percentage deviation to a thickness percentage deviation, we obviously have to multiply the former by

$$\text{Factor} = \frac{C}{A} \cdot \frac{\Delta h}{\Delta c} = \frac{C}{A \cdot (\text{slope curve at opert'g pt.})} . \text{ (III-A-1)}$$

If a finite number of counts are taken at each point, the counting rate is subject to a statistical variation due to the randomness of the radioactive emission process. Such statistical variation must be subtracted from the total variation to give the most probable variation due to thickness variations in the foil. Furthermore the statistical variation from the radioactive emission process places a practical limit on the accuracy of this technique.

Table IV (a) gives a set of sample data taken on one of the foils; and Table IV (b) summarizes the results of measurement on all the foils.

We conclude from the data that the standard deviation of the thickness measured over spots  $1/32"$  in diameter is about the order of magnitude of the precision of the measurements. We estimate that we can cite for all the foils a standard deviation of about 1.4% as measure of the spot-to-spot variation from the mean. Thus, if we



Table IV.

Spot-to-Spot Variations in Foil Thicknesses

Spot Size : 1/32 "

Part (a): Sample Data - 0.1 mil Copper Foil.

Spot No.	Counts	Sec.	Cts./min.	$\Delta c$	$(\Delta c)^2$
1	4096	828.5	297	- 1.4	1.96
2	"	770.3	319	+20.6	424.36
3	"	800.0	307	+ 8.6	73.96
4	"	831.0	296	- 2.4	5.76
5	"	844.0	291	- 7.4	54.76
6	"	827.0	297	- 1.4	1.96
7	"	842.0	292	- 6.4	40.96
8	"	853.0	288	-10.4	108.16

Av. = 298.4                      711.88

Standard Deviation (small sample theory) =  $\sqrt{\frac{711.88}{7}}$

= 10.1 , or 3.4%

Standard Deviation of Radioact. Decay Rate =  $\sqrt{\frac{1}{4096}}$

= 1.56%

C = 298.4 Cts./min.

A = 8.0 turns

Slope = 100 Cts./turn

Conversion Factor =  $\frac{298.4}{8 \times 100}$

= 0.37

Part (b): Summary of Results.

Foil	No. of Spots Measured	Total Std. Dev.	Std. Dev. of Radioac.	Net Std. Dev. in Count.Rate	Conversion Factor	Std. Dev. of Thickn.
.05mil Ni-1	9	5.8%	2.2%	5.4%	.54	2.9%
"	11	3.7	2.2	3.0	.50	1.5
"	13	3.5	2.2	2.7	.53	1.4
.05mil Ni-2	10	3.8	2.2	3.0	.48	1.4
.04mil Ni	5	3.5	2.2	2.7	.67	1.8
"	9	2.9	2.2	1.9	.71	1.4
.03mil Ni	8	2.6	2.2	1.4	.83	1.2
.05mil Cu	5	1.3	1.7	0	-	small
.1 mil Cu	8	3.4	1.6	3.0	.37	1.1





use average thickness for our computations, while the proton beam passes through the foil at a spot selected at random, a probable error in stopping power results of about 1% exists because of thickness variation alone.

We can draw the above conclusion because the  $1/32$ " spot size used is about the same as the diameter of the intense "core" of the proton beam from the Van de Graaff generator when it is well focused. We cannot as easily make the same conclusions with regard to straggling measurements, since variations of thickness within a single  $1/32$ " spot will increase the straggling without affecting average energy loss.

It is possible to make a hypothesis that the variations using a  $1/32$ " spot are due to more radical variations within the spot of this size which are not completely averaged out. This hypothesis is opposed to the hypothesis that the variations are broad and slowly changing in comparison to the  $1/32$ " distance taken as a unit. These were tested by making a series of runs in one of the nickel foils with successive spots studied being contiguous and along a straight line. The results were quite consistent with the hypothesis that the variations in foil thickness were quite gradual, and highly inconsistent with the hypothesis of more rapid, stronger variations.

This still does not obviate the possibility that very finely spaced variations may exist which average out almost completely over a  $1/32$ " spot. The possible existence of such variations therefore for spot checks of size  $10^{-6}$  to  $10^{-2}$  centimeters must still be admitted. Such variations may cause errors in the experimental results on



stopping power straggling and are discussed in the section concerned with such errors (Section IV.D.2).

The average thicknesses of the foils, measured in units of  $\text{mg}/\text{cm}^2$ , were determined by weighing them and measuring their linear dimensions. The weighing was accomplished by microbalance in the Microanalytical Laboratory, Chemistry Department, Ohio State University, through courtesy of Professor W. M. MacNevin. The measurement of the linear dimensions was accomplished under a low power microscope, and checked by steel rule and reading glass. The foils were rectangular in shape, as checked by assuring oneself of the equality of the diagonal dimensions, and therefore the area was taken to be simply the product of the two linear dimensions. Results of the foil measurements are given in Table V.

Table V.

Determination of Foil Thicknesses

Foil	Area ( $\text{cm}^2$ )	Weight (mg)	Thickness ( $\text{mg}/\text{cm}^2$ )
.05 mil Ni-1	$7.05 \pm .03$ (.43%)	$8.10 \pm .01$ (.124%)	$1.150 \pm (.45\%)$
.05 mil Ni-2	$3.28 \pm .02$ (.61%)	$3.86 \pm .01$ (.26%)	$1.175 \pm (.65\%)$
.04 mil Ni	$7.40 \pm .03$ (.40%)	$7.23 \pm .01$ (.138%)	$0.977 \pm (.45\%)$
.03 mil Ni	$7.40 \pm .03$ (.40%)	$4.73 \pm .01$ (.21%)	$0.640 \pm (.45\%)$
.05 mil Cu	$7.495 \pm .02$ (.27%)	$8.65 \pm .01$ (.116%)	$1.155 \pm (.35\%)$
.1 mil Cu	$7.42 \pm .03$ (.40%)	$16.30 \pm .01$ (.061%)	$2.20 \pm (.45\%)$

We may conclude that the probable errors inherent in the use of the thicknesses given are the statistical sum of the 1% due to non-uniformity and 0.45% due to error in measurement of average thickness. This gives a total probable error of about 1.1% in estimating average



proton path length through the foils by the above values of foil thickness.

### C. Design of Magnet Current Regulator.

It was found upon first operating the Van de Graaff generator that the current provided to the analyzing electromagnet was not sufficiently stable for the close energy resolution desired. It was found that for a given setting of the controls, the magnet current tended to swing to either side by a variable amount, giving a deviation from the mean of as much as 0.1% .

This amount can easily be translated to energy variation. If we accept a rough formula (see Section III.F, below):

$$E = (4/3) I^2 \quad , \quad \text{(III-C-1)}$$

it is easily shown that a deviation of 0.1% in the current,  $I$ , is equivalent to a deviation of 0.2% in the beam energy,  $E$ . Thus at beam voltage of 1 Mev, it was impossible to prevent the voltage from wandering as much as 2 kev to either side of the mean.

It is true that the operator has manual controls for setting the magnet current; but the variation was so erratic and sudden at times that the operator could not anticipate and counteract the more rapid swings. The disadvantages inherent in this variation are manifest:

(a) They make it difficult to maintain and read accurately the mean setting of the electromagnet current, thus preventing accurate calibration of the beam energy in terms of magnet current.

(b) Since beam position at the slit system (see Figure 3), located after the magnetic analyzer, is used to stabilize the accelerator voltage (Smith, 1952), magnetic current variations are reflected





in beam energy variations. The beam stabilizer, that is, can never prevent beam energy variations corresponding to magnet current variations.

In terms of the variables we are trying to determine, this variation would mean an uncertainty in peak position of about 1 kev added to all other uncertainties and would add greatly to the factors constituting the  $\Omega_M$  discussed in Section II.B above. It was found expedient therefore to provide some measure of regulation of the magnet current.

A brief discussion of how the magnet current is provided would be appropriate. A motor-generator set puts out a d.c. supply of maximum rated values 360 volts and 4.75 amperes. The output voltage is controlled by varying the d.c. voltage to a separately excited field winding on the generator side. The d.c. voltage for the field is obtained by full-wave rectification of a variac-controlled alternating voltage, obtained in turn from a Sola-regulated 115-volt a.c. power supply. Thus the magnet current can be varied by changing the setting of the variac supplying the field current. This actually varies the voltage from the d.c. generator; a fine control of current is obtained by means of a variable rheostat in series with the magnet coils.

A capacitance of 250  $\mu$ fd. is connected in parallel with the magnet. Since the magnet coils have a high inductive reactance (inductance estimated to be about 30 henries), fluctuations of frequency much faster than one cycle per second pass through the condensers rather than the coil. Aside from this, and the Sola



regulation mentioned above, no other regulation was in the circuit prior to the time the regulator herein described was installed.

Several possible schemes for regulation of current itself were considered and rejected. It was decided that uncontrollable resistance changes in the magnet circuit (caused by temperature changes in the coils) were slow enough to be compensated for manually by the operator. Furthermore fine control of current by a variable resistor was desired. Thus, a voltage regulator was actually used for stabilizing the current. The d.c. generator voltage is affected not only by the field current, but also by the motor speed, which may possibly experience small variations. It was decided therefore to put the regulator directly in the magnet circuit between the generator and the load, which consists of magnet coils and the control rheostats.

It was necessary under the circumstances to keep the system quite simple, since any complex electronic apparatus has a very low power efficiency and the output of the d.c. generator is rather limited. The very simplest type of regulator of the "transconductance" type is used (Hunt and Hickman, 1939).

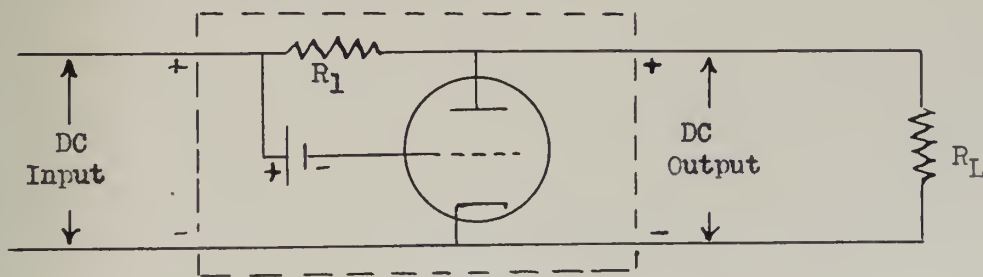


Figure 7

Figure 7 shows in schematic fashion the regulator in principle. The triode is in parallel with the load, and the current through it adds to the magnet current to give the total current required from



the d.c. source. The amount of tube current depends on the output voltage and the grid voltage. If a small positive variation occurs in the input voltage, more current flows from the source. This rise also causes a rise in grid voltage, which produces a greater current drain through the tube. With proper choice of the circuit parameters, the current increase through the tube matches the total current rise from the source - causing the same amount of current through the load. Or, from another point of view, a current rise through the tube creates additional voltage drop across  $R_1$ , which is designed to just counteract the original voltage rise at the input side - thus giving the same output voltage.

A rigorous proof of the above statements, indicating how the circuit parameters are selected is given in the appendix. Also in the appendix is a circuit diagram of the complete magnet current control and regulating system, as it exists at the present time, with further explanatory comments on its operation.

Results with the regulator have been excellent. With proper attention on the part of the operator to compensate for slow resistance changes and keep the regulator controls properly adjusted, the current variations are cut down to about one-tenth their value without regulation. This means a voltage variation of the beam of about 100 - 200 ev, which is small compared to other variations and errors.

#### D. Technique for Taking and Correcting Yield-Energy Data.

With the chosen target in place and a vacuum on the whole system, the Van de Graaff generator is started and protons produced in





accordance with standard procedure. The magnet is then "cycled" twice by running the magnet current up to a relatively high value (about 3 amperes) and then back to zero. The subsequent data is taken with ever increasing magnet current, so that one stays consistently on a reproducible magnetization curve (magnetic flux versus magnet current), without any hysteresis effects.

As and if required, the stopping foil is inserted and clamped at this point in the procedure, and the desired amount of gas (which may be zero) is introduced into the holder (Figure 4.) .

With the magnet current set at the initial (lowest) value, the accelerator voltage is set so as to send the protons through the defining slits. The proton accumulated charge is counted by an "integrator" with a mechanical register and the gamma-rays detected by the usual Geiger counter-scaler apparatus. At each current setting the data taken includes: magnet current, total gamma-ray counts (usually set to a predetermined figure), time to collect these counts, total integrator count of accumulated proton charge. Arrangements are such that the proton integrator operates only while the Geiger counter-scaler is accepting and registering gamma-ray counts.

The gamma-ray counts must be corrected for "background". This background is a function of the generator-accelerator voltage, since x-rays from the generator provide a sizable proportion of said background. Experiments made without a target indicate that accumulated background can be estimated by dividing the time (seconds) for the prescribed number of total counts in a single run at a current setting by a factor, given in Table VI. These factors are valid only





Table VI.

Factors for Determination of Background

When Operating Van de Graaff Generator

- Type Tube: Technical Associates Beta Counting Tube TA-B1.
- Location: As close to the target as possible - separated from same by thickness of target holder, 1/8" of lead, and about three millimeters of air.
- Position: (One tube) - Side to target, with center line at mid-target height. (Two tubes in parallel) - One above the other, sides to target, with mean of positions of centerlines at mid-target height.
- Shielding: Tube(s) mounted within a two-inch thick lead box, with hole in same just large enough to permit ready insertion of target holder.

Analyzing Magnet Current (amp.)	Factor by Which to Divide Length of Run in Seconds to Get Background Counts	
	One Tube	Two Tubes in Parallel
.55	3.0	2.0
.60	2.8	2.0
.65	2.6	2.0
.70	2.4	2.0
.75	2.2	1.9
.80	2.0	1.7
.85	1.8	1.5
.90	1.5	1.4
.95	1.2	1.2



if the geometry, tube type, and other factors are reproducible; and these variables are indicated in the table.

The proton integrator count for a single run is obtained by subtracting the register values before and after the run. The values thus obtained also require correcting, as a certain amount of charge leakage occurs through paths other than that which actuates the register. By experimentally checking the integrator register counts per unit time against galvanometer readings of current from the Faraday cage to the integrator, it has been found that integrator readings must be increased by an amount corresponding to about 35 counts per minute of time for the run. Such counts, when corrected, thus provide a more constant ratio between the figure for total integrator counts and the actual number of protons striking the target.

The "yield", on an arbitrary scale, is the result of dividing the corrected gamma-ray counts by the corrected proton integrator count.

These data are taken at successively higher magnet current settings. The desirable current increments between successive readings for our experimental work was as follows: for sharp peaks, current increments of 0.5 ma. are necessary; for broader peaks, data every 1 ma. are sufficient.

If gas stopping is being studied during any sequence of individual runs, the manometer, thermometer (see Figure 4), and time of day are recorded just before gas introduction, just after gas introduction, just before the gas is finally removed, and just after the gas is removed. Readings at intervals between start and finish may



also be made if desired.

The yield can be plotted against magnet current, or if the analyzing current-proton energy relationship has been established (called "calibration" herein) the yield can be plotted versus proton energy to give a more proper spectrum. For our purposes only the first type of plot has been required, as it is possible to read the peak maximum values and the statistical measurements of width directly in terms of magnet current and then convert to the proton energy scale.

Table VII gives a sample set of data for a single peak, with yield computations. Figure 8(a) shows the plot of the resonance peak (unshifted) for this particular set of data; Figure 8(b) is a plot of the same peak, shifted by insertion of stopping material. The probable error of the position of each point is indicated by the size of the crosses. The error in horizontal direction is based on personal observation and judgment; the error in the vertical direction is determined from standard statistical deviations of the total number of gamma-ray counts ( $P.E. = 0.67 \sqrt{\text{No. of Counts}}$ ). In the latter case, the actual probable error is somewhat greater, but the largest errors come from counting statistical errors and give a rough basis for estimating the extent to which our smooth curve has to follow the experimental points.

#### E. Target Preparation.

The target materials used were either lithium fluoride or aluminum. The targets were formed by coating a blank tantalum disc with a thin coating of the target substance. The coating was





Table VII.

Sample Set of Data for Computation of Yield and Plotting of Peak

Peak Covered: 340.4 kev - F<sup>19</sup> .

Target Used: LiF-2

No Stopping Medium Interposed.

One Geiger Tube Used.

Magnet Current (amp)	Proton Int. Counts	Time (sec)	Correc. to Prot. Counts	Net Proton Counts	Gamma Counts	B'grnd. Corr.to Gam.Cts	Net Gamma Cts.	Yield
.4900	49	28.6	17	66	32	9	23	.3
10	82	45.0	26	108	64	14	50	.5
20	83	56.6	33	116	64	18	46	.4
30	59	34.0	20	79	64	11	53	.7
40	94	57.2	33	127	128	18	110	.9
50	84	46.8	27	111	128	15	113	1.0
60	80	43.4	25	105	256	14	242	2.3
70	69	41.8	24	93	256	13	243	2.6
80	61	37.7	22	83	512	12	500	6.0
90	62	44.0	26	88	1024	14	1010	11.5
.5000	43	32.0	19	62	1024	10	1014	16.4
10	71	38.4	22	93	2048	12	2036	21.9
20	64	37.4	22	86	2048	12	2036	23.7
30	105	60.0	35	140	4096	19	4077	29.1
40	136	72.0	42	178	4096	23	4073	22.9
50	57	33.6	20	77	2048	11	2037	26.5
60	53	36.3	21	74	2048	11	2037	27.5
70	83	53.6	31	114	2048	17	2031	17.8
80	61	38.0	22	83	1024	12	1012	12.2
90	70	46.2	27	97	1024	14	1010	10.4
.5100	83	62.6	37	120	1024	20	1004	8.4
10	224	84.0	49	273	512	26	486	1.8
20	85	55.0	32	117	256	17	239	2.0
30	67	39.0	23	90	128	12	116	1.3
40	77	43.6	25	102	128	14	114	1.1
60	70	41.5	24	94	128	13	115	1.2
80	110	62.7	37	147	128	20	108	.7

These results are plotted in Figure 8(a).



# YIELD CURVE

340.4 KEV PEAK, WITHOUT FOIL, 2 DEC. 1952

TARGET: LiF-2

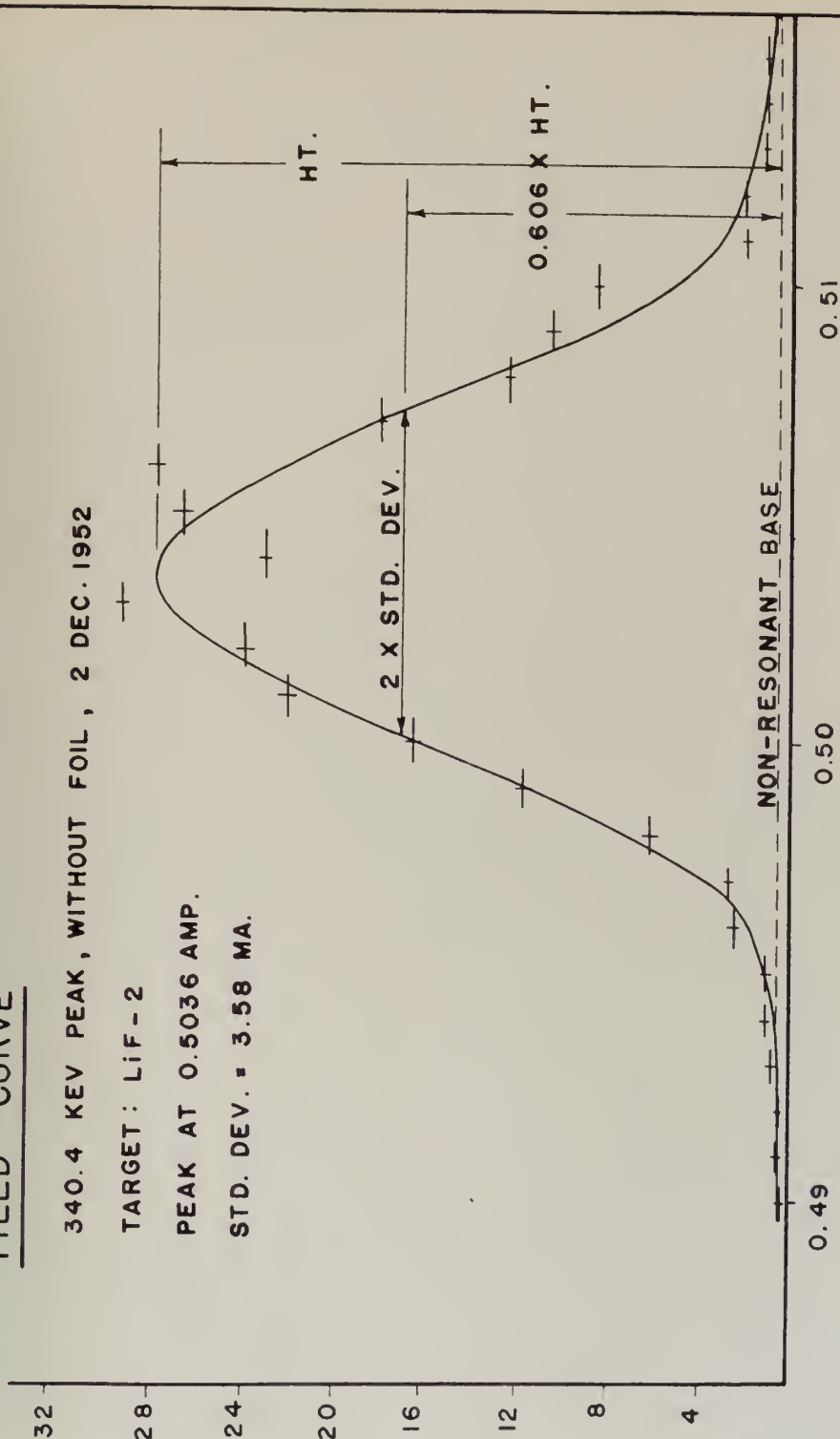
PEAK AT 0.5036 AMP.

STD. DEV. = 3.58 MA.

YIELD (ARB. UNITS)

MAGNET CURRENT (AMP.)

FIG. 8(a)





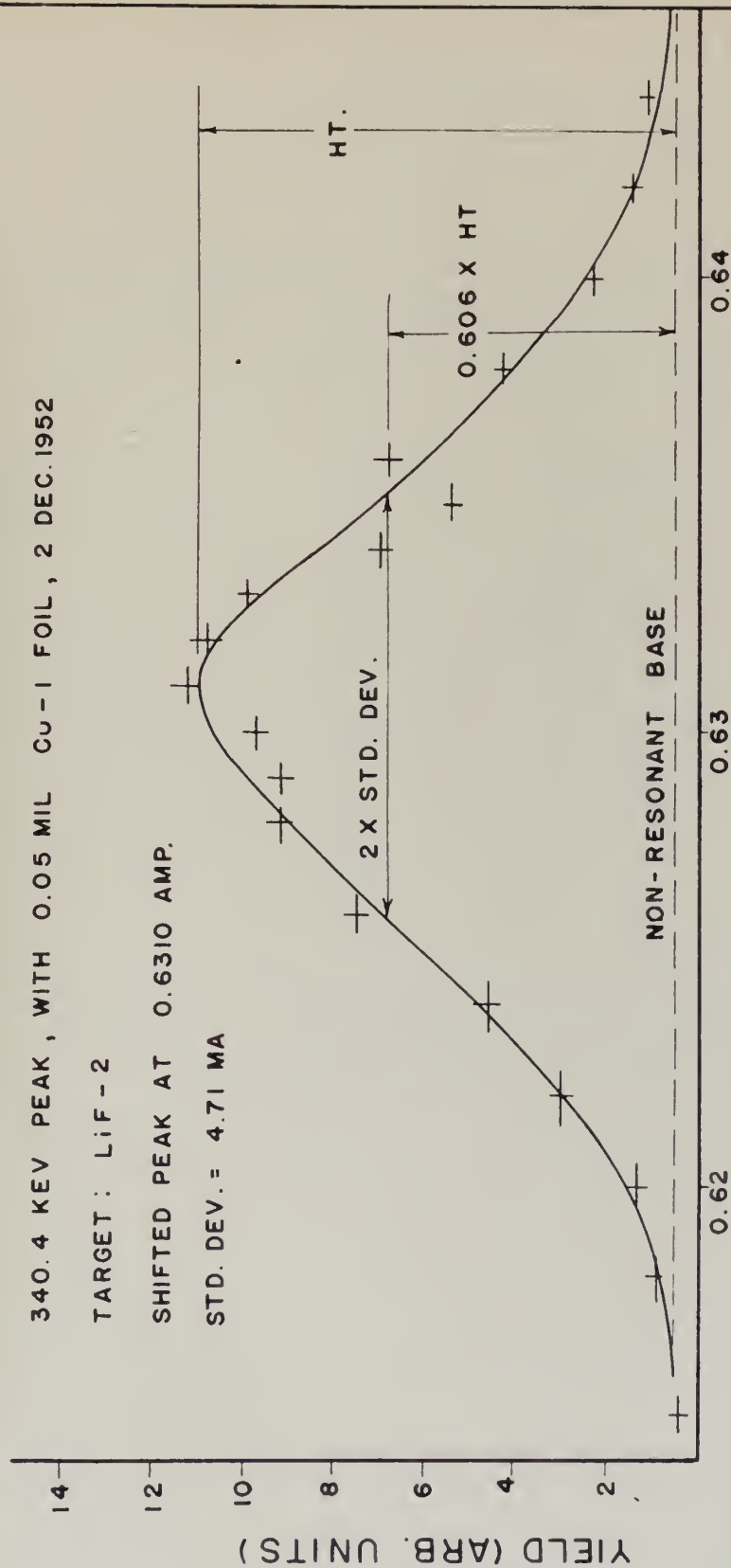
# YIELD CURVE

340.4 KEV PEAK, WITH 0.05 MIL CU-1 FOIL, 2 DEC. 1952

TARGET: LiF-2

SHIFTED PEAK AT 0.6310 AMP.

STD. DEV. = 4.71 MA



MAGNET CURRENT (AMP.)

FIG. 8(t)



Table VIII.

List of Resonance Energy Values for Proton-Gamma Process in  
Materials Used as Targets

Element	Reference	Resonance Energy (kev)	Width at Half Ht. = $\Gamma_{\text{nat}}$ (kev)	$\Omega_{\text{nat}}$ = $.42 \Gamma_{\text{nat}}$
$\text{Li}^7$	(1)	$441.1 \pm .5$	$12.2 \pm .5$	5.1
$\text{F}^{19}$	(1)	340.4	2.3	.97
		598	37	15.5
		669	7.5	3.15
		873.5	5.2	2.2
		935.3	8.0	3.35
$\text{Al}^{27}$	(2)	503	From 1	Negl.
		630	ev at	"
		771	600 kev,	"
		986	to 1 kev	.1
		1112	at 1.4	.1
		1165	Mev	.2
		1176		.2

References: (1) Ajzenberg and Lauritsen, 1952.  
(2) Brostrom, Huus, and Tangen, 1947.





performed by a rather standard technique of evaporation in a vacuum (Strong, 1945). The materials selected were those for which the energy resonance levels and peak widths are known with reasonable accuracy. The levels for lithium, fluorine, and aluminum as obtained from the latest and best references are tabulated in Table VIII.

A succession of targets were made and used, before some were obtained which were entirely satisfactory. A satisfactory target must have the following qualities:

(a) The target should be thick enough to give high yields of gamma-rays per proton count, thus providing good counting "statistics".

(b) On the other hand, the target thickness should be small enough that target thickness,  $T$ , and  $\Omega_T$  (Section II.B) can be minimized, thus minimizing the effect of errors in their estimation. And under any circumstances  $T$  must be much less than the energy difference between adjacent peaks, to avoid interference from other peaks when a certain one is analyzed.

(c) A fair uniformity of target thickness should be provided, so that when a proton beam is somewhat diffused over the target, the same values of  $T$  and  $\Omega_T$  will apply to all portions of the beam.

#### F. Analysis of Auxiliary Statistical Variables.

Preliminary to the primary calculations of stopping power are those calculations of the other variables which are a part of equations (II-B-4) to (II-B-7), inclusive. These calculations require a knowledge of the calibration relation between analyzing magnet



current and proton energy. Unfortunately an accurate determination of this relation requires in turn a knowledge of target thickness,  $T$ , which is one of the variables referred to above. Originally a rough assumption as to the proper calibration relation had to be assumed and calculations made by the process of successive approximations. In this report we may start with reasonably accurate information on the mean calibration curve, which has actually been obtained at a later stage in the experiment (See Section III.H).

Within a limited range it is found by plotting calibration data on log-log graph paper that the calibration relation can be expressed by a formula of the type:

$$E = K I^a, \quad (\text{III-F-1})$$

where  $E$  represents proton beam energy (Mev) and  $I$  is analyzing magnet current (amperes). (See Figure 9.)

Besides  $K$  and  $a$ , we wish to find the value of  $F$ , where

$$F = \frac{dE}{dI} = a K I^{a-1}, \quad (\text{III-F-2})$$

which is used to translate magnet current variations into energy variations at some particular peak. It has been found, using data to be presented later (Section III.H), that the values for  $K$ ,  $a$ , and  $F$  given in Table IX are fairly accurate.

Let us now analyze some of the statistical distributions in energy a little more closely. It is necessary for our purposes that the statistical spread in these distributions be expressed in terms of the standard deviation about the mean or its square, the variance. Many of the distributions are of such a type that the spread is not usually expressed thus, and calculations must be made to permit



Table IX.

Values of constants  $K$ ,  $a$ , and  $F$  ( $= dE/dI$ ) in the  
Magnet Current-Proton Energy Relationship:  $E = K I^a$ .

Current (amp)	Approx. Energy (Mev)	$K$	$a$	$F$
.50	.344	1.355	1.975	1.362
.55	.417	1.353	1.972	1.490
.60	.494	1.350	1.970	1.620
.65	.579	1.348	1.967	1.748
.70	.669	1.345	1.960	1.870
.75	.765	1.339	1.950	1.986
.80	.868	1.332	1.935	2.09
.85	.972	1.323	1.920	2.19
.90	1.076	1.315	1.905	2.28
.95	1.181	1.305	1.887	2.35

translation to those statistical variables we employ in common for all the distributions. Resonance curves for example have their spread expressed in terms of a width of peak at half the maximum height.

#### 1. Method of Obtaining $\Omega_{nat}$ .

As just noted, it is necessary to translate the natural peak's width at half height, designated as  $\sqrt{\phantom{x}}_{nat}$ , to the standard deviation  $\Omega_{nat}$ . We are immediately faced with a somewhat difficult situation, since the theoretical computation of  $\Omega_{nat}$  takes one into complications of both a mathematical and a practical nature.

The shape of the theoretical resonance curve is given by the well known Breit-Wigner formula (Breit and Wigner, 1936), modified for the proton-gamma reaction (Bethe, 1937):





$$\sigma = G_p \cdot \frac{1}{\sqrt{E}} \cdot \frac{K_1}{(E - E_{\text{res}})^2 + K_2} \quad , \quad (\text{III-F-3})$$

where  $\sigma$  is the probability cross-section for an atom to undergo the proton-gamma reaction.  $G_p$  is the barrier penetration factor for the proton in trying to pierce the Coulomb potential barrier of the atom, and at high proton energies (compared with Coulomb barrier height) it is close to unity, whereas at low proton energies it equals approximately  $\exp(-K'/\sqrt{E})$ .

This expression is difficult to deal with mathematically, but we may make further simplifications for the sake of discussion. Since most of the resonances used are extremely narrow compared to the proton energy ( $E$ ) exciting them, the factor  $G_p/\sqrt{E}$  is very slowly varying in the immediate vicinity of the peak, and can be taken as constant. We then have a resonance peak with a shape given by the formula:

$$\sigma \approx \frac{K}{(E - E_{\text{res}})^2 + K_2} \quad . \quad (\text{III-F-4})$$

By definition,  $\Omega_{\text{nat}}^2$  is then given by

$$\Omega_{\text{nat}}^2 = \frac{\int_{E_-}^{E_+} \frac{K \, dE}{1 + K_2/(E - E_{\text{res}})^2}}{\int_{E_-}^{E_+} \frac{K \, dE}{(E - E_{\text{res}})^2 + K_2}} \quad . \quad (\text{III-F-5})$$

The difficulty arises when we try to decide what limits to take for  $E_+$  and  $E_-$ , on either side of the peak.  $E_-$  cannot go below zero, but there is no natural upper limit to select. The value of the



denominator is finite with limits zero to infinity; but the value of the numerator increases without limit as  $E_+$  approaches infinity. Thus the value of the standard deviation will depend upon where we choose to take this upper limit and becomes somewhat arbitrary. The inclusion of the factor  $G_p/\sqrt{E}$  does not simplify our task, since the numerator still diverges with increasing value of  $E_+$ .

To avoid the decision as to where precisely we cut off the "tails" of the distribution, we shall employ the same approximation used by Madsen and Venkateswarlu (1948b). Noting that the resonance curves are rather similar in shape to a Gaussian, or "normal", distribution curve, one may assume that the ratio of the standard deviation to the width at half-maximum height is the same for a theoretical resonance curve as for the true Gaussian shaped curve. From tables of the latter function it is easily found that as a consequence

$$\Omega_{\text{nat}} = 0.42 \sqrt{\Gamma_{\text{nat}}} \quad . \quad (\text{III-F-6})$$

Table VIII, which gives the resonance widths for the target materials used, also gives the values of  $\Omega_{\text{nat}}$  computed by the above formula.

## 2. Method of Determining $\Omega_T$ .

The distribution curve for energy loss in the target material is quite simple. We may assume that the proton stopping power is practically constant over the small energy variation the beam undergoes in the thin target, so that this distribution curve has the shape of a rectangle. That is, if  $y(\Delta E_T)$  is the frequency variable, then it is defined as:



$$y = \left\{ \begin{array}{ll} 0, & \text{for } \Delta E_T < 0 \quad \text{and} \quad \Delta E_T > T ; \\ k, & \text{for } 0 < \Delta E_T < T . \end{array} \right\} \quad (\text{III-F-7})$$

Then,

$$\begin{aligned} \Omega_T^2 &= \frac{1}{k T} \int_0^T k (\Delta E - \frac{1}{2}T)^2 d(\Delta E) , \\ &= T^2/12 , \end{aligned} \quad (\text{III-F-8})$$

so that

$$\Omega_T = .288 T . \quad (\text{III-F-9})$$

### 3. Determination of $\Omega_S$ .

The distribution of energies of protons passing through the slit cannot be known with the degree of certainty one would like. Experience indicates that for a narrow slit the beam energy stabilizer can usually hold the center of the beam within the edges of the slit quite well. The maximum variation in proton energy which will still permit the beam center to pass through the slit has been computed by Smith (1952) to be:

$$\delta E_S \approx \frac{E w}{200} , \quad (\text{III-F-10})$$

where  $w$  is the width of the slit in millimeters, and  $\delta E_S$  and  $E$  are in the same units. This formula is probably not highly accurate in view of the assumptions and approximations involved in the derivation.

To provide a check, the shift in location of a peak at 669 kev was determined experimentally when the slit position was shifted by  $\frac{1}{2}$  millimeter. The shift in peak position was 1.2 ma. of magnet current, which corresponds according to Table IX to a beam energy shift of  $1.87 \times 1.2 = 2.25$  kev. These values are consistent with an equation:



$$\delta E_S = \frac{E w}{150} \quad . \quad (III-F-11)$$

This experiment probably does not give a highly accurate answer, but it is considered an improvement numerically over the theoretical formula's prediction; and we shall use equation (III-F-11) therefore.

If we assume that energy variations in the accelerator are such that a proton is equally likely to pass through the slit with any value in the corresponding spread of  $\delta E_S$ , we have a rectangular distribution; and as in equation (III-F-9) we obtain:

$$\Omega_S = .288 E w / 150 = E w / 520 \quad . \quad (III-F-12)$$

Since for all the experiments herein described,  $w$  equals one millimeter, the formula becomes:

$$\Omega_S = E / 520 \quad , \quad (III-F-13)$$

where the units of  $E$  and  $\Omega_S$  are the same.

#### 4. Determination of $\Omega_M$ .

The factor  $\Omega_M$  is impossible to obtain directly, and it can only be guessed at when the resonance peaks' widths are analyzed. There is no reason to believe that it is even constant from one day to another under what are presumed to be similar operating conditions. Since current variations cause greater beam voltage variations with higher energies, we may guess that  $\Omega_M$  will generally increase with increasing proton energy, though this is by no means certain.





### G. Analysis of Unshifted Resonance Peaks and Determination of Target Thicknesses.

Table X gives the analysis of the statistical variations of most of the resonance peaks studied without stopping media interposed. This analysis is based upon formula (II-B-5), and shows all computed values for  $\Omega_T^2 + \Omega_M^2$ . Observation of these results leads to the following conclusions:

(a) There are comparatively large uncertainties present in all of the data presented, so that the final probable error in the estimation of  $\Omega_{T+M}$  is on the order of 1 kev or more. This is especially evident from the size and number of negative values obtained, since all values should be positive for variances.

(b) There seems to be little reason to believe that  $\Omega_M$  is large enough to consider, except in a few cases. We shall therefore ignore it in our computations but must consider its possible influence when the matter of errors in results is discussed.

(c) For low energy values  $\Omega_T$  is at a maximum, whereas  $\Omega_S$  is at a minimum. Therefore in determination of target thickness, greater weight should be given to data obtained from lower energy peaks.

In order to express the target thickness in terms of stopping power, we must standardize such values to a specific value of proton energy (1 Mev is usual). This means that after having determined target thickness at a certain proton energy we must convert this value to thickness for a 1 Mev proton beam. This can be done if we know the relative stopping power of the target substance at 1 Mev compared to the stopping power of the target at the energy of the



Table X. (Two Pages)

## Analysis of Contributions to Variances in Unshifted

## Resonance Peaks.

Line	Date	Target	Peak Energy, (kev)	Magnet Current, (amp)	F (Table IX)
1	8-29-52	LiF-1	340.4	.50	1.362
2	"	"	441.1	.566	1.533
3	"	"	669	.70	1.870
4	9-24-52	Al-3	503	.60	1.620
5	"	"	630	.68	1.820
6	"	"	986	.85	2.170
7	"	"	1112	.91	2.255
8	9-26-52	Al-3	630	.68	1.820
9	10-16-52	LiF-1	669	.70	1.870
10	"	"	873.5	.80	2.086
11	"	"	935.3	.83	2.135
12	10-17-52	Al-3	630	.68	1.820
13	"	"	986	.86	2.185
14	"	"	1112	.91	2.255
15	10-23-52	LiF-1	441.1	.566	1.533
16	12-2-52	LiF-2	340.4	.50	1.362
17	"	"	669	.70	1.870
18	"	"	873.5	.81	2.103
19	"	"	935.3	.84	2.153
20	12-18-52	LiF-4	441.1	.57	1.540
21	"	"	669	.70	1.870
22	"	"	873.5	.805	2.095
23	"	"	935.3	.835	2.144



Table X. (Concl.)

Line	$\Omega_0$ (ma)	$\Omega_0$ (kev)	$\Omega_0^2$ (kev <sup>2</sup> )	$\Omega_{nat}^2$ (kev <sup>2</sup> ) Table VIII	$\Omega_S^2$ (kev <sup>2</sup> ) (III-F-13)	$\Omega_T^2 + \Omega_M^2$ (kev <sup>2</sup> ) (II-B-5)
1	1.90	2.60	6.75	0.94	0.43	5.38
2	4.95	7.60	57.7	26.0	0.72	31.0
3	3.34	6.25	39.1	9.9	1.66	27.5
4	0.80	1.30	1.69	Negl.	0.94	0.75
5	0.90	1.64	2.69	"	1.47	1.22
6	0.84	1.82	3.31	0.01	3.60	- 0.30
7	1.35	3.05	9.30	0.01	4.58	4.71
8	1.1	2.00	4.00	Negl.	1.47	2.53
9	1.65	3.10	9.61	9.9	1.66	- 1.95
10	1.2	2.50	6.25	4.84	2.82	- 1.41
11	1.9	4.05	16.40	11.23	3.24	1.93
12	1.15	2.10	4.41	Negl.	1.47	2.94
13	0.93	2.03	4.12	0.01	3.60	0.51
14	1.03	2.32	5.38	0.01	4.58	0.79
15	3.45	5.30	28.1	26.0	0.72	1.40
16	3.58	4.88	23.8	0.94	0.43	22.4
17	2.82	5.27	27.8	9.9	1.66	16.2
18	2.97	6.25	39.0	4.84	2.82	31.3
19	3.02	6.50	42.2	11.23	3.24	27.7
20	3.2	4.93	24.3	26.0	0.72	- 0.24
21	1.43	2.67	7.13	9.9	1.66	- 4.43
22	1.2	2.51	6.30	4.84	2.82	- 1.36
23	1.85	3.97	15.76	11.23	3.24	1.29





Table XI.

Computations of Target Thickness (kev)

Target	Peak Energy (Mev)	Conv. Factor $= \sqrt{E}$	$\Omega_T^2$ (kev <sup>2</sup> )	$\Omega_T$ (kev)	$T = \Omega_T / .288$	T at 1 Mev (kev)
LiF-1	.3404	.583	5.38	2.32	8.05	4.7
"	.4411	.664	31.0	5.57	19.3	12.8
"	.4411	.664	1.4	1.18	4.1	2.7
"	.669	.818	27.5	5.24	18.2	14.9
"	.669	.818	nega.	-	-	-
"	.8735	.935	"	-	-	-
"	.9353	.970	1.93	1.39	4.82	4.7
LiF-2	.3404	.583	22.4	4.73	16.4	9.56
"	.669	.818	16.2	4.02	13.9	11.4
"	.8735	.935	31.3	5.60	19.4	18.1
"	.9353	.967	27.7	5.26	18.2	17.6
LiF-4	.4411	.664	nega.	-	-	-
"	.669	.818	"	-	-	-
"	.8735	.935	"	-	-	-
"	.9353	.967	1.27	1.135	3.94	3.8
Al-3	.503	.710	0.75	0.866	3.00	2.13
"	.630	.794	1.22	1.105	3.83	3.04
"	.630	.794	2.53	1.59	5.51	4.37
"	.630	.794	2.94	1.714	5.95	4.72
"	.986	.993	nega.	-	-	-
"	.986	.993	0.51	0.714	2.47	2.45
"	1.112	1.055	4.71	2.17	7.53	7.94
"	1.112	1.055	0.79	0.889	3.08	3.25



particular peak analyzed.

Bohr (1948) indicates that within this energy region which we are concerned with, the stopping power is inversely proportional to the square root of proton energy. To the extent that data is available in this region, such dependence is roughly confirmed (Madsen and Venkateswarlu, 1948a; Kahn, 1953; and Figure 11 herein). In view of the approximate nature of the data given in Table X, it is sufficiently accurate to convert target thickness to the 1 Mev standard energy by multiplying the target thickness by the square root of the proton energy at which the specific measurement was made.

Table XI gives the target thickness analysis, with the aid of the data derived in Table X. In view of the approximate nature of the final results, it is desirable to use other means to aid in the selection of definite answers. If the targets are thin the maximum value of the yield at a certain resonance peak will be a rough measure of the relative thickness of the target. Thus a comparison of the maxima of the various peaks for the various lithium fluoride targets will add additional information on which to base final judgment. It is especially desirable to do this for determination of the thickness of target LiF-4, since it is evidently so thin as to make detection from an experimental peak width practically impossible. Table XII gives this data, as taken from experimental results. The table indicates that in a rough sort of way, the relative yield from the various lithium fluoride targets are in the ratio:

$$\text{LiF-1} : \text{LiF-2} : \text{LiF-4} = 0.3 : 1 : 0.1$$



Table XII.

Resonance Peak Maxima for Lithium Fluoride Targets

Peak	Maximum Yields		
	* LiF-1	LiF-2	LiF-4
340.4 kev	24.6	28.0	-
441.1	2.2	-	2.15
441.1	2.9	-	-
669	10.5	86	2.65
669	6.7	-	-
#873.5	7.1	310	67
#935.3	4.4	136	24

\* Evidently the target LiF-1 has a somewhat variable thickness. We can speak only of its average value.

# Counting geometry somewhat variable.

Table XIII.

Target Thicknesses (kev) for Various Proton Energies

Lithium Fluoride Targets				Aluminum Target	
Proton Energy (Mev)	LiF-1	LiF-2	LiF-4	Proton Energy (Mev)	Al-3
1.000	4.0	12.0	1.0	1.000	3.0
.3404	6.8	20.6	1.8	.503	4.2
.4411	6.0	18.0	1.6	.630	3.8
.598	5.2	15.6	1.2	.771	3.4
.669	4.8	14.6	1.2	.986	3.0
.8735	4.2	12.8	1.0	1.112	2.8
.9353	4.2	12.4	1.0		

On the basis of all information available, we can now make an estimate of target thicknesses for all targets. Table XIII gives



the thickness estimated at 1 Mev, and also gives the computed values of target thickness at various resonant energies. In the computation the target thickness is assumed, as before, to be inversely proportional to the square root of the energy.

#### H. Energy-Current Calibration.

Since we can now find the value of  $E_0$  for each peak measured, by use of equation (II-B-4), we may find the calibration curves for accelerator beam energy ( $E_0$ ) versus analyzing magnet current ( $I$ ). All data from experiment and previous analysis is listed in Table XIV in such a fashion that the calibration curves can be put on a logarithmic scale. The curves themselves are depicted in Figure 9.

Table XV is a list of data similar to Table XIV, except that the data are for single resonance peaks and are not taken as part of a complete calibration series. Their use is indicated below.

In using and interpreting the calibration curves, several significant points have been discovered:

(a) If the data is plotted to a logarithmic scale, vertically and horizontally, the calibration line drawn is almost a straight line. This indicates that an empirical formula of the type  $E = K I^a$  is approximately valid over the whole energy range, and is quite accurate within smaller limits. (This justifies equation (III-F-1).) This is a change from the previous custom (Grove, 1950; Taylor, 1952; Russell, 1952), by which data was plotted as  $\sqrt{E}$  versus  $I$  and the best straight line drawn. This older type of plot presumes that an empirical formula of the type  $E = K (I+b)^2$  is valid. Plotting of a typical set of calibration data from Table XIV according to the





Table XIV. (Two Pages)

Calibration Data

Date; *Target; Slit Setting, mm.	$E_{\text{nat}}$ (Mev)	$\frac{1}{2}T$ (Mev)	$E_0$ (Mev)	$\log E_0$	I (amp)	$\log I$
8-29-52	.3404	.0034	.3438	$\bar{1}.5363$	.4973	$\bar{1}.6966$
LiF-1	.4411	.0030	.4441	$\bar{1}.6475$	.5665	$\bar{1}.7532$
4.25	.669	.0024	.6714	$\bar{1}.8270$	.6996	$\bar{1}.8448$
	.8735	.0021	.8756	$\bar{1}.9423$	.8020	$\bar{1}.9042$
9-26-52	.503	.0021	.5051	$\bar{1}.7034$	.6032	$\bar{1}.7805$
A 1-3	.630	.0019	.6319	$\bar{1}.8006$	.6763	$\bar{1}.8301$
4.75	.986	.0015	.9875	$\bar{1}.9945$	.8563	$\bar{1}.9326$
	1.112	.0014	1.1134	0.0467	.9095	$\bar{1}.9588$
10-16-52	.669	.0024	.6714	$\bar{1}.8270$	.7023	$\bar{1}.8465$
LiF-1	.8735	.0021	.8756	$\bar{1}.9423$	.8030	$\bar{1}.9047$
4.75	.9353	.0021	.9374	$\bar{1}.9719$	.8315	$\bar{1}.9199$
10-17-52	.630	.0019	.6319	$\bar{1}.8006$	.6789	$\bar{1}.8318$
Al-3	.986	.0015	.9875	$\bar{1}.9945$	.8573	$\bar{1}.9331$
4.75	1.112	.0014	1.1134	0.0467	.9103	$\bar{1}.9592$
12-2-52	.3404	.0103	.3507	$\bar{1}.5449$	.5036	$\bar{1}.7021$
LiF-2	.669	.0073	.6763	$\bar{1}.8301$	.7036	$\bar{1}.8473$
3.75	.8735	.0064	.8799	$\bar{1}.9444$	.8074	$\bar{1}.9071$
	.9353	.0062	.9415	$\bar{1}.9738$	.8377	$\bar{1}.9231$
12-3-52	.503	.0021	.5051	$\bar{1}.7034$	.6115	$\bar{1}.7864$
Al-3	.630	.0019	.6319	$\bar{1}.8006$	.6838	$\bar{1}.8349$
3.75	.986	.0015	.9875	$\bar{1}.9945$	.8640	$\bar{1}.9365$

\* Slit setting equals reading of position micrometer minus one-half the reading of the slit width micrometer. It essentially indicates the position of the middle of the slit.



Table XIV. (Concl.)

Date; Target; Slit Setting, mm.	$E_{nat}$ (Mev)	$\frac{1}{E}T$ (Mev)	$E_0$ (Mev)	$\log E_0$	I (amp)	$\log I$
12-18-52	.4411	.0008	.4419	$\bar{1}.6453$	.5690	$\bar{1}.7551$
LiF-4	.669	.0006	.6696	$\bar{1}.8258$	.6995	$\bar{1}.8448$
3.75	.8735	.0005	.8740	$\bar{1}.9415$	.8052	$\bar{1}.9059$
	.9353	.0005	.9358	$\bar{1}.9712$	.8334	$\bar{1}.9209$
12-19-52	.503	.0021	.5051	$\bar{1}.7034$	.6095	$\bar{1}.7850$
41-3	.630	.0019	.6319	$\bar{1}.8006$	.6817	$\bar{1}.8336$
4.25	.771	.0017	.7727	$\bar{1}.8880$	.7562	$\bar{1}.8786$
	.986	.0015	.9875	$\bar{1}.9945$	.8620	$\bar{1}.9355$
	1.112	.0014	1.1134	0.0467	.9176	$\bar{1}.9627$
1-9-53	.4411	.0008	.4419	$\bar{1}.6453$	.5700	$\bar{1}.7559$
LiF-4	.669	.0006	.6696	$\bar{1}.8258$	.7028	$\bar{1}.8468$
3.50	.8735	.0005	.8740	$\bar{1}.9415$	.8074	$\bar{1}.9071$
	.9353	.0005	.9358	$\bar{1}.9712$	.8367	$\bar{1}.9226$
1-19-53	.669	.0006	.6696	$\bar{1}.8258$	.7014	$\bar{1}.8460$
LiF-4	.8735	.0005	.8740	$\bar{1}.9415$	.8080	$\bar{1}.9074$
3.50	.9353	.0005	.9358	$\bar{1}.9712$	.8367	$\bar{1}.9226$
1-22-53(am)	.669	.0006	.6696	$\bar{1}.8258$	.7040	$\bar{1}.8476$
LiF-4	.8735	.0005	.8740	$\bar{1}.9415$	.8072	$\bar{1}.9070$
3.50						
1-22-53(pm)	.669	.0006	.6696	$\bar{1}.8258$	.7014	$\bar{1}.8460$
LiF-4	.8735	.0005	.8740	$\bar{1}.9415$	.8056	$\bar{1}.9061$
3.50	.9353	.0005	.9358	$\bar{1}.9712$	.8335	$\bar{1}.9209$



Table XV. (Two Pages)

Data for Single Peaks (Unshifted)

Date; Target; Slit Setting, mm.	$E_{\text{nat}}$ (Mev)	$\frac{1}{2}T$ (Mev)	$E_0$ (Mev)	$\log E_0$	$I$ (amp)	$\log I$
10-23-52 LiF-1 4.75	.4411	.0030	.4441	$\bar{1}.6475$	.5670	$\bar{1}.7536$
10-28-52 LiF-1 4.75	.9353	.0021	.9374	$\bar{1}.9719$	.8320	$\bar{1}.9201$
10-31-52 LiF-1 4.75	.9353	.0021	.9374	$\bar{1}.9719$	.8303	$\bar{1}.9192$
1-12-53(am) LiF-4 3.50	.669	.0006	.6696	$\bar{1}.8258$	.7009	$\bar{1}.8457$
1-12-53(pm) LiF-4 3.50	.669	.0006	.6696	$\bar{1}.8258$	.7001	$\bar{1}.8452$
1-13-53 LiF-4 3.50	.669	.0006	.6696	$\bar{1}.8258$	.6998	$\bar{1}.8450$
1-14-53 LiF-4 3.50	.669	.0006	.6696	$\bar{1}.8258$	.7002	$\bar{1}.8452$
1-15-53 LiF-4 3.50	.669	.0006	.6696	$\bar{1}.8258$	.7023	$\bar{1}.8465$
1-19-53 LiF-4 3.50	.669	.0006	.6696	$\bar{1}.8258$	.7024	$\bar{1}.8466$





Table XV. (Concl.)

Date; Target; Slit Setting, mm.	$E_{\text{nat}}$ (Mev)	$\frac{1}{E}T$ (Mev)	$E_0$ (Mev)	$\log E_0$	$I$ (amp)	$\log I$
1-20-53 LiF-4 3.50	.669	.0006	.6696	$\bar{1}.8258$	.6996	$\bar{1}.8449$
1-21-53 LiF-4 3.50	.669	.0006	.6696	$\bar{1}.8258$	.7030	$\bar{1}.8470$
1-23-53 LiF-4 3.50	.669	.0006	.6696	$\bar{1}.8258$	.7018	$\bar{1}.8462$



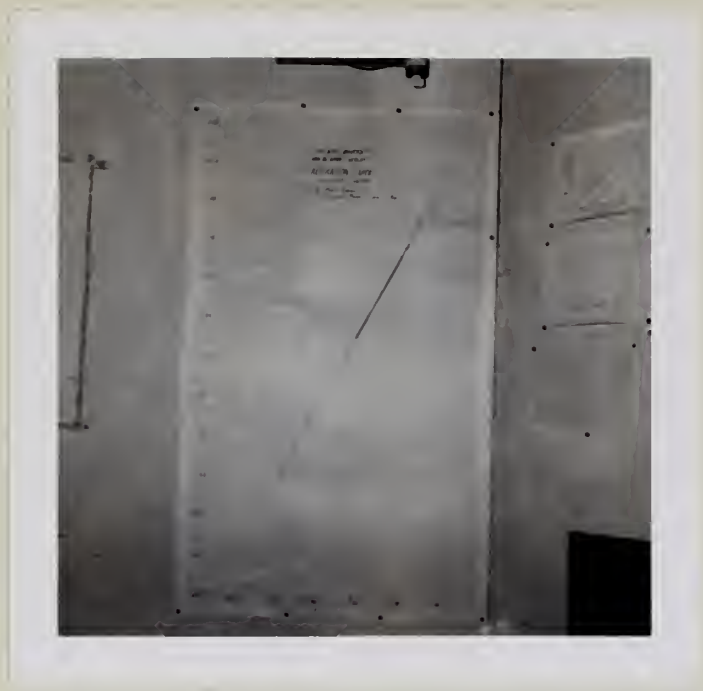


Figure 9.



previous custom and comparing such a plot with the double-logarithmic plot has indicated that the latter plot has less curvature than the corresponding plot by the older method. In view of the fact, however, that a slight curvature does exist for the calibration curves, even on the logarithmic plots, it was considered more accurate to use the curves directly rather than to use a straight line formula giving the closest fit over the whole energy range. The empirical formula (III-F-1) and Table IX are to be used only for computations at localized energy regions.

(b) Different calibration series give curves which are generally slightly displaced from one another, although they are essentially parallel. This indicates that personal errors during a series of runs are small compared to those discrepancies between different daily series. Every effort was made in doing the experimental work to use a standardized technique in operation of the accelerator and auxiliary apparatus; but some variation from day to day seemed unavoidable. Such variations may be due to: (1) lack of precise control as to the horizontal and vertical position of the beam axis (as indicated by the neutral beam, undeviated by the magnetic field); (2) lack of control over the temperature of the magnet itself. The first effect means that inhomogeneities in the magnetic field may be sufficient to be noticeable. The latter effect is related to the fact that magnetic elements in an electromagnet are more easily aligned when the iron is at a higher temperature, so that the same current gives a slightly greater deviating flux. The fact that different curves are closely parallel means that once



a few typical calibration curves have been plotted to give the general trend, further curves may be indicated by having data for only a single calibration point on the curve. This fact has been utilized in the latter part of the research, and Table XV gives the data for these single calibration points.

(c) It is of some interest to note the actual variation of the calibration data for one specific value of energy, to give an idea as to the spread in the calibration curves over a six months' period. A check of Tables XIV and XV shows that for the 669 kev fluorine resonance peak, by use of the same target and the same slit position, the average value of the analyzing current was .7014 amperes, with extremes of .6696 and .7040 amperes. The standard deviation of all readings from the mean is .0014 amperes. If on the other hand, one were given the current at about this point, the extreme energy variation corresponding to this calibration curve variation would be 8.2 kev (determined by using factor F, Table IX). The standard deviation in energy comes out to be 2.6 kev from the mean calibration line, or a probable error, if one used the mean line, of about 1.7 kev. This fact indicates that if we have some additional information as to the proper position of the true calibration curve, such as by a single calibration point, a much better choice can be made for energy corresponding to a certain value of magnet current; and the probable error in such a case would undoubtedly be substantially less than 1 kev. It should be noted that this conclusion is justified only if the technique is used for data taken on the same magnet cycle as the calibration point. A recycling of the magnet may require a new curve. (For examples, see Table XIV, data for 1-22-53, a.m. and p.m.)





#### IV. Experimental Results on Stopping Power.

##### A. Possible Sources of Systematic Error and Corrections Required.

When the experimental data on stopping are analyzed, the possibility of certain consistent factors requiring correction must be considered.

##### 1. Nuclear Collision Losses.

It can be visualized that proton-nuclear collisions, though elastic, will result in a certain small amount of energy loss by the proton in the laboratory system. The usual formulas for stopping power do not include this effect, and therefore in theory the nuclear stopping effect should be subtracted from experimental data in order to give a result which can be compared with theory.

Bohr (1948) has derived a formula for nuclear stopping, given as follows:

$$\Delta_p E = N \cdot \Delta x \cdot \frac{2\pi z^2 Z^2 e^4}{M_a v^2} \cdot \ln \frac{2}{\zeta} \quad , \quad (\text{IV-A-1})$$

$$\text{where } \zeta = 2 z Z^{4/3} \frac{m}{M} \left( \frac{v_0}{v} \right)^2 \quad . \quad (\text{IV-A-2})$$

In order to determine the magnitude of this effect, an example was calculated for hypothetical circumstances conducive to a large answer. For energy loss due to nuclear collisions of protons of mean velocity  $0.8 \times 10^9$  cm/sec (energy of 332 kev) passing through a 0.05 mil nickel foil, the calculated value of  $\Delta_p E$  is 0.171 kev. It can be seen by comparison with electronic stopping energy losses for the foils (Figure 10) that the nuclear effect is



only on the order of 0.1% of the total stopping effect. The nuclear stopping may therefore be neglected.

## 2. Increase of Path Length by Scattering.

Another effect, also due primarily to nuclear collisions, is the deviation from the beam axis of many protons, especially for the case of slow protons through large thicknesses of matter. This effect is observable visually during stopping experiments with gases. The excitation of the gas atoms by the proton beam brings about the emission of light which marks the proton paths. It can be seen that the beam does indeed diverge in a very narrow cone from the entrance foil to the gas chamber. Such effect increases the average amount of matter traversed by the beam. The geometry of our chamber (Figure 4) is such that the target subtends at the entrance foil an angle of  $5.6^\circ$  to each side of the axis. Any proton deviated so much as to pass outside this cone does not hit the target and cannot contribute to the gamma ray yield and thus has no effect on experimental values of stopping power. Only at very low proton energies (as noted visually) does there exist an appreciable deviation of the protons away from the axis. Even in such circumstances the correction for longer path length is only a fraction of  $\cos 5.6^\circ$ , or less than one-half of one percent. At higher energies the correction is still less. Since this correction is much less than the over-all experimental error expected, we shall ignore it.

## 3. Carbonization of Foils.

There is a tendency for all parts exposed to the beam to accumulate a dark deposit of what is called "carbon", though it



probably includes a moderate percentage of hydrogen. This deposit is a well-known problem for many accelerators. It is presumably a result of deposition of volatile hydrocarbons on surfaces plus subsequent molecular breakdown by proton bombardment and by localized heating. It is even possible that if a foil or target is heated to a high temperature, hydrocarbon molecules in gaseous form may be decomposed upon random collision with the spot heated by the beam, even if there is no tendency otherwise to adhere as a semi-permanent or permanent film. The sources of the volatile hydrocarbons are several, the most probable ones being:

- (a) vapors from the oil diffusion pump of the vacuum system;
- (b) volatile vapors from organic substances such as vacuum rings and gaskets in the system;
- (c) vaporized solvents from freshly applied sealing paint (such as glyptal) used to stop small leaks;
- (d) vapors from small amounts of acetone or similar penetrating fluids used for leak testing;
- (e) vapors from residual amounts of organic solvents used for cleaning parts of the system.

These factors are listed in such an order that the first ones are most difficult to avoid, and the latter ones the easiest. Fortunately, our experience seems to indicate that the very ones hardest to avoid are actually the ones having the least noticeable effect, and vice versa.

Under normal operating conditions it was our practice to discard a foil or target if the blackening became appreciable. This was





especially necessary for the foil; evidently the greater diffuseness of the beam on the targets and their greater ability to conduct the heat away prevented rapid "carbonization" of the targets.

In connection with the foils, this carbonizing added small amounts to the stopping. The effect was checked by determining energy loss through the foils at intervals throughout their use, Figure 10, which gives the energy loss in the various foils as function of the entering proton energy, shows this effect clearly. Note especially the progressive increase in stopping power by the .05 mil copper foil for subsequent days (on the order of 2 kev per operating day for 1 Mev protons). Also note the radical shift in energy loss through the .05 mil nickel foil (#2), which occurred after a rather severe carbonizing due to release of gaseous hydrocarbons into the gas chamber from incompletely dried applications of glyptal.

Foil stopping power data were discarded when it was evident that such carbonizing had contributed to abnormally high values of energy loss. This data is needed, however, when the carbonized foils are used as windows for the experiments on gas stopping power. It should be mentioned that the greatest problem did occur in the gas stopping power experiments. In the foil stopping power experiments, the whole system was continually pumped by the vacuum pumps; but in the gas experiments, the gas chamber was closed off and any hydrocarbon molecules trapped therein had many chances to strike the hot foil and be decomposed and deposited there. The examples of severe carbonizing



mentioned in the preceding paragraph occurred during experiments on gases.

#### 4. Accurate Computation of Mean Energy of Protons in Medium.

It is usually customary in giving experimental results for stopping power to consider that  $\Delta E/\Delta x$  equals  $dE/dx$  for a value of  $E$  which is the arithmetic average of the initial and exit energies of the beam in the stopping medium ( $= \frac{E_0 + E_0'}{2}$ , for example, in case the stopping material is a foil). This approximation is appropriate when  $\Delta E$  is small compared to  $E$ . Warshaw (1949) has commented on this matter and proposes a formula to give a correction to  $\Delta E/\Delta x$  so that the correct value for stopping can be obtained at the arithmetic mean value of energy. His formula assumes that the stopping power curve over the region from  $E_0$  to  $E_0'$  is a straight line. He finds that the corrections thus computed are less than his probable error but worth including to insure a correct shape for his curves.

Our values of both  $\Delta E$  and  $E$  are in most cases larger than Warshaw's, and we may also find a slight correction advantageous. Rather than Warshaw's formula correcting stopping power we prefer one which provides a correction to the arithmetic mean energy to give the true mean (designated as  $E_m$ ). In deriving the formula for this correction let us make an assumption as to the shape of the stopping power curve which is more accurate than the linear shape assumed by Warshaw. Assume that

$$\frac{dE}{dx} = k E^{-\gamma} \quad . \quad (IV-A-3)$$



Theory indicates, as we have noted before, that the exponent  $\gamma$  should have a value of 0.5 (See Section III-G). Experimental results (Madsen and Venkateswarlu, 1948a; Kahn, 1953) show that  $\gamma$  is slightly dependent on  $Z$  and on  $E$ , but has in the cases wherein we are required to use it ( $E \approx 600$  kev) an average value of about 0.45.

The thickness of the medium traversed,  $\Delta x$ , is easily seen to be given by:

$$\Delta x = \int_{E_0}^{E'_0} \frac{dE}{dE/dx} = \frac{1}{k} \int_{E_0}^{E'_0} E^{\gamma} \cdot dE \quad (\text{IV-A-4})$$

$$= \frac{1}{k(\gamma+1)} (E'^{\gamma+1}_0 - E_0^{\gamma+1}) \quad (\text{IV-A-5})$$

Now the correct value of mean energy,  $E_m$ , to use is that for which

$$\frac{dE}{dx}(E_m) = \Delta E / \Delta x = \frac{E'_0 - E_0}{\Delta x} \quad (\text{IV-A-6})$$

Solving for  $\Delta x$  and substituting equation (IV-A-3) gives:

$$\Delta x = \frac{E'_0 - E_0}{k E_m^{-\gamma}} \quad (\text{IV-A-7})$$

If we equate the two expressions for  $\Delta x$  and solve for  $E_m$ , we obtain:

$$E_m = \left[ \frac{1}{\gamma+1} \cdot \frac{E'^{\gamma+1}_0 - E_0^{\gamma+1}}{E'_0 - E_0} \right]^{1/\gamma} \quad (\text{IV-A-8})$$

If we replace  $E'_0$  by  $E_a + \frac{1}{2}\Delta E$ , and  $E_0$  by  $E_a - \frac{1}{2}\Delta E$ , where  $E_a$  is the arithmetic average, we find:

$$E_m = \left[ \frac{1}{\gamma+1} \cdot \frac{(E_a + \frac{1}{2}\Delta E)^{\gamma+1} - (E_a - \frac{1}{2}\Delta E)^{\gamma+1}}{\Delta E} \right]^{1/\gamma} \quad (\text{IV-A-9})$$





If we expand the parenthetical expressions according to the binomial formula, we find:

$$E_m = \left[ E_a + \frac{1}{24} \gamma (\gamma - 1) \frac{(\Delta E)^2}{E^{2-\gamma}} + \text{other terms} \right]^{1/\gamma}, \quad (\text{IV-A-10})$$

where the other terms are successive terms in  $(\Delta E)^n / E^{n-\gamma}$ , for  $n = 2, 4, 6$ , etc., with fractional coefficients for the terms.

For  $\Delta E$  appreciably less than  $E$ , this series converges rapidly, so that the other terms in the above equation may be neglected.

Then let us expand the bracketed expression in equation (IV-A-10) once again by the binomial formula, to obtain:

$$E_m \approx E_a - \frac{(1-\gamma) (\Delta E)^2}{24 E_a} + \text{additional terms}, \quad (\text{IV-A-11})$$

where the additional terms can once more be dropped when  $\Delta E$  is appreciably less than  $E$ .

Then we see, substituting 0.45 for  $\gamma$ , that

$$E_m = E_a - \delta E, \quad (\text{IV-A-12})$$

where

$$\delta E \approx \frac{.55 (\Delta E)^2}{24 E_a}. \quad (\text{IV-A-13})$$

We use this correction and apply it below in cases where it exceeds 1 kev.

##### 5. Corrections Required for Impurities in the Materials Studied.

One possible source of consistent error which should be carefully checked is the impurities in the elements studied.

The metals are quickly disposed of. A semi-quantitative





spectrographic analysis was carried out <sup>1</sup> with sample foils from the same set as those used, with the following results:

(a) For copper, the impurities present are as follows: calcium with the order of magnitude of 0.1%, magnesium less than 0.1%, and a trace of silicon.

(b) For nickel, the impurities present are as follows: cobalt to an amount between 0.1 to 0.5%, plus traces of magnesium, molybdenum, beryllium, and iron.

The error in stopping power is not as great as the percentage of impurities. Each of the impurities tends to produce an error only to the extent that its stopping power varies from the stopping power of the prime constituent, so that the closer the impurity is to the primary element in the table of elements, the less the effect of the impurity on the stopping power measured. With these considerations in mind, it becomes clear that the impurities in foils of either nickel or copper are such in quantity and type that no appreciable error can result by considering the foils as pure.

The gases however require more careful study. The gases<sup>2</sup> as they are supplied by the company are guaranteed to be pure to the following extent:

---

1

The analysis was carried out by Mr. Sam Wohlfort at the Spectrographic Laboratory, Department of Chemistry, Ohio State University, through the courtesy of Professor W.H. MacNevin.

2

The nitrogen and argon were obtained in pressurized K cylinders from the Linde Air Products Company; while the rarer gases came from the same company in glass flasks at approximately atmospheric pressure.



- (a) Commercial nitrogen used is stated to be 99.7% pure.
- (b) The argon supplied is stated to be 99.6% pure.
- (c) The neon impurities are negligible.
- (d) The krypton may have as much as 1% xenon present.
- (e) The xenon may have as much as 2% krypton present.

Since the above amounts are maximum values, the exact extent of the impurities for our samples was still somewhat in doubt. There existed a still more serious factor in connection with the latter three gases, which were supplied in one liter or one-half liter glass flasks. Difficulties were encountered in the attachment of the flasks to the system in such a way as to be absolutely air-tight when the duct system is under partial or complete vacuum. The results were that a certain amount of air contamination was probable for the gases in each of the three flasks, before final gas-tightness was attained. It was considered necessary therefore that an analysis be made on the gases in the flasks after the possible contamination occurred.

The analysis was carried out by mass-spectrograph<sup>1</sup>, and results are as given in Table XVI.

In order to determine the effects of these impurities, it is necessary to note that the amount of matter traversed is indicated by the measured values of path length, gas pressure, and gas temperature. Since the pressures used are quite low (a few centimeters of

The analysis was carried out by Mr. Leonard Mauk, at the Mass-Spectrographic Laboratory, Department of Chemistry, Ohio State University, through the courtesy of Professor H.L. Johnston and Dr. David White.



mercury) the ideal gas relationships are valid, and the variables cited above are sufficient to give the number of molecules per square centimeter of cross-section perpendicular to the proton path. For the rare gases, the atomic stopping power is the same as the molecular stopping power; and since the impurities are given as volume percent (equivalent to mole percent), the corrective factor to be applied to the experimental results is the relative molecular stopping power of the impure gas as compared to that for the pure gas.

Table XVII gives the values assumed for atomic and molecular stopping power for the various elements and compounds concerned. It has been necessary in some cases to make rough preliminary estimates of stopping power from the data taken in our experiments, so that the values taken can be justified only by the final answer. Fortunately, highly accurate values are not necessary in this particular set of computations. The sources of data are indicated in the table.

Table XVIII tabulates the calculations of the corrective factors for the gases neon and xenon. It is quite evident from the analysis of the gases in Table XVI that no appreciable leakage into the system occurred for the krypton experiments, so that no correction is required for this gas. The correction factors computed must divide the experimental results to obtain final corrected results.

We have neglected any effect of possible impurities in nitrogen and argon. This is justified for two reasons. First, the gas chamber was supplied with nitrogen or argon directly from the pressurized tank, so that the filling system up to the inlet valve of the chamber





Table XVI.

Impurities in Volume Percent in Gases, As

Determined by Mass Spectrograph

Impurity	Primary Gas		
	Neon	Krypton	Xenon
H <sub>2</sub> O	2.72%	-	0.02%
N <sub>2</sub>	8.15	0.16%	3.73
O <sub>2</sub>	1.11	.011	.72
A	.102	-	.017
CO <sub>2</sub>	.59	.005	-
Kr	1.19	-	.172
Ne	-	.026	.07

Table XVII.

Approximate Values of Atomic and Molecular Stopping  
Power of Various Gaseous Constituents for Protons at  
Energies of 500 and 1000 kev

Atom or Molecule	Atomic Stopping Power (ev-cm <sup>2</sup> x 10 <sup>15</sup> )		Molecular Stopping Power (ev-cm <sup>2</sup> x 10 <sup>15</sup> )		Ref.
	500 kev	1000 kev	500 kev	1000 kev	
H	1.1	0.6	2.2	1.2	(2)
C	7.25	4.35	-	-	(2)
N	8.0	4.9	16.0	9.8	(1)
O	8.8	5.5	17.6	11.0	(3)
Ne	10.1	6.45	10.1	6.45	(3)
A	14.4	9.8	14.4	9.8	(1)
Kr	21.1	14.2	21.1	14.2	(1)
Xe	24.2	16.25	24.2	16.25	(1)
H <sub>2</sub> O	-	-	11.0	6.7	(4)
CO <sub>2</sub>	-	-	24.85	15.35	(4)

- (1) Estimated from preliminary results, present research.
- (2) Extrapolation from data given by Livingston and Bethe (1937).
- (3) Interpolated value, according to atomic number, from values obtained by references (1) and (2).
- (4) Obtained by addition of atomic stopping powers.



Table XVIII.

Computation of Impurity Correction Factors, to Convert Experimentally  
Determined Atomic Stopping Power to the Correct Value - Valid for  
Protons of 500 and 1000 kev .

Molecule	$\sigma_{\text{mol}}$ ( $\times 10^{15}$ )		Relative $\sigma_{\text{mol}}$		Vol. %	(Vol.%) $\times$ (Rel. $\sigma$ )	
	500 kev	1000 kev	500 kev	1000 kev		500 kev	1000 kev
(a) Neon							
Neon	10.1	6.45	1.00	1.00	86.15	86.15	86.15
H <sub>2</sub> O	11.0	6.7	1.09	1.04	2.7	2.94	2.81
N <sub>2</sub>	16.0	9.8	1.58	1.52	8.15	12.9	12.4
O <sub>2</sub>	17.6	11.0	1.74	1.70	1.1	1.91	1.87
A	14.4	9.8	1.43	1.52	.1	.14	.15
CO <sub>2</sub>	24.85	15.35	2.46	2.38	.6	1.48	1.43
Kr	21.1	14.2	2.09	2.20	1.2	2.51	2.64
					<u>100.0</u>	<u>103.03</u>	<u>107.45</u>
(b) Xenon							
Xenon	24.2	16.25	1.00	1.00	95.3	95.3	95.3
Ne	10.1	6.45	.42	.40	.1	.04	.04
N <sub>2</sub>	16.0	9.8	.66	.60	3.7	2.44	2.22
O <sub>2</sub>	17.6	11.0	.73	.68	.7	.51	.48
Kr	21.1	14.2	.87	.87	.2	.17	.17
					<u>100.0</u>	<u>98.46</u>	<u>98.21</u>

Summary: To correct experimental data, divide by factors:

Prime Stopping Substance	Proton Energy	
	500 kev	1000 kev
Neon	1.080	1.075
Xenon	.985	.982



was under a positive pressure relative to atmospheric. This prevented inward leaking of air, so that most of the impurities present could be attributed to those originally present in the gas containers purchased. In regard to these original impurities, we note that the percentage allowed is small. Furthermore such impurities are primarily air constituents. Table XVII shows that the molecular stopping power of nitrogen, oxygen, and argon are all very close together, so that small amounts of one gas in the other as impurity would have an extremely small effect on stopping power.

#### 6. Possible Errors Due to Air Leakage During Experiment.

It was discovered during most of the experiments on the gases that the gas chamber pressure increased slowly, by varying amounts at different times. At the worst, this change amounted to about 25% of the initial pressure. This indicated a leak of some kind into the gas system during operation. Continual monitoring of the pressure indicated that such leaking occurred at a fairly constant rate for a single filling, although the rate varied from one day to the next. The errors due to such leaking could be allowed for therefore, provided the type of gas leaking were known. It might be possible that the leakages were either of air, or of the gas being studied, through the filling system. The possibility also existed that a combination of both effects in unknown proportions occurred.

Great precautions were taken to reduce this effect to a minimum, and frequent observation was made on the rate of leakage into the chamber with no gas present. Except for a couple of times when definite air-leakage was shown (data taken on these days showed radi-



cal departures from other data on the same gas, and were discarded), no appreciable pressure change was discovered in the evacuated and closed gas chamber over periods of several hours duration.

Despite these checks for air leaks, the effect persisted during periods that gases being studied were in the system. After some discussion with other persons in the departments of physics and chemistry who worked with high vacuums, it was concluded that the effect was due to the entrapment of minute bubbles of gas in the stop-cock grease at the stop-cock which occurred during the filling process. Such bubbles gradually traveled to the low pressure port and discharged the gas into the chamber. The prominence of such effect depends upon many factors - type of stop-cock used, type of vacuum grease used, amount of vacuum grease applied, pressure with which the valve of the stop-cock is forced onto its seat. It is concluded that the main difficulty was due to use of a type of grease used for ordinary chemical applications, but not especially suited for high vacuum work. For future workers, Apiezon, Type II, grease, applied strictly in accordance with instructions on the label and in sparing quantities, is recommended.

Notwithstanding the failure to reduce the effect of pressure change to zero, the experiments made and precautions taken insured that a negligible proportion was due to air leakage. All that is necessary for our analysis is to know the precise value of gas pressure in the chamber at the time that a resonance peak is measured. Since the pressure in the system at various times during the sequence of runs was recorded, and followed very closely a linear





change with time, pressures and variables dependent upon time can be determined through a simple linear formula for each gas filling. These formulas will be given in the compilation of data where they apply.

## B. Stopping Power Results - Foils.

### 1. Determination of Energy of Displaced Peaks, Foils Inserted.

Tables XIX and XX show the tabulated data and results of determination of displaced peak energy values ( $E_0'$ ). The values of  $I'$ , the displaced peak position on a magnet current scale, are given by the yield plots (Figure 8(b), for example). The values of  $E_0'$  are then determined from the calibration curves (Figure 9). The proper calibration curve to use on any particular day is determined by one or more calibration points taken in the same sequence of runs. This is discussed in detail in Section III.H, above.

### 2. Computation of Foil Stopping Power.

Tables XXI and XXII indicate in tabulated form the computations for stopping power of nickel and copper, respectively. The definitions and methods of computing the variables specified in the column headings are already completely set forth. Stopping power is computed both in the "experimental" units and also, as atomic stopping power, in those units closer to basic theory. A column is provided for tabulation of values of  $\sigma/z^{1/3}$ . Since Bohr's theory for stopping of slow particles in heavy media provides that stopping power is proportional to  $z^{1/3}$  (Equation I-B-74), such a tabulation gives a better means of comparing the results of stopping power ex-



Table XIX.

Determination of Shifted Resonance Peak Positions in the Energy Spectrum, with Various Nickel Foils Inserted into the Proton Beam.

Foil	Date*	E <sub>0</sub> (Mev)	Shifted Peak Position			
			I' (amp)	log I'	#log E' <sub>0</sub>	E' <sub>0</sub> (Mev)
.05mil Ni-1	8-29-52	.6714	.7848	$\bar{1}.8948$	$\bar{1}.9241$	.8397
"	"	.8756	.8696	$\bar{1}.9393$	0.0115	1.0268
"	9-26-52	.9875	.9150	$\bar{1}.9614$	0.0517	1.1264
.05mil Ni-2	1-19-53	.6696	.7908	$\bar{1}.8981$	$\bar{1}.9245$	.8404
"	"	.8740	.8776	$\bar{1}.9433$	0.0107	1.0249
"	"	.9358	.9015	$\bar{1}.9550$	0.0330	1.0790
##	1-21-53	.6696	.7955	$\bar{1}.9006$	$\bar{1}.9274$	.8461
##	"	.8740	.8823	$\bar{1}.9456$	0.0130	1.0304
##	"	.9358	.9075	$\bar{1}.9578$	0.0360	1.0864
.04 mil Ni	10-16-52	.6714	.7720	$\bar{1}.8876$	$\bar{1}.9084$	.8098
"	"	.8756	.8620	$\bar{1}.9355$	0.0027	1.0062
"	"	.9374	.8860	$\bar{1}.9474$	0.0261	1.0619
"	10-17-52	.6319	.7560	$\bar{1}.8785$	$\bar{1}.8905$	.7771
"	"	.9875	.9069	$\bar{1}.9576$	0.0435	1.1053
"	10-23-52	.4441	.6681	$\bar{1}.8248$	$\bar{1}.7870$	.6123
##	10-28-52	.9374	.8868	$\bar{1}.9478$	0.0270	1.0641
##	10-31-52	.9374	.8870	$\bar{1}.9479$	0.0283	1.0673
.04 mil Ni	12-19-52	.9875	.9145	$\bar{1}.9612$	0.0440	1.1066
"	1-9-53	.6696	.7765	$\bar{1}.8901$	$\bar{1}.9080$	.8091
"	"	.8740	.8650	$\bar{1}.9370$	$\bar{1}.9986$	.9968
.03 mil Ni	1-22-53	.6696	.7519	$\bar{1}.8762$	$\bar{1}.8840$	.7656
"	"	.8740	.8427	$\bar{1}.9257$	$\bar{1}.9805$	.9561
"	"	.9358	.8707	$\bar{1}.9399$	0.0079	1.0184

Notes: \* The dates not only serve to identify the various sets of data extracted from plotted yield curves, but also indicate the proper calibration curve to use (Fig.9).

# Obtained from calibration curves (Fig. 9), with use of Tables XIV and XV.

## Appreciable carbon accumulation indicated.



Table XX.

Determination of Shifted Resonance Peak Positions in the Energy Spectrum, with Various Copper Foils Inserted in the Proton Beam.

Foil	Date	$E_0$ (Mev)	Shifted Peak Position			
			$I'$ (amp)	$\log I'$	$\log E_0$	$E_0'$ (Mev)
.05 mil Cu	12-2-52	.3507	.6310	$\bar{1}.8000$	$\bar{1}.7372$	.5460
"	"	.6763	.7860	$\bar{1}.8954$	$\bar{1}.9215$	.8346
"	"	.8799	.8735	$\bar{1}.9413$	0.0080	1.0186
"	"	.9415	.8970	$\bar{1}.9528$	0.0298	1.0710
"	12-3-52	.6319	.7705	$\bar{1}.8868$	$\bar{1}.8996$	.7936
"	"	.9875	.9212	$\bar{1}.9644$	0.0485	1.1182
"	12-18-52	.4419	.6760	$\bar{1}.8299$	$\bar{1}.7956$	.6246
# "	"	.6696	.7834	$\bar{1}.8940$	$\bar{1}.9188$	.8295
# "	"	.8740	.8710	$\bar{1}.9400$	0.0073	1.0170
# "	"	.9358	.8960	$\bar{1}.9523$	0.0307	1.0732
# "	1-12-53	.6696	.7860	$\bar{1}.8954$	$\bar{1}.9203$	.8323
# "	" (pm)	.6696	.7855	$\bar{1}.8951$	$\bar{1}.9210$	.8337
0.1 mil Cu	1-22-53	.4419	.7580	$\bar{1}.8797$	$\bar{1}.8877$	.7721
"	"	.6696	.8485	$\bar{1}.9287$	$\bar{1}.9819$	.9592
"	"	.8735	.9214	$\bar{1}.9644$	0.0515	1.1259

# Appreciable carbon accumulation indicated.

See also the notes in Table XIX.





Table XXI (Two Pages)

Stopping Power Computation for Nickel

Line	Foil Number	Foil Thickness (mg/cm <sup>2</sup> )	E <sub>0</sub> (kev)	E <sub>0</sub> (kev)	Δ E (kev)	E <sub>a</sub> (kev)
1	.05mil Ni-1	1.150	671.4	839.7	168.3	755.6
2	"	"	875.6	1026.8	151.2	951.2
3	"	"	987.5	1126.4	138.9	1057.0
4	.05mil Ni-2	1.175	669.6	840.4	170.8	755.0
5	"	"	874.0	1024.9	150.9	949.4
6	"	"	935.8	1079.0	143.2	1007.4
<sup>##</sup> 7	"	"	669.6	846.1	176.5	757.8
<sup>##</sup> 8	"	"	874.0	1030.4	156.4	952.2
<sup>##</sup> 9	"	"	935.8	1086.4	150.6	1011.1
10	.04 mil Ni	0.977	671.4	809.8	138.4	740.6
11	"	"	875.6	1006.2	130.6	940.9
12	"	"	937.4	1061.9	124.5	999.6
13	"	"	631.9	777.1	145.2	704.5
14	"	"	987.5	1105.3	117.8	1046.4
15	"	"	444.1	612.3	168.2	528.2
<sup>##</sup> 16	"	"	937.4	1064.1	126.7	1000.8
<sup>##</sup> 17	"	"	937.4	1067.3	129.9	1002.4
18	.04 mil Ni	0.977	987.5	1106.6	119.1	1047.0
19	"	"	669.6	809.1	139.5	739.4
20	"	"	874.0	996.8	122.8	935.4
21	.03 mil Ni	0.640	669.6	765.6	96.0	717.6
22	"	"	874.0	956.1	82.1	915.0
23	"	"	935.8	1018.4	82.6	977.1

<sup>##</sup> Appreciable carbon accumulation indicated.



Table XXI. (Concl.)

Stopping Power Computation for Nickel

Line	$\delta E$ (kev)	$E_m$ (kev)	Stopping Power (kev-cm <sup>2</sup> /mg)	# $\sigma$ , At. Stpg. Power (ev-cm <sup>2</sup> )	# $\sigma/Z^{1/3}$	Prob. Error, %
1	negl.	757	146.3	14.27	4.70	1.5
2	"	951	131.5	12.51	4.12	2.0
3	"	1057	120.7	11.77	3.88	2.0
4	"	755	149.3	14.18	4.67	1.5
5	"	949	128.3	12.51	4.12	2.0
6	"	1007	121.9	11.88	3.91	2.0
7	Carbon accumulation renders invalid.					
8	"	"	"	"		
9	"	"	"	"		
10	negl.	741	141.7	13.80	4.55	2.0
11	"	941	133.7	13.02	4.29	2.0
12	"	1000	127.4	12.42	4.09	2.0
13	"	704	148.7	14.48	4.77	2.0
14	"	1046	120.4	11.74	3.87	2.5
15	1.2	527	172.0	16.78	5.52	1.5
16	Carbon accumulation renders invalid.					
17	"	"	"	"		
18	ngl.	1047	122.0	11.89	3.92	2.5
19	"	739	142.8	13.91	4.58	2.0
20	"	935	125.7	12.25	4.04	2.0
21	"	718	150.0	14.62	4.81	3.0
22	"	915	128.2	12.50	4.12	3.0
23	"	977	129.0	12.57	4.14	3.0

<sup>#</sup>/<sub>17</sub> Values tabulated in these columns to be multiplied by 10<sup>-15</sup>.



Table XXII. (Two Pages)

Stopping Power Computation for Copper

Line	Foil Number	Foil Thickness (mg/cm <sup>2</sup> )	E <sub>0</sub> (kev)	E' <sub>0</sub> (kev)	ΔE (kev)	E <sub>a</sub> (kev)
1	.05 mil Cu	1.155	350.7	546.0	195.3	448.4
2	"	"	676.3	834.6	158.3	755.5
3	"	"	879.9	1018.6	138.7	949.2
4	"	"	941.5	1071.0	129.5	1006.2
5	"	"	631.9	793.6	161.7	712.8
6	"	"	987.5	1118.2	130.7	1049.6
7	"	"	441.9	624.6	182.7	533.2
# 8	"	"	669.6	829.5	159.9	749.6
# 9	"	"	874.0	1017.0	143.0	945.5
#10	"	"	935.8	1073.2	137.4	1004.5
#11	"	"	669.6	832.3	162.7	751.0
#12	"	"	669.6	833.7	164.1	751.6
13	0.1 mil Cu	2.20	441.9	772.1	330.2	607.0
14	"	"	669.6	959.2	289.6	814.4
15	"	"	873.5	1125.9	252.4	997.8

# Appreciable carbon accumulation indicated.



Table XXII. (Concl.)

Stopping Power Computation for Copper

Line	$\delta E$ (kev)	$E_m$ (kev)	Stopping Power (kev-cm <sup>2</sup> /mg)	# $\sigma$ , At. Stpg. Power (ev-cm <sup>2</sup> )	# $\sigma/Z^{1/3}$	Prob. Error, %
1	1.9	446	169.0	17.86	5.815	1.5
2	negl.	755	137.0	14.48	4.715	2.0
3	"	949	120.0	12.68	4.13	2.0
4	"	1006	112.0	11.83	3.85	2.0
5	"	713	139.9	14.78	4.81	1.5
6	"	1050	113.1	11.95	3.89	2.0
7	1.4	532	158.0	16.70	5.44	1.5
8	Carbon accumulation renders invalid.					
9	"	"	"	"		
10	"	"	"	"		
11	"	"	"	"		
12	"	"	"	"		
13	4.1	603	150.1	15.87	5.165	1.5
14	2.4	812	131.6	13.90	4.525	1.5
15	1.4	996	114.7	12.11	3.94	1.5

# Values tabulated in these columns to be multiplied by  $10^{-15}$ .





periments on different elements.

### 3. Discussion of Errors in Experimental Data and Results.

Probable errors in the individual values of stopping power obtained are difficult to judge accurately, but even an approximate idea of such deviations would be useful.

Values obtained from the literature for the resonance energy values used are probably correct to about  $\pm 1$  kev on the average. Some are known with better accuracy, since they are quoted to tenths of a kev. Many other peak values are determined in relation to those few peaks whose energy have been accurately obtained by absolute methods, and thus their error may be much larger. The value of 1 kev is considered a rough average for all those used herein.

Errors in target thickness are likely to be of the same order of magnitude. However, although such errors affect the values taken for  $E_0$ , they cause at the same time an erroneous shift in the calibration curve used which introduces an error of the same order of magnitude in the value of  $E_0'$ . Thus for  $\Delta E$ , these two errors largely cancel. We will therefore neglect such errors.

The important errors to be considered in  $E_0'$  are due to error in obtaining the proper value of  $I'$  (value of shifted peak position in the magnet current spectrum) and to an error in choice of the calibration curve used. In regard to the former it must be noted that the stopping phenomenon not only shifts the peak but also broadens it, so that the position of the maximum point is more difficult to estimate. Whereas the undeviated peak can be judged to an accuracy of about 0.1 milliamperes, or about 0.2 kev, the deviated peak has a



greater probable error - probably on the order of 1 kev.

In regard to the error from calibration inaccuracies, let us refer to Section III.H wherein a typical value of probable error is about 1.7 kev by use of the mean curve. We can improve on this, however, since we determine one or more calibration points during a given day's sequence of operations. A value of 1 kev should be about the proper value for this error.

Summarizing the above, we see that the probable error in  $E_0'$  is about 1.4 kev and about 1 kev for  $E_0$ , so that the probable error from the difference of these two is about 1.7 kev. We feel it necessary to add to this an estimate for surface impurities, primarily carbon, of about 1.4 kev (see Section IV.A.3.). This gives a final probable error in  $\Delta E$  of about 2.2 kev.

The percentage error which this figure provides depends on the value of  $\Delta E$ . Reference to Tables XXI and XXII indicates that the probable error varies from 0.7% for thick foils and low proton energies to 2.7% for thin foils and high proton energies. To take into account the possible increase in path length at low energies, let us raise the lower figure to 1 kev.

It has already been shown in Section III.B. that the probable error in foil thicknesses is about 1.1%. This means that the probable error in values for foil stopping power varies between 1.5% and 3%. Tables XXI and XXII tabulate the estimates of probable error for individual values of stopping power.

It must be emphasized that the probable errors given are based on the assumption of all errors conforming to the Gaussian theory of



# ENERGY LOSS PROTONS THRU FOILS

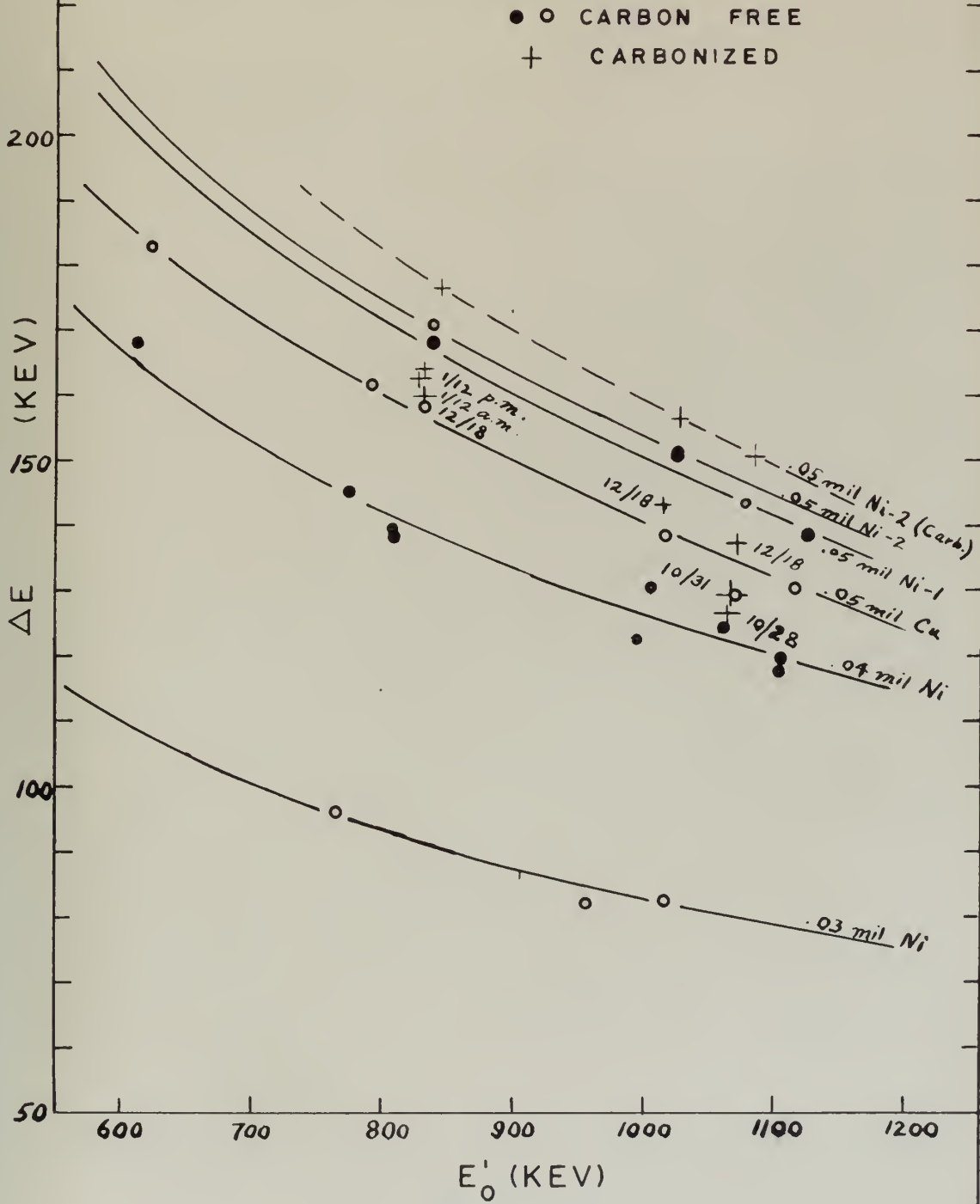


FIG. 10





errors, with positive and negative errors equally likely. Furthermore this analysis does not guarantee that unknown errors of either a consistent or random nature have not caused the tabulated values of probable error to be less than they should be.

### C. Stopping Power Results - Gases.

#### 1. Energy Loss in Window Foils.

It is evident that in obtaining the energy loss through the gas in the chamber, it is necessary not only to subtract  $E_0$  from  $E_0'$ , but from this difference to subtract the energy loss in the window foil (Equation II-B-9). Since for windows we used the same foils on which the stopping power measurements were made, we can determine the value of window foil energy loss,  $\Delta E_F$ , by making use of a chart whereon is drawn for each foil used a curve showing foil energy loss versus proton energy at the foil entrance,  $E_0'$ . Using the data provided in Table XXI and XXII, this can be readily accomplished. Figure 10 gives these curves. It should be noted that certain points are plotted which indicate clearly the effect of carbon accumulation. Such data enable one to make a better estimate of  $\Delta E_F$  so as to include carbonizing when appropriate.

#### 2. Energy of Displaced Peaks, Gases and Window Foils Inserted.

These values are determined precisely as they are for the case of foils alone (Section IV.B.1). Tables XXIII-XXVII, inclusive, show this determination.

#### 3. Determination of the Formula for Atomic Stopping Power of Gases.

The fundamental conversion formulas for stopping power have al-



ready been evaluated. It is necessary however to develop a formula which will give atomic stopping power as a function of gas temperature (T), pressure (p), and beam energy loss. The other factor, path distance, is already known from measurement of the length of the gas chamber (Figure 4). This distance,  $\Delta x$ , is 10.56 cm. From Section I.A., we see that

$$\sigma \text{ (ev-cm}^2\text{)} = \frac{10^3}{N} \cdot \frac{\Delta E}{10.56} , \quad (\text{IV-C-1})$$

where  $\Delta E$  is measured in kev.

The gas pressures used are so low that the ideal gas relations are sufficiently accurate for our purposes. Then, under standard conditions,

$$N_{\text{STP}} = \frac{6.023 \times 10^{23}}{22,414} \cdot n , \quad (\text{IV-C-2})$$

where n is the number of atoms per molecule of the gas considered. Furthermore,

$$N = \frac{p}{76} \frac{273}{T} \cdot N_{\text{STP}} , \quad (\text{IV-C-3})$$

where p is measured in centimeters of mercury, and T is measured in degrees Kelvin.

Combination of the above formula gives the relation sought:

$$\left. \begin{aligned} \sigma &= G \cdot \Delta E , \\ \text{where } G &= \frac{T}{1.021 \times 10^{18} \cdot p \cdot n} \end{aligned} \right\} \quad (\text{IV-C-4})$$

Since p and T are functions of time (Section IV.A.6), it is possible to determine G as a function of time for each gas filling. Table



Table XXIII.

Determination of Shifted Resonance Peak Positions in the  
Energy Spectrum, with Nitrogen Gas and Window Foil Inserted  
in the Beam.

Window Foil	Date	$E_0$ (Mev)	Shifted Peak Position			
			$I'$ (amp)	$\log I'$	* $\log E'_0$	$E'_0$ (Mev)
.04 mil Ni	10-27-52	.3438	.6820	$\bar{1}.8338$	$\bar{1}.8040$	.6368
"	"	.4441	.7237	$\bar{1}.8596$	$\bar{1}.8543$	.7150
"	"	.6006	.7846	$\bar{1}.8946$	$\bar{1}.9225$	.8366
"	"	.6714	.8132	$\bar{1}.9102$	$\bar{1}.9525$	.8964
"	"	.8756	.8936	$\bar{1}.9511$	0.0318	1.0760
"	"	.9374	.9164	$\bar{1}.9621$	0.0533	1.1306
.04 mil Ni	10-28-52	.3438	.6852	$\bar{1}.8358$	$\bar{1}.8085$	.6434
"	"	.4441	.7255	$\bar{1}.8606$	$\bar{1}.8563$	.7183
"	"	.6006	.7856	$\bar{1}.8952$	$\bar{1}.9234$	.8383
"	"	.6714	.8150	$\bar{1}.9112$	$\bar{1}.9544$	.9003
"	"	.8756	.8940	$\bar{1}.9513$	0.0321	1.0767
"	"	.9374	.9168	$\bar{1}.9623$	0.0535	1.1311
.03 mil Ni	1-23-53	.3413	.7050	$\bar{1}.8482$	$\bar{1}.8295$	.6753
"	"	.4419	.7413	$\bar{1}.8700$	$\bar{1}.8716$	.7440
"	"	.6696	.8269	$\bar{1}.9175$	$\bar{1}.9622$	.9166
"	"	.8740	.9045	$\bar{1}.9544$	0.0368	1.0884
"	"	.9358	.9279	$\bar{1}.9675$	0.0580	1.1429

\* Obtained from calibration curves (Fig. 9), with the use of Tables XIV and XV.



Table XXIV.

Determination of Shifted Resonance Peak Positions in the  
Energy Spectrum, with Argon Gas and Window Foil Inserted  
in the Beam.

Window Foil	Date	$E_0$ (Mev)	Shifted Peak Position			
			$I'$ (amp)	$\log I'$	$^* \log E_0$	$E_0'$ (Mev)
.04 mil Ni	10-29-52	.3438	.7492	$\bar{1}.8746$	$\bar{1}.8837$	.7651
"	"	.4441	.7852	$\bar{1}.8950$	$\bar{1}.9238$	.8391
"	"	.6006	.8427	$\bar{1}.9257$	$\bar{1}.9840$	.9638
"	"	.6714	.8668	$\bar{1}.9379$	0.0077	1.0179
"	"	.8756	.9370	$\bar{1}.9717$	0.0740	1.1858
.04 mil Ni	10-30-52	.3438	.6978	$\bar{1}.8437$	$\bar{1}.8235$	.6660
"	"	.4441	.7415	$\bar{1}.8701$	$\bar{1}.8750$	.7499
"	"	.6006	.7990	$\bar{1}.9025$	$\bar{1}.9385$	.8680
"	"	.8756	.9054	$\bar{1}.9568$	0.0450	1.1092
"	"	.9374	.9280	$\bar{1}.9675$	0.0658	1.1636
.04 mil Ni	10-30-52 p.m.	.8756	.9080	$\bar{1}.9581$	0.0474	1.1153

\* Obtained from calibration curves (Fig. 9), with use of Tables XIV and XV.





Table XXV.

Determination of Shifted Resonance Peak Positions in the  
Energy Spectrum, with Neon Gas and Window Foil Inserted in  
the Beam.

Window Foil	Date	$E_0$ (MeV)	Shifted Peak Position			
			$I'$ (amp)	$\log I'$	$*\log E_0'$	$E_0'$ (MeV)
# .05mil Ni-2	1-20-53	.3413	.7164	$\bar{1}.8552$	$\bar{1}.8453$	.7003
"	"	.4419	.7572	$\bar{1}.8792$	$\bar{1}.8910$	.7780
"	"	.5986	.8180	$\bar{1}.9128$	$\bar{1}.9553$	.9022
"	"	.6696	.8440	$\bar{1}.9263$	$\bar{1}.9810$	.9572
"	"	.8740	.9210	$\bar{1}.9643$	0.0535	1.1311
"	"	.9358	.9452	$\bar{1}.9755$	0.0746	1.1874
# .05mil Ni-2	1-21-53	.3413	.7220	$\bar{1}.8585$	$\bar{1}.8475$	.7039
"	"	.4419	.7617	$\bar{1}.8818$	$\bar{1}.8921$	.7800
"	"	.6696	.8469	$\bar{1}.9278$	$\bar{1}.9802$	.9554
"	"	.8740	.9250	$\bar{1}.9661$	0.0535	1.1311
"	"	.9358	.9466	$\bar{1}.9762$	0.0725	1.1817

\* Obtained from calibration curves (Fig. 9), with the use of Tables XIV and XV.

# Foil was blackened by heavy carbon deposit during runs on 20 January. Target thickness was checked before use on 21 January (Figure 10).



Table XXVI.

Determination of Shifted Resonance Peak Positions in the  
Energy Spectrum, with Krypton Gas and Window Foil Inserted  
in the Beam.

Window Foil	Date	$E_0$ (Mev)	Shifted Peak Position			
			$I'$ (amp)	$\log I'$	* $\log E_0$	$E'_0$ (Mev)
.04 mil Ni	1-9-53	.4419	.7518	$\bar{1}.8761$	$\bar{1}.8818$	.7617
"	"	.5986	.8130	$\bar{1}.9101$	$\bar{1}.9472$	.8855
"	"	.6696	.8422	$\bar{1}.9254$	$\bar{1}.9765$	.9473
"	"	.8740	.9206	$\bar{1}.9641$	0.0515	1.1259
.05 mil Cu	1-12-53	.3413	.7070	$\bar{1}.8494$	$\bar{1}.8332$	.6811
"	"	.4419	.7492	$\bar{1}.8746$	$\bar{1}.8814$	.7610
"	"	.5986	.8110	$\bar{1}.9090$	$\bar{1}.9478$	.8867
"	"	.6696	.8404	$\bar{1}.9245$	$\bar{1}.9775$	.9495
"	"	.8740	.9170	$\bar{1}.9624$	0.0503	1.1228
"	"	.9358	.9394	$\bar{1}.9729$	0.0705	1.1762

\* Obtained from calibration curves (Fig. 9), with use of Tables XIV and XV.



Table XXVII.

Determination of Shifted Resonance Peak Positions in the  
Energy Spectrum, with Xenon Gas and Window Foil Inserted  
in the Beam.

Window Foil	Date	$E_0$ (Mev)	Shifted Peak Position			
			$I'$ (amp)	$\log I'$	$*\log E'_0$	$E'_0$ (Mev)
.05 mil Cu	1-14-53	.3413	.7270	$\bar{1}.8615$	$\bar{1}.8572$	.7198
"	"	.4419	.7728	$\bar{1}.8881$	$\bar{1}.9080$	.8091
"	"	.5986	.8268	$\bar{1}.9174$	$\bar{1}.9645$	.9215
"	"	.6696	.8561	$\bar{1}.9325$	$\bar{1}.9932$	.9845
"	"	.8740	.9292	$\bar{1}.9681$	0.0613	1.1516
.05 mil Ni-2	1-19-53	.3413	.7351	$\bar{1}.8663$	$\bar{1}.8635$	.7303
"	"	.4419	.7747	$\bar{1}.8891$	$\bar{1}.9073$	.8078
"	"	.5986	.8300	$\bar{1}.9191$	$\bar{1}.9647$	.9219
"	"	.6696	.8581	$\bar{1}.9335$	$\bar{1}.9923$	.9824
"	"	.8740	.9517	$\bar{1}.9785$	0.0791	1.1998

\* Obtained from calibration curves (Fig. 9), with use of Tables XIV and XV.





Table XXVIII. (Two Pages)

Computation of  $G(t)$  , a Factor Required in Computing Stopping Power of Gases (Equation IV-C-4).

Date	T° Abs., Initial: Final :	p (cm), Initial: Final :	* G, Initial: Final :	Hour, t, Initial: Final :	* G(t)
<u>(a) Nitrogen</u>					
10-27-52	298.5	2.02	72.3	-	72.3
	299.5	2.03	72.3		
10-28-52	297.4	2.076	70.1	9:45	70.1 - 0.847(t-9.25)
	298.9	2.20	66.5	14:00	
1-23-53	298.1	3.915	37.25	-	37.25
<u>(b) Argon</u>					
10-29-52	297.5	5.29	55.1	10:15	55.1 - 0.392(t-10.25)
	298.8	5.60	53.3	14:50	
10-30-52	297.8	3.10	94.0	12:30	94.0 + 0.20(t-12.5)
a.m.	299.2	3.09	94.8	16:30	
10-30-52	299.2	3.25	90.1	-	90.1
p.m.					
<u>(c) Neon</u>					
1-20-53	298.0	4.685	62.25	13:27	62.25 - 0.925(t-13.45)
	298.2	4.815	60.6	15:14	
1-21-53	298.0	4.28	68.2	11:05	68.2
	298.0	4.39	66.4	11:25	66.4
	298.0	4.515	64.6	13:10	64.6
	298.5	4.85	60.25	14:00	60.25
	298.5	4.86	60.1	14:10	60.1

\* Values tabulated are to be multiplied by  $10^{-18}$  .



Table XXVIII. (Concl.)

Date	T <sup>o</sup> Abs., Initial: Final :	p (cm), Initial: Final :	* G, Initial: Final :	Hour, t, Initial: Final :	* G(t)
<u>(d) Krypton</u>					
1-9-53	297.5	2.183	133.4	13:55	133.4-0.85(t-13.916)
	298.5	2.675	109.3	16:45	
1-12-53	298.0	2.097	142.0	13:00	142.0 - 4.16(t-13.0)
	298.5	2.27	131.6	15:30	
<u>(e) Xenon</u>					
1-14-53	298.5	2.183	133.9	10:30	133.9 - 12(t-10.5)
	299.0	2.482	117.9	11:50	
1-19-53	298.5	2.204	132.7	13:33	132.7-12.84(t-13.55)
	298.0	2.482	117.5	14:44	
1-19-53	298.4	3.36	87.0	16:00	87.0

\* Values tabulated are to be multiplied by  $10^{-18}$  .



XXVIII shows the values of  $G(t)$  for each sequence of runs in studying gas stopping power.

#### 4. Computation of Gas Stopping Power.

Tables XXIX through XXXIII, inclusive, give the computations in tabulated form for stopping power of the gases nitrogen, argon, neon, krypton, and xenon. The various factors involved have already been fully defined and explained. The results are expressed in the same units as the foil stopping power, and with the same end in view. (See Section IV.B.2)

#### 5. Discussion of Errors in Gas Stopping Power Results.

As in the case with the foils, we should expect the probable error in position of the undeviated peak to be on the order of 1 kev. Errors in the value of the shifted peak are, as before, about 1.4 kev. We have to subtract from the energy shift the energy loss in the window foil. The values of the curves plotted in Figure 10 are correct to roughly 2 kev, and an additional 1.5 kev variation in the stopping power of the carbon film is estimated. These probable errors combine statistically to give an over-all probable error in  $\Delta E$  of about 3 kev. This amounts to about 1% for large values of  $\Delta E$  and up to 4% for the smallest values of energy loss in the gas.

The probable error in pressure readings is estimated to be 1%, and the uncertainty in the quality and quantity of impurities, though doubtful, is taken to cause probable errors in stopping power of about 1% for nitrogen and argon, and about 2% for the rarer gases.



Table XXIX. (Three Pages)

Computation of Stopping Power of Nitrogen ( $\frac{1}{2}N_2$ )

Line	Foil	Date	Time	$E_0$ (kev)	* $\Delta E_F$ (kev)	$E_3$ (kev)
1	.04 mil Ni	10-27-52	11:00	636.8	164.5	472.3
2	"	"	12:30	715.0	154.5	560.5
3	"	"	13:45	836.6	141.0	695.6
4	"	"	15:00	896.4	136.5	759.9
5	"	"	16:00	1076.0	124.0	952.0
6	"	"	17:00	1130.6	120.0	1010.6
7	.04 mil Ni	10-28-52	10:30	643.4	165.5	477.9
8	"	"	11:15	718.3	155.5	562.8
9	"	"	12:15	838.3	142.5	695.8
10	"	"	13:00	900.3	137.5	762.8
11	"	"	13:30	1076.7	125.0	951.7
12	"	"	14:00	1131.1	121.5	1009.6
13	.03 mil Ni	1-23-53	13:50	675.3	102.5	572.8
14	"	"	14:05	744.0	97.5	646.5
15	"	"	14:20	916.6	86.5	830.1
16	"	"	14:40	1088.4	79.0	1009.4
17	"	"	14:55	1142.9	77.0	1065.9

\* Allowance made for slight carbonization of foil on 27 and 28 October (Figure 10).





Table XXIX. (Cont.)

Line	$E_o$ (kev)	$\Delta E =$ $E'_3 - E_o$ (kev)	$E_a =$ $\frac{1}{2}(E_o + E'_3)$ (kev)	$\delta E$ (kev)	$E_m$ (kev)	Correction Factor for Impurities (Divide)
1	343.8	128.5	408.0	negl.	406	1.0
2	444.1	116.4	502.3	"	501	"
3	600.6	95.0	648.1	"	648	"
4	671.4	88.5	715.6	"	716	"
5	875.6	76.4	913.8	"	914	"
6	937.4	73.2	974.0	"	974	"
7	343.8	134.1	410.8	1.0	409	"
8	444.1	118.7	503.4	negl.	502	"
9	600.6	95.2	648.2	"	648	"
10	671.4	91.5	717.1	"	717	"
11	875.6	76.1	913.6	"	914	"
12	937.4	72.2	973.5	"	973	"
13	341.3	231.5	457.0	2.7	452	"
14	441.9	204.6	544.2	1.8	541	"
15	669.6	160.5	749.8	negl.	748	"
16	874.0	135.4	941.7	"	942	"
17	935.8	130.1	1000.8	"	1001	"

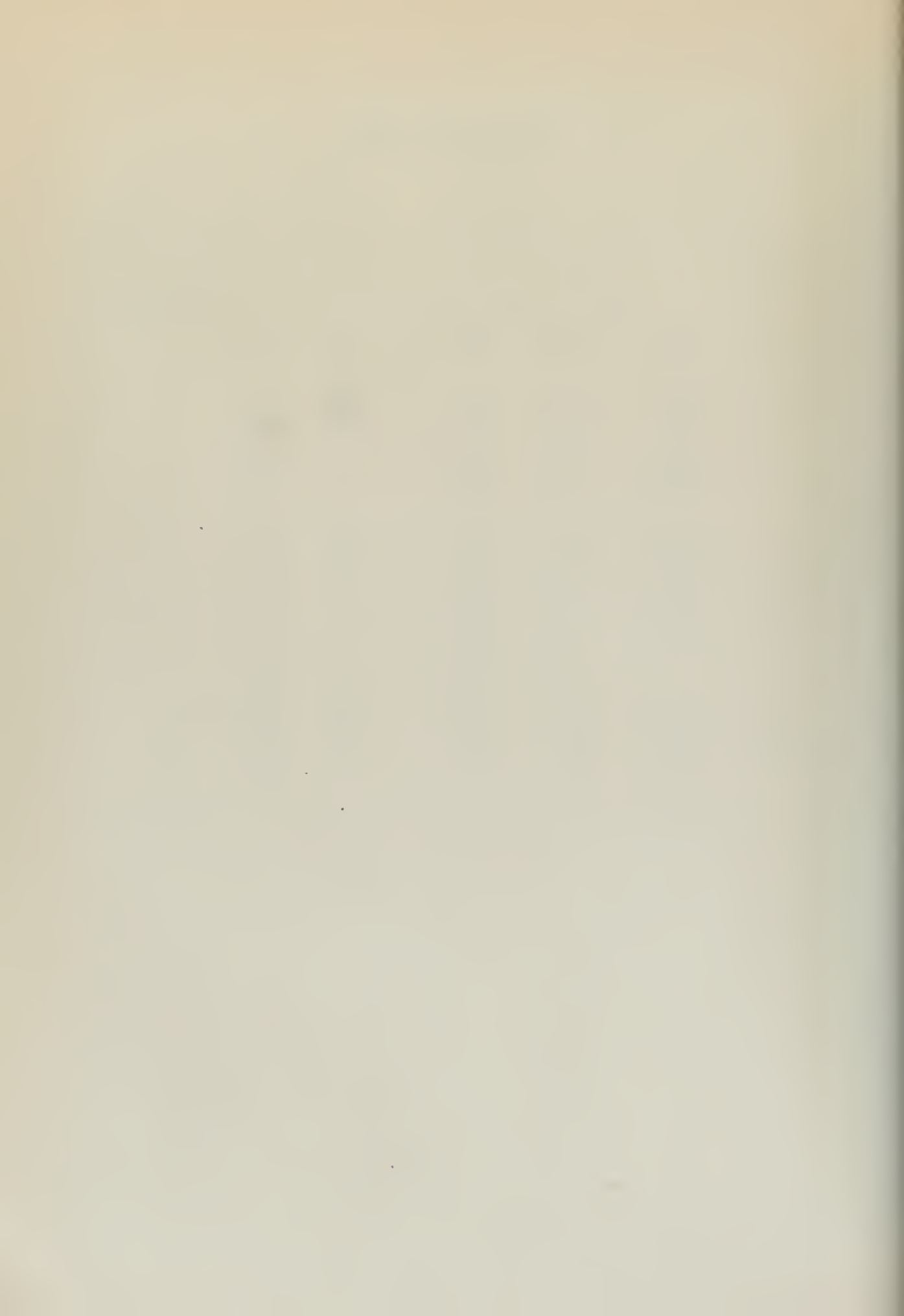


Table XXIX. (Concl.)

Line	Corrected $\Delta E$ (kev)	* G (Multip.)	<sup>#</sup> $\sigma$ , At. Stopping	<sup>#</sup> $\sigma/Z^{1/3}$	Stopping Power (kev-cm <sup>2</sup> /mg)	Prob. Error, %
1	128.5	72.3	9.30	4.86	400	4.0
2	116.4	"	8.42	4.40	362	4.0
3	95.0	"	6.87	3.59	296	4.5
4	88.5	"	6.40	3.34	275	4.5
5	76.4	"	5.53	2.89	238	4.5
6	73.2	"	5.30	2.77	228	4.5
7	134.1	69.5	9.32	4.87	401	4.0
8	118.7	68.8	8.16	4.26	351	4.0
9	95.2	68.0	6.47	3.38	278	4.0
10	91.4	67.3	6.15	3.21	264	4.5
11	76.1	66.9	5.09	2.66	219	4.5
12	72.2	66.5	4.80	2.51	207	4.5
13	231.5	37.25	8.62	4.50	371	2.5
14	204.6	"	7.62	3.98	328	3.0
15	160.5	"	5.98	3.12	257	3.5
16	135.4	"	5.05	2.64	217	3.5
17	130.1	"	4.85	2.53	209	4.0

\* Data in this column to be multiplied by  $10^{-18}$  .

<sup>#</sup> Data in these columns to be multiplied by  $10^{-15}$  .



Table XXX. (Two Pages)

Computation of Stopping Power of Argon

Line	Foil	Date	Time	$E_0'$ (kev)	$^*\Delta E_F$ (kev)	$E_3'$ (kev)
1	.04 mil Ni	10-29-52	10:30	765.1	152.0	613.1
2	"	"	11:15	839.1	144.5	694.6
3	"	"	12:30	963.8	134.5	829.3
4	"	"	13:00	1017.9	130.5	887.4
5	"	"	14:00	1185.8	120.0	1065.8
6	"	10-30-52	13:15	666.0	164.5	501.5
7	"	"	14:00	749.9	154.5	595.4
8	"	"	14:45	868.0	144.0	724.0
9	"	"	15:30	1109.2	126.0	983.2
10	"	"	16:00	1163.6	122.5	1041.1
11	"	" (pm)	17:30	1115.3	126.0	989.3

\* Allowance is made for moderate carbonization of the window foil (Figure 10).

Line	$E_0$ (kev)	$\Delta E = E_3 - E_0$ (kev)	$E_a = \frac{1}{2}(E_0 + E_3)$ (kev)	$\delta E$ (kev)	$E_m$ (kev)	Correction Factor for Impurities (Divide)
1	343.8	269.3	478.4	2.8	476	1.0
2	444.1	250.5	569.3	2.5	567	"
3	600.6	228.7	714.9	1.7	713	"
4	671.4	216.0	779.4	1.4	778	"
5	875.6	190.2	970.7	negl.	971	"
6	343.8	157.7	422.6	1.3	421	"
7	444.1	151.3	519.7	1.0	519	"
8	600.6	123.4	662.3	negl.	662	"
9	875.6	107.6	929.4	"	929	"
10	937.4	103.7	989.2	"	989	"
11	875.6	113.7	932.4	negl.	932	"





Table XXX. (Concl.)

Line	Corrected $\Delta E$ (kev)	* G (Multip.)	# $\sigma$ , At. Stopping Power	# $\sigma/Z^{1/3}$	Stopping Power (kev-cm <sup>2</sup> /mg)	Prob. Error, %
1	269.3	55.0	14.81	5.66	224	2.0
2	250.5	54.7	13.71	5.24	207	2.5
3	228.7	54.2	12.39	4.73	187	2.5
4	216.0	54.0	11.66	4.45	176	2.5
5	190.2	53.6	10.20	3.89	154	3.0
6	157.7	94.2	14.87	5.68	224.5	3.5
7	151.3	94.3	14.28	5.45	215	3.5
8	123.4	94.5	11.67	4.45	176	4.0
9	107.6	94.6	10.19	3.89	154	4.0
10	103.7	94.7	9.82	3.75	148.5	4.0
11	113.7	90.1	10.24	3.91	155	4.0

\* Data in this column to be multiplied by  $10^{-18}$ .

# Data in these columns to be multiplied by  $10^{-15}$ .



Table XXXI. (Two Pages)

Computation of Stopping Power of Neon

Line	Foil	Date	Time	$E_0$ (kev)	* $\Delta E_F$ (kev)	$E_3$ (kev)
1	.05 mil Ni-2	1-20-53	13:35	700.3	190.0	510.3
2	"	"	13:55	778.0	179.0	599.0
3	"	"	14:15	902.2	165.5	736.7
4	"	"	14:30	957.2	160.0	797.2
5	"	"	14:50	1131.1	144.5	986.6
6	"	"	15:05	1187.4	140.0	1047.4
7	"	1-21-53	11:05	703.9	198.0	505.9
8	"	"	11:25	780.0	185.5	594.5
9	"	"	13:10	955.4	164.5	790.9
10	"	"	14:00	1131.1	146.0	985.1
11	"	"	14:10	1181.7	141.0	1040.7

\* The foil was blackened by heavy carbon deposit during run on 20 January. Carbonized target checked for stopping power and used again 21 January. This effect has been taken into account.

Line	$E_0$ (kev)	$\Delta E =$ $E_3 - E_0$ (kev)	$E_a =$ $\frac{1}{2}(E_0 + E_3)$ (kev)	$\delta E$ (kev)	$E_m$ (kev)	Correction Factor for Impurities (Divide)
1	341.3	169.0	425.8	1.5	424	1.081
2	441.9	157.1	520.4	1.1	519	1.080
3	598.6	138.1	667.6	negl.	668	1.078
4	669.6	127.6	733.4	"	733	1.078
5	874.0	112.6	930.3	"	930	1.076
6	935.8	111.6	991.6	"	992	1.075
7	341.3	164.6	423.6	1.5	422	1.081
8	441.9	152.6	518.2	1.0	517	1.080
9	669.6	121.3	730.2	negl.	730	1.078
10	874.0	111.1	929.5	"	929	1.076
11	935.8	104.9	988.2	"	988	1.075



Table XXXI. (Concl.)

Line	Corrected $\Delta E$ (kev)	* G (Mult.)	# $\sigma$ , At. Stopping Power	# $\sigma/Z^{1/3}$	Stopping Power (kev-cm <sup>2</sup> /mg)	Prob. Error, %
1	156.2	62.1	9.70	4.50	290	3.5
2	145.4	61.8	8.99	4.17	269	3.5
3	128.1	61.5	7.88	3.66	235.5	4.0
4	118.4	61.3	7.26	3.37	217	4.0
5	104.7	61.0	6.38	2.97	191	4.0
6	103.8	60.7	6.30	2.93	188	4.0
7	152.1	68.2	10.37	4.82	310	3.5
8	141.3	66.4	9.38	4.35	280	3.5
9	112.6	64.6	7.27	3.38	217	4.0
10	103.3	60.25	6.22	2.89	186	4.0
11	97.6	60.1	5.86	2.73	175	4.0

\* Data in this column to be multiplied by  $10^{-18}$  .

# Data in these columns to be multiplied by  $10^{-15}$  .



Table XXXII. (Two Pages)

Computation of Stopping Power of Krypton

Line	Foil	Date	Time	$E_0$ (kev)	$\Delta E_F$ (kev)	$E_3$ (kev)
1	.04 mil Ni	1-9-53 pm	15:10	761.7	146.0	615.7
2	"	"	15:45	885.5	134.5	751.0
3	"	"	16:05	947.3	130.0	817.3
4	"	"	16:35	1125.9	118.5	1007.4
5	.05 mil Cu	1-12-53pm	13:25	681.1	178.5	502.6
6	"	"	13:55	761.0	169.0	592.0
7	"	"	14:15	886.7	156.0	730.7
8	"	"	14:45	949.5	152.0	797.5
9	"	"	15:00	1122.8	138.0	984.8
10	"	"	15:20	1176.2	133.0	1043.2

Line	$E_0$ (kev)	$\Delta E =$ $E_3 - E_0$ (kev)	$E_a =$ $\frac{1}{2}(E_0 + E_3)$ (kev)	$\delta E$ (kev)	$E_m$ (kev)	Correction Factor for Impurities (Divide)
1	441.9	173.8	528.8	1.3	527	1.0
2	598.6	152.4	674.8	negl.	675	"
3	669.6	147.7	743.4	"	743	"
4	874.0	133.4	940.7	"	941	"
5	341.3	161.3	421.9	1.4	420	"
6	441.9	150.1	516.9	1.0	516	"
7	598.6	132.1	664.6	negl.	665	"
8	669.6	127.9	733.5	"	733	"
9	874.0	110.8	929.4	"	929	"
10	935.8	107.4	989.5	"	989	"





Table XXXII. (Concl.)

Line	Corrected $\Delta E$ (kev)	* G (Mult.)	# $\sigma$ , At. Stopping Power	# $\sigma/Z^{1/3}$	Stopping Power (kev-cm <sup>2</sup> /mg)	Prob. Error, %
1	173.8	122.7	21.3	6.46	153.5	3.5
2	152.4	117.8	17.95	5.44	129	3.5
3	147.7	114.9	16.98	5.15	122	3.5
4	133.4	110.7	14.77	4.48	106.5	4.0
5	161.3	140.3	22.65	6.87	163	3.5
6	150.1	138.2	20.75	6.29	149.5	3.5
7	132.1	136.8	18.07	5.48	130	4.0
8	127.9	134.7	17.21	5.22	124	4.0
9	110.8	133.7	14.81	4.49	107	4.0
10	107.4	132.3	14.22	4.31	102.5	4.0

\* Data in this column to be multiplied by  $10^{-18}$  .

# Data in these columns to be multiplied by  $10^{-15}$  .



Table XXXIII. (Two Pages)

Computation of Stopping Power of Xenon

Line	Foil	Date	Time	$E_0'$ (kev)	* $\Delta E_F$ (kev)	$E_3'$ (kev)
1	.05 mil Cu	1-14-53	10:35	719.8	183.5	536.3
2	"	"	11:05	809.1	172.5	636.6
3	"	"	11:10	921.5	161.0	760.5
4	"	"	11:20	984.5	154.5	830.0
5	"	"	11:35	1151.6	139.5	1012.1
6	.05mil Ni-2	1-19-53	14:00	730.3	184.5	545.8
7	"	"	14:15	807.8	174.0	633.8
8	"	"	14:30	921.9	161.5	760.4
9	"	"	14:40	982.4	155.5	826.9
10	"	"	16:00	1199.8	136.0	1063.8

\* Allowance made for carbonization of window foil (Fig. 10).

Line	$E_0$ (kev)	$\Delta E =$ $E_3' - E_0$ (kev)	$E_a =$ $\frac{1}{2}(E_0 + E_3')$ (kev)	$\delta E$ (kev)	$E_m$ (kev)	Correction Factor for Impurities (Divide)
1	341.3	195.0	438.8	2.0	437	.985
2	441.9	194.7	539.2	1.6	538	.985
3	598.6	161.9	679.5	negl.	679	.984
4	669.6	160.4	749.8	"	750	.983
5	874.0	138.1	943.0	"	943	.982
6	341.3	204.5	443.5	2.2	441	.985
7	441.9	191.9	537.8	1.6	536	.985
8	598.6	161.8	679.5	negl.	679	.984
9	669.6	157.3	748.2	"	748	.983
10	874.0	189.8	968.9	"	969	.982



Table XXXIII. (Concl.)

Line	Corrected $\Delta E$ (kev)	* G (Mult.)	# $\sigma$ , At. Stopping Power	# $\sigma/Z^{1/3}$	Stopping Power (kev-cm <sup>2</sup> /mg)	Prob. Error, %
1	198.0	132.9	26.3	6.96	120.5	3.5
2	197.8	126.9	25.1	6.64	115	3.5
3	164.7	125.9	20.72	5.48	95	3.5
4	163.3	123.9	20.22	5.35	92.7	3.5
5	140.6	120.9	16.99	4.49	77.8	4.0
6	208	126.9	26.4	6.98	121	3.0
7	194.9	123.7	24.1	6.38	110.5	3.5
8	164.5	120.5	19.85	5.25	91	3.5
9	160.1	118.3	18.95	5.01	86.9	3.5
10	193.3	87.0	16.8	4.44	77	3.5

\* Data in this column to be multiplied by  $10^{-18}$  .

# Data in these columns to be multiplied by  $10^{-15}$  .



Thus, the probable error amounts to 2% to 4.5% for nitrogen and argon, and 2.5% to 4.5% for the other gases studied. The higher values are valid for smaller values of energy loss, and vice versa. Tables XXIX through XXXIII include columns for the probable errors computed in this fashion.

#### D. Straggling in Stopping Power.

##### 1. Computation.

We shall consider  $\Omega^2 / \Delta x$  as the measure of stopping power straggling, and assume it to be valid for  $E_m$ , the mean value of energy for the protons passing through the stopping medium. Results were considered only for the foils. Results for the gases are not easily obtained by using the technique employed for our stopping power experiments. There are two reasons for this:

(1) Straggling results for window foils must be known with great accuracy in order to subtract such effects from the overall results provided for gas plus window foil. Such accuracy for the foils has not been obtained.

(2) The statistical spread of the resonance peaks, with both gas and window foil inserted, is so large that adjacent peaks interfere somewhat with one another. This introduces uncertainty in how much of the yield data are ascribable to each individual peak.

Table XXXIV gives the data and computations for straggling effect in proton stopping power. The column headings have already been defined and discussed in previous sections. The basic formula for determination of  $\Omega^2$  is equation (II-B-10).





For reasons which have been explained in Section III.G., the values of  $\Omega_M$  are not usually large enough to consider. Thus the values of  $\Omega_M'^2 - \Omega_M^2$  are not considered in the final determination of  $\Omega^2$ .

In obtaining the values of  $\Omega'_0$  and  $\Omega_0$  from the yield curves the following rules of procedure were used (see Figures 8 (a) and (b) for illustration):

(a) The non-resonance portion of the yield was estimated and subtracted from the yield values to give only the resonance portion of the yield for analysis. This is estimated as the level which the yield curve seems to approach on either side. Since displacement of the non-resonance portion of the curve should not affect its height, the same non-resonance datum level should be taken for corresponding shifted and unshifted peaks. In case the non-resonance base lines do not appear equal, some compromise has to be reached.

(b) If the peaks appear Gaussian in shape, we can estimate the standard deviation quite accurately by taking a half of the peak width at 60.6% of its height above the datum level. This is easily proved by reference to any table of the error function, or normal distribution.

(c) If the peak is not Gaussian in shape, the standard deviation must be computed by numerical analysis in accordance with basic definition.

(d) The influences of adjacent peaks must be subtracted if they



Table XXXIV. (Two Pages)

Computation of Straggling in Stopping  
Power of Copper and Nickel Foils

Line	Date	Foil	$\Delta x =$ Thickness (mg/cm <sup>2</sup> )	Resonance Peak Ener. (kev)	I' (amp)	F'
1	8-29-52	.05mil Ni-1	1.150	669	.7848	2.06
2	10-16-52	.04 mil Ni	0.977	669	.7720	2.03
3	"	"	"	873.5	.8620	2.21
4	10-17-52	"	"	630	.7560	2.00
5	"	"	"	986	.9069	2.29
6	10-23-52	"	"	441.1	.6681	1.79
7	1- 9-53	"	"	669	.7765	2.04
8	12- 2-52	.05 mil Cu	1.155	340.4	.6310	1.70
9	"	"	"	669	.7860	2.06
10	"	"	* "	873.5	.8735	2.14
11	"	"	1.18	935.3	.8970	2.27
12	12-18-52	"	"	669	.7834	2.06
13	"	"	"	873.5	.8710	2.13
14	"	"	1.155	935.3	.8960	2.27

\* 3% added to thickness because of carbonization.

Line	$E'_0$ (kev)	$E'_m$ (kev)	$\Omega'_0$ (ma)	$\Omega'_0$ (kev)	$\Omega'^2_0$	$\Omega^2_0$
1	839.7	757	4.9	10.10	102.0	39.1
2	809.8	741	4.13	8.39	70.4	9.61
3	1006.2	941	4.5	9.95	99.0	6.25
4	777.1	704	4.5	9.00	81.0	4.41
5	1105.3	1046	4.75	10.88	118.4	4.12
6	612.3	527	6.0	10.74	115.5	28.1
7	809.1	739	4.35	8.87	78.7	12.04
8	546.0	446	4.71	8.00	64.0	23.8
9	834.6	755	4.71	9.70	94.1	27.8
10	1018.6	949	5.18	11.10	123.2	39.0
11	1071.0	1006	5.5	12.49	156.0	42.2
12	829.5	749	4.4	9.06	82.1	7.13
13	1017.0	945	4.3	9.16	83.9	6.30
14	1073.2	1004	4.6	10.21	104.3	15.76



Table XXXIV. (Concl.)

Line	$\Omega_o'^2 - \Omega_o^2$	$\Omega_S'$	$\Omega_S'^2$	$\Omega_S^2$	$\Omega_S'^2 - \Omega_S^2$	$\Omega^2$ (kev <sup>2</sup> )	$\Omega^2/\Delta x$ (kev <sup>2</sup> -cm <sup>2</sup> /mg)
1	62.9	1.61	2.59	1.66	0.93	62.0	53.9
2	60.8	1.56	2.43	1.66	0.77	60.0	61.4
3	92.75	1.93	3.72	2.82	0.90	91.85	94.0
4	76.6	1.49	2.22	1.47	0.75	75.85	77.6
5	114.3	2.13	4.54	3.60	0.94	113.4	116.2
6	87.4	1.18	1.39	0.72	0.67	86.7	88.8
7	66.7	1.55	2.40	1.66	0.74	66.0	67.6
8	40.2	1.05	1.10	0.43	0.67	39.5	34.2
9	66.3	1.60	2.56	1.66	0.90	65.4	56.5
10	84.2	1.96	3.84	2.82	1.02	83.2	72.0
11	113.8	2.06	4.24	3.24	1.00	112.8	95.5
12	75.0	1.59	2.53	1.66	0.87	74.1	62.8
13	77.6	1.96	3.84	2.82	1.02	76.6	64.9
14	88.5	2.06	4.24	3.24	1.00	87.5	75.6



seem to be present to any extent.

For the sake of comparison with theory, values of straggling are plotted in Figure 15.

## 2. Discussion of Errors.

It is difficult to make good estimates of probable errors of straggling results, since many factors of indeterminable size are present. The best estimate of the size of the random errors can be gained by noting the spread in the results as tabulated and as plotted in Figure 15. It will be noted that the values for copper are much more self-consistent than those for nickel. This may be due to the fact that the data for copper were in general taken at a later period than the data for nickel, and the improvement in technique and procedures obtained with practice tended to make later results more precise. On the other hand, the amount of data is not sufficient to insure that such self-consistency for the copper results is more than pure chance.

Factors leading to large errors in the straggling results include such matters as are listed:

- (a) There is reason to think that the target LiF-1, which was used for some of the earlier data is somewhat uneven. Since the beam without the foil interposed is concentrated but is more diffuse with the foil interposed, the portion of spread in corresponding peaks due to target thickness may not cancel in the subtraction of the peak variances.
- (b) As indicated in Section III.B, very fine, undetectable thickness variations may cause a straggling effect in addition to the





theoretical stopping power variations. This error is always positive. If we are willing to accept theoretical predictions in stopping as roughly correct, the experimental results may indicate the lack of appreciable contribution due to this factor. (See Figure 15).



## V. Summary of Results.

The results on stopping power are summarized in Table XXXV, giving the values for stopping power in  $\text{kev-cm}^2/\text{mg}$ , and in Table XXXVI which gives the results for atomic stopping power ( $\sigma$ ) in  $\text{ev-cm}^2$ . Figure 11 gives in graphical form the results for stopping power, while Figures 12, 13, and 14 give in graphical form the atomic stopping power results expressed as  $\sigma/Z^{1/3}$ .

The results in stopping power straggling, expressed as  $\frac{d}{dx} (\Omega^2)$  are given in Table XXXVII and Figure 15.



Table XXXV. (Two Pages)

SUMMARY OF DATA ON STOPPING POWER FOR PROTONS

(kev-cm<sup>2</sup>/mg)

(a) Nickel

Proton Energy (kev)	Stopping Power	Prob. Error, %
527	172.0	1.5
704	148.7	2.0
718	150.0	3.0
739	142.8	2.0
741	141.7	2.0
755	145.3	1.5
757	146.3	1.5
915	128.2	3.0
935	125.7	2.0
941	133.7	2.0
949	128.3	2.0
951	131.5	2.0
977	129.0	3.0
1000	127.4	2.0
1007	121.9	2.0
1046	120.4	2.5
1047	122.0	2.5
1057	120.7	2.0

(b) Copper

Proton Energy (kev)	Stopping Power	Prob. Error, %
446	169.0	1.5
532	158.0	1.5
603	150.1	1.5
713	139.9	1.5
755	137.0	2.0
812	131.6	1.5
949	120.0	2.0
996	114.7	1.5
1006	112.0	2.0
1050	113.1	2.0

(d) Nitrogen ( $\frac{1}{2}$ N<sub>2</sub>)

Proton Energy (kev)	Stopping Power	Prob. Error, %
406	400	4.0
409	401	4.0
452	371	2.5
501	362	4.0
502	351	4.0
541	328	3.0
648	278	4.0
648	296	4.5
716	275	4.5
717	264	4.5
748	257	3.5
914	219	4.5
914	238	4.5
942	217	3.5
973	207	4.5
974	228	4.5
1001	209	4.0

(c) Argon

Proton Energy (kev)	Stopping Power	Prob. Error, %
421	224.5	3.5
476	224	2.0
519	215	3.5
567	207	2.5
662	176	4.0
713	187	2.5
778	176	2.5
929	154	4.0
932	155	4.0
971	154	3.0
989	148.5	4.0



Table XXXV. (Concl.)

(e) Neon

Proton Energy (kev)	Stopping Power	Prob. Error, %
422	310	3.5
424	290	3.5
517	280	3.5
519	269	3.5
668	235.5	4.0
730	217	4.0
733	217	4.0
929	186	4.0
930	191	4.0
988	175	4.0
992	188	4.0

(f) Krypton

Proton Energy (kev)	Stopping Power	Prob. Error, %
420	163	3.5
516	149.5	3.5
527	153.5	3.5
665	130	4.0
675	129	3.5
733	124	4.0
743	122	3.5
929	107	4.0
941	106.5	4.0
989	102.5	4.0

(g) Xenon

Proton Energy (kev)	Stopping Power	Prob. Error, %
437	120.5	3.5
441	121	3.0
536	110.5	3.5
538	115	3.5
679	91	3.5
679	95	3.5
748	86.9	3.5
750	92.7	3.5
943	77.8	4.0
969	77	3.5





# SUMMARY OF DATA ON ATOMIC

## STOPPING POWER FOR PROTONS ( $10^{-15}$ ev-cm<sup>2</sup>)

### (a) Nickel

Proton Energy (Kev)	Atomic Stopping Power	Prob. Error, %
527	16.78	1.5
704	14.48	2.0
718	14.62	3.0
739	13.91	2.0
741	13.80	2.0
755	14.18	1.5
757	14.27	1.5
915	12.50	3.0
935	12.25	2.0
941	13.02	2.0
949	12.51	2.0
951	12.51	2.0
977	12.57	3.0
1000	12.42	2.0
1007	11.88	2.0
1046	11.74	2.5
1047	11.89	2.5
1057	11.77	2.0

### (c) Argon

Proton Energy (Kev)	Atomic Stopping Power	Prob. Error, %
421	14.87	3.5
476	14.81	2.0
519	14.28	3.5
567	13.71	2.5
662	11.67	4.0
713	12.39	2.5
778	11.66	2.5
929	10.19	4.0
932	10.24	4.0
971	10.20	3.0
989	9.82	4.0

### (b) Copper

Proton Energy (Kev)	Atomic Stopping Power	Prob. Error, %
446	17.86	1.5
532	16.70	1.5
603	15.87	1.5
713	14.78	1.5
755	14.48	2.0
812	13.90	1.5
949	12.68	2.0
996	12.11	1.5
1006	11.83	2.0
1050	11.95	2.0

### (d) Nitrogen ( $\frac{1}{2}$ N<sub>2</sub>)

Proton Energy (Kev)	Atomic Stopping Power	Prob. Error, %
406	9.30	4.0
409	9.32	4.0
452	8.62	2.5
501	8.42	4.0
502	8.16	4.0
541	7.62	3.0
648	6.47	4.0
648	6.87	4.5
716	6.40	4.5
717	6.15	4.5
748	5.98	3.5
914	5.09	4.5
914	5.53	4.5
942	5.05	3.5
973	4.80	4.5
974	5.30	4.5
1001	4.85	4.0



(e) Neon

Proton Energy (Kev)	Atomic Stopping Power	Prob. Error, %
422	10.37	3.5
424	9.70	3.5
517	9.38	3.5
519	8.99	3.5
668	7.88	4.0
730	7.27	4.0
733	7.26	4.0
929	6.22	4.0
930	6.38	4.0
988	5.86	4.0
992	6.30	4.0

(f) Krypton

Proton Energy (Kev)	Atomic Stopping Power	Prob. Error, %
420	22.65	3.5
516	20.75	3.5
527	21.30	3.5
665	18.07	4.0
675	17.95	3.5
733	17.21	4.0
743	16.98	3.5
929	14.81	4.0
941	14.77	4.0
989	14.22	4.0

(g) Xenon

Proton Energy (Kev)	Atomic Stopping Power	Prob. Error, %
437	26.30	3.5
441	26.40	3.0
536	24.10	3.5
538	25.10	3.5
679	19.85	3.5
679	20.72	3.5
748	18.95	3.5
750	20.22	3.5
943	16.99	4.0
969	16.80	3.5



Table XXXVII.

SUMMARY OF DATA ON STOPPING POWER STRAGGLING OF

PROTONS  $\left( \frac{d}{dx} (\Omega^2) \right)$

(kev<sup>2</sup>-cm<sup>2</sup>/mg)

(a) Nickel

<u>Proton Energy</u> <u>(kev)</u>	<u>Straggling in Stopping Power</u> <u>(Variance per Unit Thickness)</u>
527	88.8
704	77.6
739	67.6
741	61.4
757	53.9
941	94.0
1046	116.2

(b) Copper

<u>Proton Energy</u> <u>(kev)</u>	<u>Straggling in Stopping Power</u> <u>(Variance per Unit Thickness)</u>
446	34.2
749	62.8
755	56.5
945	64.9
949	72.0
1004	75.6
1006	95.5



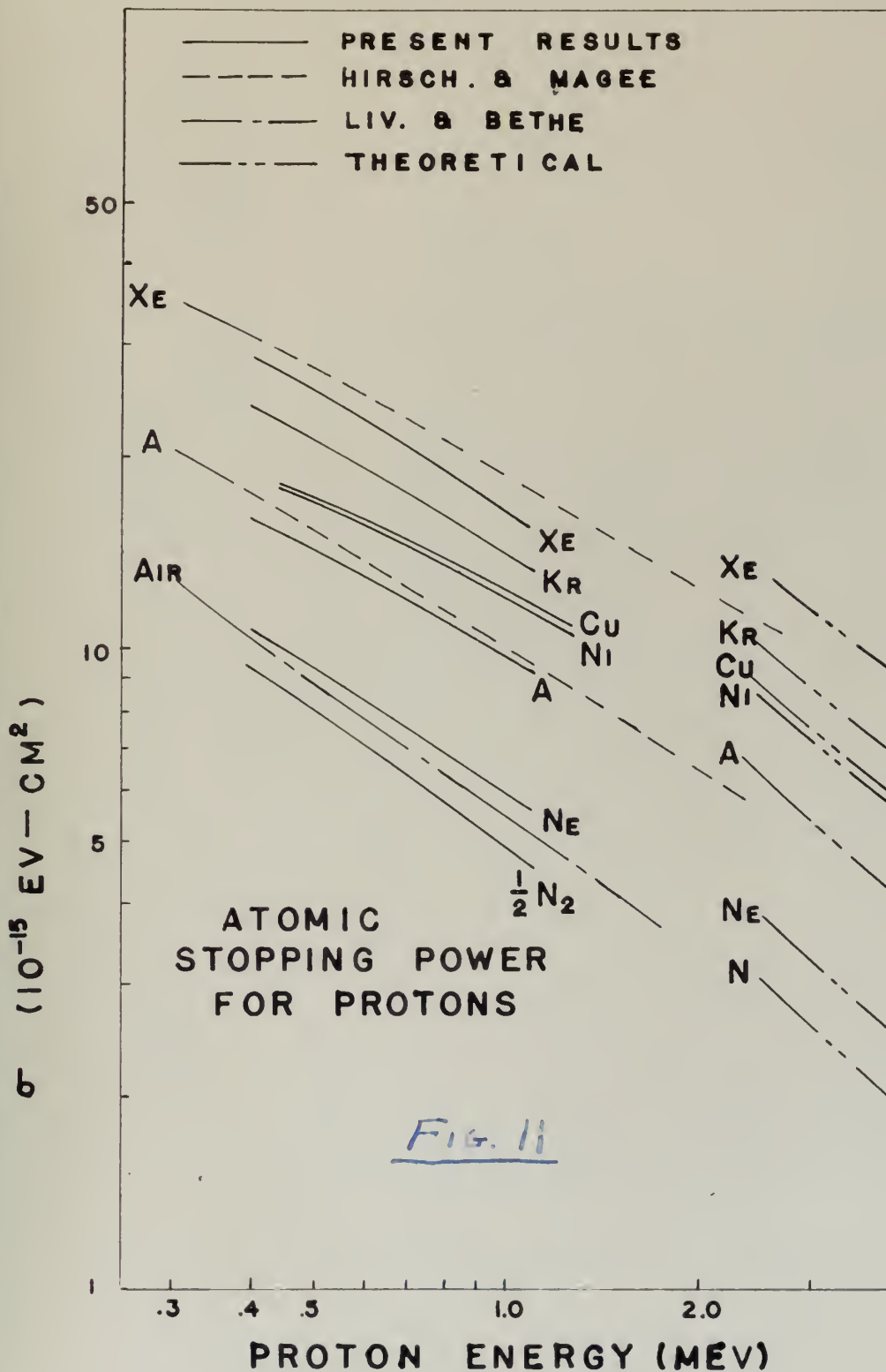
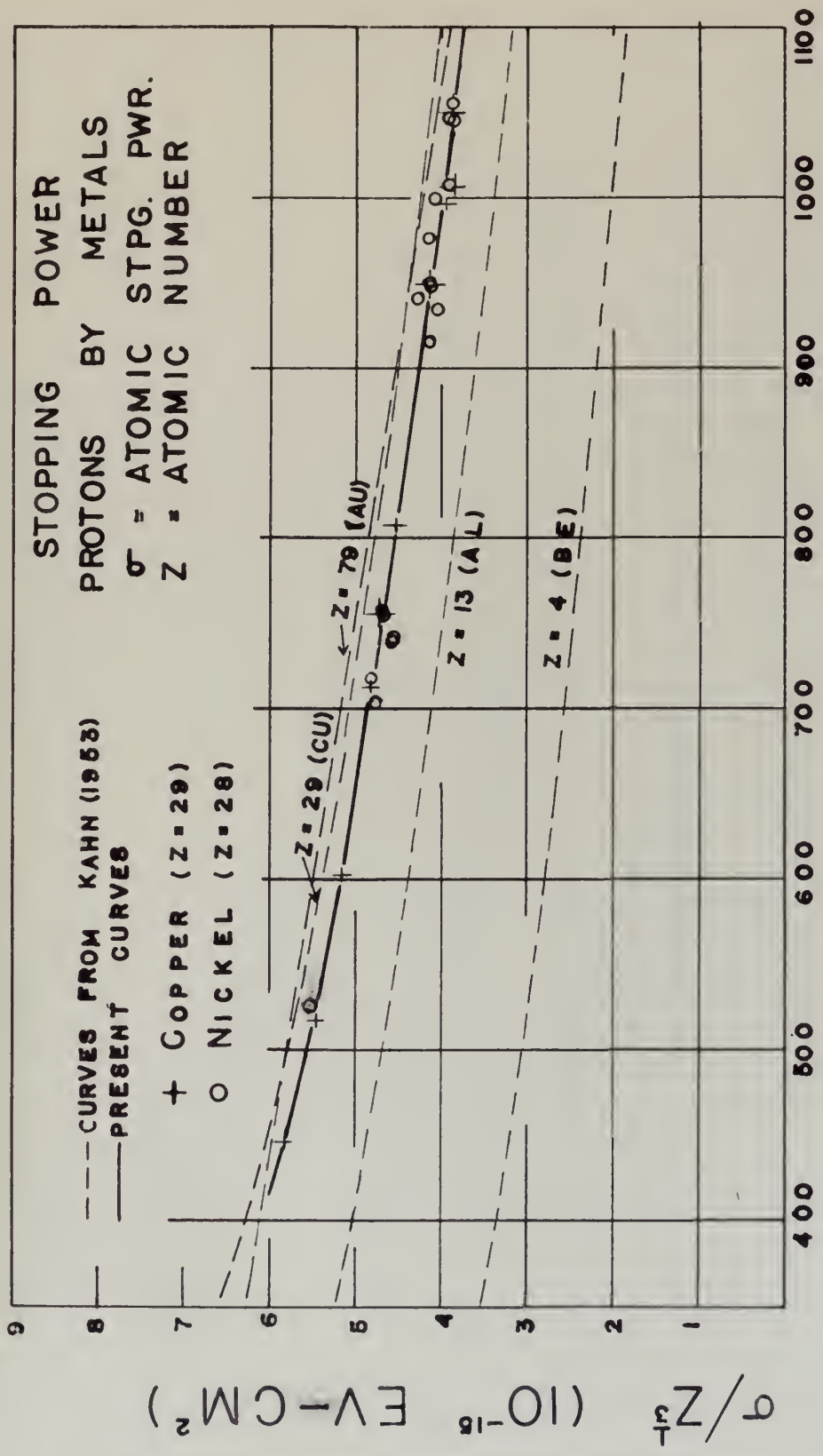


FIG. 11







PROTON ENERGY (KEV)

Fig. 12



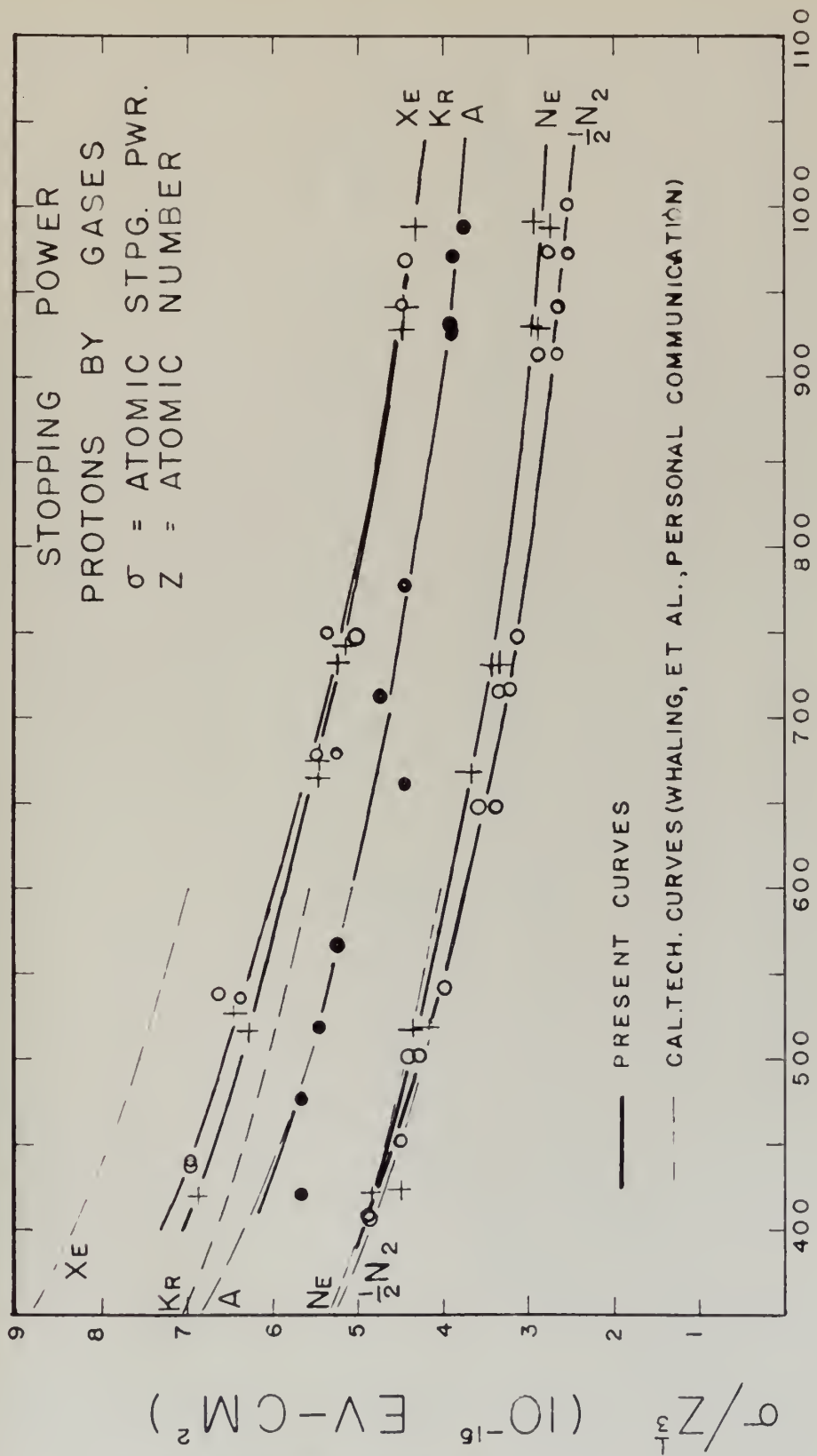


FIG. 13



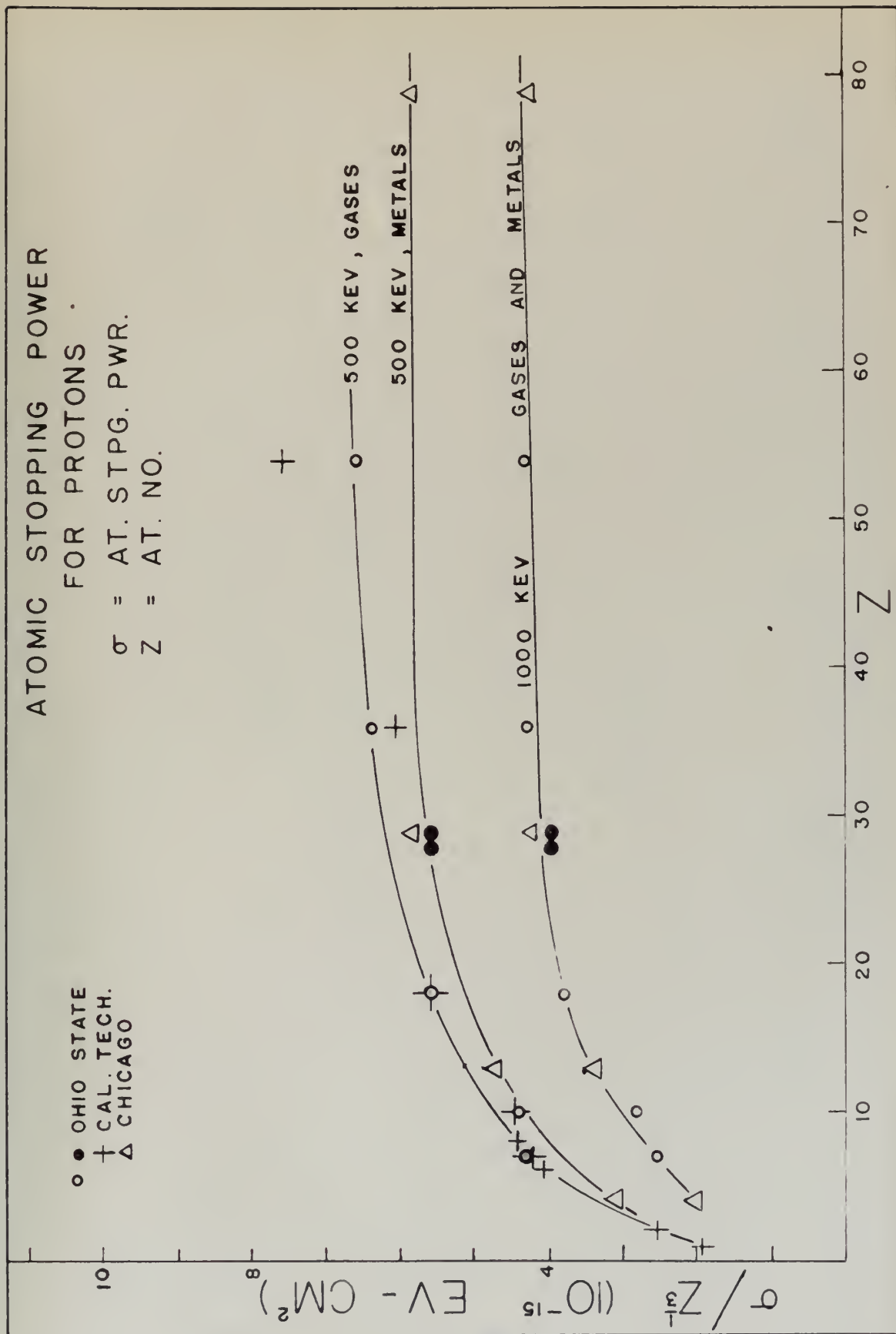


Fig. 14



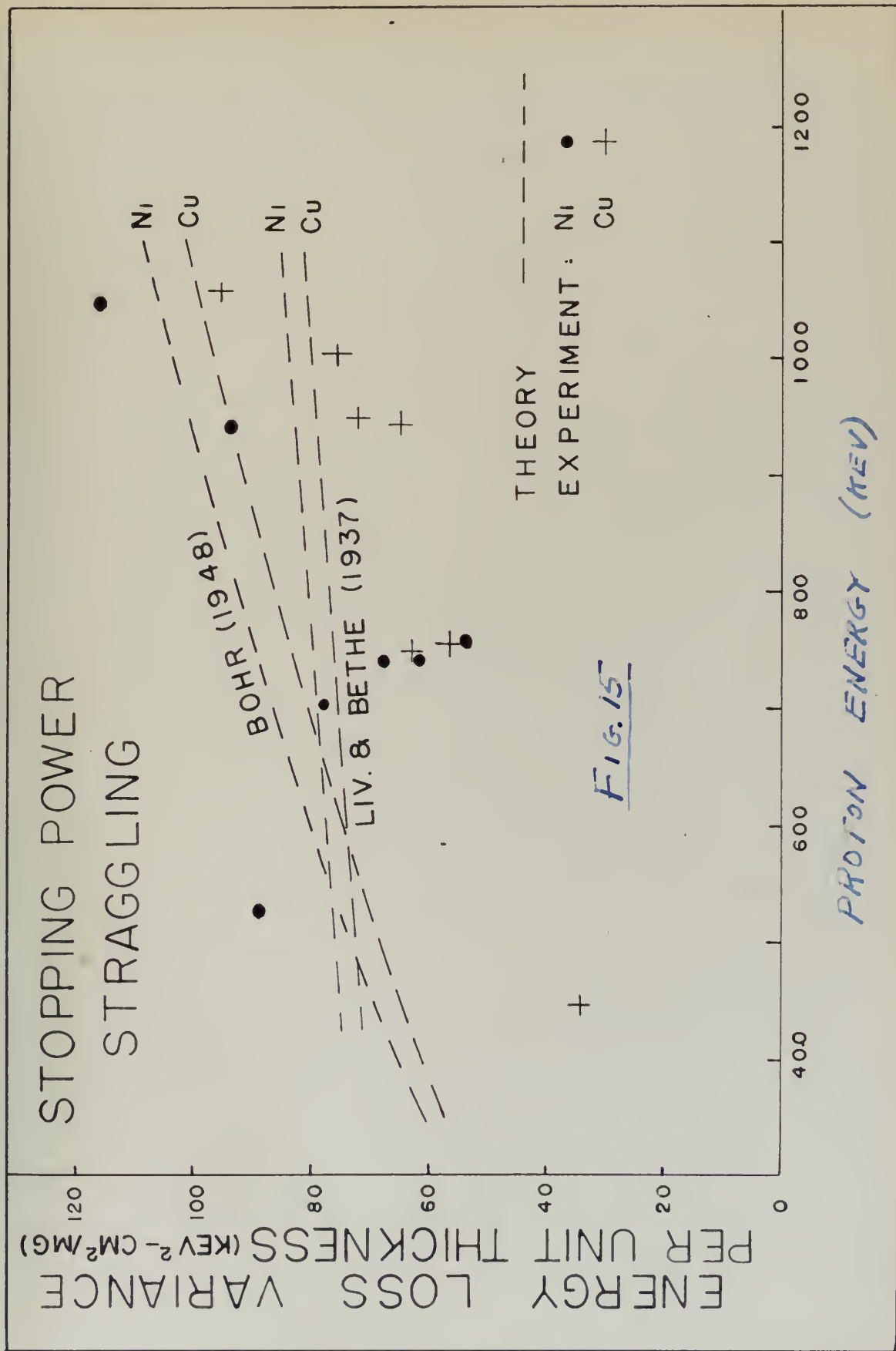


FIG. 15





## VI. Conclusion - Discussion of Results.

### A. Comparison of Present Results with Other Published Results.

#### 1. Stopping Power - Comparison with Theory.

In Figure 11, we have plotted mean curves obtained from our results on atomic stopping power. Superimposed on our resulting curves are curves obtained from theoretical predictions. The set of curves on the right side of the figure are obtained by use of equation (I-B-69), as modified by inclusion of the correction  $C_K$  in the manner indicated by equation (I-B-83). The values of  $I_{av}$  were obtained from Mano (1934), and are listed in Table II. The values of  $C_K$  were obtained from the graphs of Walske (1952). As this theoretical computation cannot be expected to be very accurate in the energy region of interest to us, (primarily due to the failure to include corrections for deficiency in stopping power of L and higher shell electrons), it is not surprising that the theoretical curves tend toward too high a value as the proton energy decreases. It is seen that a smooth curve of transition could easily be drawn from our experimental curves to approach the theoretical curves at higher energies.

The computed curves of Hirschfelder and Magee (1948), which traverse the energy region of interest to us, are plotted for the gases argon and xenon. Since their approach has included the stopping power corrections for all shells, one may expect their curves to agree better with experimental data than those based on the older formulations. In both cases the experimental curves lie below the



theoretical curves by about 5 to 10%. It would be unreasonable to expect better agreement (except by accident), since the theoretical considerations on which Hirschfelder and Magee based their analyses were admittedly approximate.

Livingston and Bethe's (1937) curve for proton atomic stopping power in air is likewise plotted, as a rough comparison with our results for nitrogen. Here, too, experiment seems to be about 10% below the predictions in this energy region.

No effort is made to include the predictions by Bohr's (1948) formula for slow particles in heavy media (Equation I-B-24), since it is not expected to give quantitatively correct answers. As a matter of fact, the formula gives predictions for  $\sigma/z^{1/3}$  of  $8.5 \text{ ev-cm}^2$  at 500 kev proton energy and  $6.1 \text{ ev-cm}^2$  at 1000 kev. Comparison with Figure 14 shows that these values are consistently higher than experiment by an appreciable amount. The theory can be checked however for correctness of dependence on  $Z$  and  $v$ . The plots of  $\sigma/z^{1/3}$  all seem to show that for heavy media the value of this variable is almost independent of  $Z$ . This conforms to the predicted variation of atomic stopping power with atomic number - at least for elements of atomic number  $\gtrsim 30$ . The inverse dependence on  $v$  predicted by Bohr's theory can be checked by determining from Figure 11 whether the dependence on  $E$  is as the inverse square root of the latter variable. Since Figure 11 is plotted on a log-log scale, the slope of the curve should determine this exponent. It is seen that all the curves have a slope of approximately minus one-half, in accordance with the theory. The



heavier gases are more nearly in accord, as is expected. The lighter gases show a steeper slope, and the metals a somewhat less steep slope. The anomalous results from the metals will be discussed in the concluding section.

## 2. Stopping Power - Comparison with Other Experimental Information.

The sources of other experimental information have already been indicated in Section I.C. Figures 12, 13, and 14 give data on  $\sigma/Z^{1/3}$  in such a way that the comparison of our results with that reported from other laboratories is readily seen.

In regard to the metals, Figure 12 includes results, attributed to Kahn. Our curve for copper is about 4% below that of Kahn, which discrepancy is not alarming. Kahn has matched his curves to Warshaw's (1949) work at the 350-400 kev region, but our curve for copper can be matched with Warshaw's just as easily. The data of Madsen (1953) on copper is much different from other experimental data and is not included. The earlier work of Madsen and Venkateswarlu (1948a) on beryllium is essentially in agreement with the curve given by Kahn, so that a separate curve for this contribution is unnecessary in Figure 12, although credit is certainly due to these earlier workers.

Our data for gases is compared in Figure 13 with the data from the California Institute of Technology up to 600 kev, reported by Dunbar, et al. (1952). The work of Weyl (1952) on the lighter gases, especially on argon, up to the maximum energy he utilized of 400 kev, agrees with the data from the California Institute of Technology, so that his results are not explicitly included. It can be seen that





our data agree well with other results for the lighter gases. The data for krypton differ by a little more than the probable error, but the results for xenon differ by much more than the probable error.

### 3. Comparison of Results of Straggling Measurements with Theory.

There are no experimental measurements of stopping power straggling with which we can compare our results on nickel and copper. Since Madsen and Venkateswarlu's (1948b) measurements for beryllium checked so well with the theory of Bohr (1948), it is of special interest to check our results with theory.

Equations (I-B-95) and (I-B-96) provide the relation, according to Bohr (1948), for theoretical prediction of straggling. They are readily evaluated in the cases of the metals nickel and copper. We should note that according to (I-B-96) the number of effective electrons,  $Z'$ , becomes about 27 for 500 kev protons and 39 for 1000 kev protons. Since the latter figure is considerably more than the total number of electrons in the copper or nickel atom, it is obvious that the estimate is too high. We have seen in subsection 1, however, that Bohr's use of the Thomas-Fermi model gives too high an answer for stopping power, which leads us to the suspicion that the formula obtained from the model (I-B-72) gives too large a value.

Evaluation of the theoretical predictions according to Livingston and Bethe (1937) is a little more difficult. (See equation I-B-97). The values of  $I_n^1$  are not known precisely, nor is  $\kappa_n$  easy to evalu-





ate. A calculation was made indicating the contribution made by the term in which these constants appear, using  $4/3$  for each  $\eta_n$  and the ionization energy  $I_n$  in place of the average excitation energy  $I'_n$ . This gives a value to this expression of about 8.5 for 500 kev protons and about 11.5 for 1000 kev protons, valid both for copper and nickel. For  $Z'$  we must subtract from the atomic numbers of the element studied the oscillator strength of the K and L electrons, in accordance with the criterion of equation (I-B-71). Using the values computed by Hönig (1933) for oscillator strength we get for  $Z'$  values of 19.8 for nickel and 20.8 for copper.

The theoretical curves and experimental data are plotted in Figure 15. It can be seen that our results are too scattered to permit us to make any positive statements. The following conclusions seem to be indicated, however: The theory of Livingston and Bethe is imperfect in that it does not permit gradual changes in the value of  $Z'$ , the effective number of electrons; that of Bohr takes account of this change with proton energy, but does not include the extra term stemming from the kinetic energy effect of the orbital electrons. On the other hand, the equation of Bohr over-estimates the number of effective electrons, and in this particular region this error nearly cancels the failure to include the kinetic energy effects. The experimental results roughly follow the trends with energy as predicted by Bohr (1948) though they seem to indicate that in absolute value, theory may give too high a prediction in this region.



## B. Concluding Comments.

This dissertation should not be concluded without some comment on the general significance of the experimental results on stopping power in this energy region. There are a few discrepancies between the results reported by the various experimenters, including the writer, but nevertheless there is sufficient agreement to detect the pattern of the stopping power effect at these moderately low proton energies. Figures 12, 13, and 14 - especially the latter - bring out a very interesting fact. Above 700 kev there is little difference between the stopping power of gases and the solids studied except the predicted variation with atomic number. Below 700 kev however the results indicate a consistency among the gases or among the metals, but a definite variation between the two groups of elements.

Theory has not developed to the extent of permitting a definite explanation of this effect. In a qualitative way, however, we may speculate upon the possibility that those special effects in condensed media (conducting and non-conducting) discussed in Section I.B.6 may provide the explanation desired. Whereas the polarization effects in condensed media of high atomic number are considered to have a negligible effect in view of the small proportion of loosely bound electrons contributing to polarization, this presumption may no longer be valid at low proton energies at which only the outer electrons contribute to the stopping power phenomenon. Since theoreticians have admitted that deficiency in stopping may



exist for both conducting and non-conducting types of condensed media, we cannot state whether our resulting difference between the gases and metals in stopping of low energy protons is due to the special conducting properties of the metals, or simply to their condensed state. It is proper and desirable, of course, to make no final judgment on such a matter until experiments are forthcoming on the stopping power of non-conducting elements in the solid state for protons in this energy region.

One comment may be made on the stopping power of neon, which according to Figure 14 appears to have an anomalously low value of stopping power. This is not too surprising however upon some consideration of theory. The theoretical prediction of smooth variation with atomic number is a result of Bohr's use of the Thomas-Fermi statistical model of the atom, which is well-known to be least valid for the light elements. Since neon contains only closed shells, its outer electrons lie deeper in the Coulombian potential well than those of the atoms adjacent in the atomic table. Its electrons are therefore likely to be less effective than those of the neighboring atoms, even aside from the general trend with atomic number.



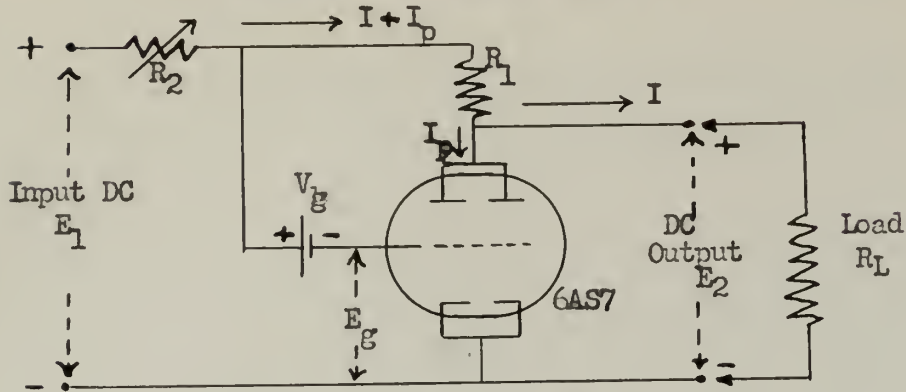
APPENDIX





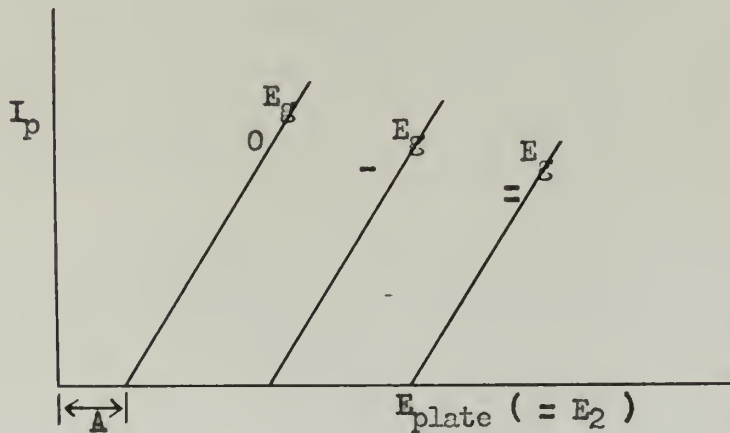
## Basic Theory and Design Details of Voltage

### Regulator for Magnet Circuit



Basic Circuit of Regulator

Figure App-1



Theoretical Triode Characteristic Curves

Figure App-2

Figure App-1 shows the basic circuit of the voltage regulator for the magnet circuit. Figure App-2 gives the characteristic curves for an ideal triode. The tube used, 6AS7, has characteristic curves quite close to the ideal case - at least in region in which we expect to operate. The characteristics may be theoretically expressed



by the following formula:

$$I_p = \frac{E_2 - A + \mu E_g}{R_p} , \quad (\text{App-I-1})$$

where  $\mu$  is the tube amplification factor,  $R_p$  is the plate resistance of the tube, and the other symbols are obvious from the above figures.

From Figure App-1 we can see that

$$E_2 = I R_L , \quad (\text{App-I-2})$$

and

$$E_2 = E_1 - (I + I_p)(R_1 + R_2) . \quad (\text{App-I-3})$$

Also we note that

$$E_g = E_1 - (I + I_p) R_2 - V_g . \quad (\text{App-I-4})$$

The above four independent equations can be reduced to a single equation by the elimination of the three variables  $E_g$ ,  $E_2$ , and  $I_p$ . By doing so we may get an equation for  $I$ , which can be reduced to the following form:

$$I = \frac{A + \mu V_g + r E_1}{R_p + R_L (1 + \mu) + \frac{r R_L}{R_1 + R_2}} , \quad (\text{App-I-5})$$

with

$$r = R_p - \mu R_1 . \quad (\text{App-I-6})$$

From these last two equations we note that  $I$  is independent of  $E_1$  when  $r = 0$ , or when  $R_1 = R_p / \mu$ . Since this last factor is the reciprocal of the transconductance of the tube, the criterion that output current (and output voltage) be constant is that conductance of the plate resistor equal the transconductance of the tube - whence the name of the regulator type: "transconductance".



Unfortunately no actual tube characteristic curves correspond to the ideal curves, so that different operating points on the actual chart have different values of transconductance. The proper value for  $R_1$  is taken then as the reciprocal of triode transconductance at some mean operating point located in the most linear portion of the actual set of curves.

Once  $R_1$  is selected then  $r$  may vary from zero only if the characteristic point at which we are operating is one with a different transconductance value than the one used to select  $R_1$ . If the actual characteristic curves are not too different from the ideal (this is one reason for selection of the 6AS7 tube - the others are its high current capacity and its low transconductance, permitting a reasonably low value for  $R_1$ ), then  $r$  will not deviate markedly from zero. We see thus from equation (App-I-5) that  $I$  is affected very little by variations in  $r$  of the order of magnitude expected.

We note also that if  $r$  is approximately zero,  $I$  is not only practically independent of  $E_1$  but also of variations in  $R_2$ . This resistance is not needed theoretically but has a very good use in actual practice. Assuming that  $r$  is small enough to be considered zero, we may use equations (App-I-2), (App-I-3), and (App-I-5) to determine that:

$$I_p = \frac{1}{(R_1 + R_2)} \left[ E_1 - \frac{(R_L + R_1 + R_2)(A + \mu V_g)}{R_p + R_L (1 + \mu)} \right], \quad (\text{App-I-7})$$

We see that  $I_p$  does depend significantly on  $R_2$ . This enables us to vary  $I_p$  appreciably without markedly changing  $I$  or  $E_2$ .





The value of this will be seen in a moment.

The system must be flexible enough so that any desired value of regulated current may be obtained from about 0.4 amperes to about 1.2 amperes. (During the process of cycling the magnet, a maximum current of not less than 3 amperes is desirable, but precise regulation is not required in this process, and the design is made so that the regulator may be removed from the system by a single switching operation.) This means that  $E_2$  must be allowed to vary at will without affecting the regulation effect. It happens that lines of constant transconductance can be drawn on the characteristic chart for the tube selected, which lines proceed in general from the lower left side of the chart to the upper right side. If the system is designed so that the operating point, even if it changes, stays on or near the line selected to match  $R_1$ , then the regulation property remains for all operating currents. In case the system characteristics cannot be made to follow the proper transconductance line (which we may call the operating line) exactly, changes in the value of  $R_2$  can be made to bring one exactly to said operating line. In practice it is quite easy to determine the proper value of  $R_2$  to keep the system operating at the proper transconductance. With  $r$  slightly different from zero, any change in  $R_2$  will make a just perceptible change in current  $I$ .  $R_2$  is simply changed until the position is reached for which slight changes make no appreciable changes in magnet current.

Gross changes in magnet current are effected by changes in  $E_1$ , which is caused in turn by changing the setting on the field current





variac, as explained in Section III.C. In order to prevent the regulator from opposing this desired current change, it is necessary to change simultaneously some other factor in the equation (App-I-5) on which the current depends. Obviously  $V_g$  is the only one which it is practicable to change. We provide this bias by means of a bank of batteries across a potentiometer, the middle connection of which, being variable, can provide a variable value of  $V_g$ . This potentiometer is then "ganged" with the variac, so that they are changed together. By proper selection of the potentiometer resistance and battery voltage, the value of grid bias will change along with the plate voltage ( $E_2$ ) so that the operating point moves approximately along the line of proper transconductance on the characteristic chart.

The complete diagram of the magnet control panel, including all the control and regulator elements, is given in Figures App-3(a) and App-3(b), separated into the upper and lower sections. This separation can easily be carried out in practice if necessary, permitted by the use of multiply-ganged connectors between the two sections.



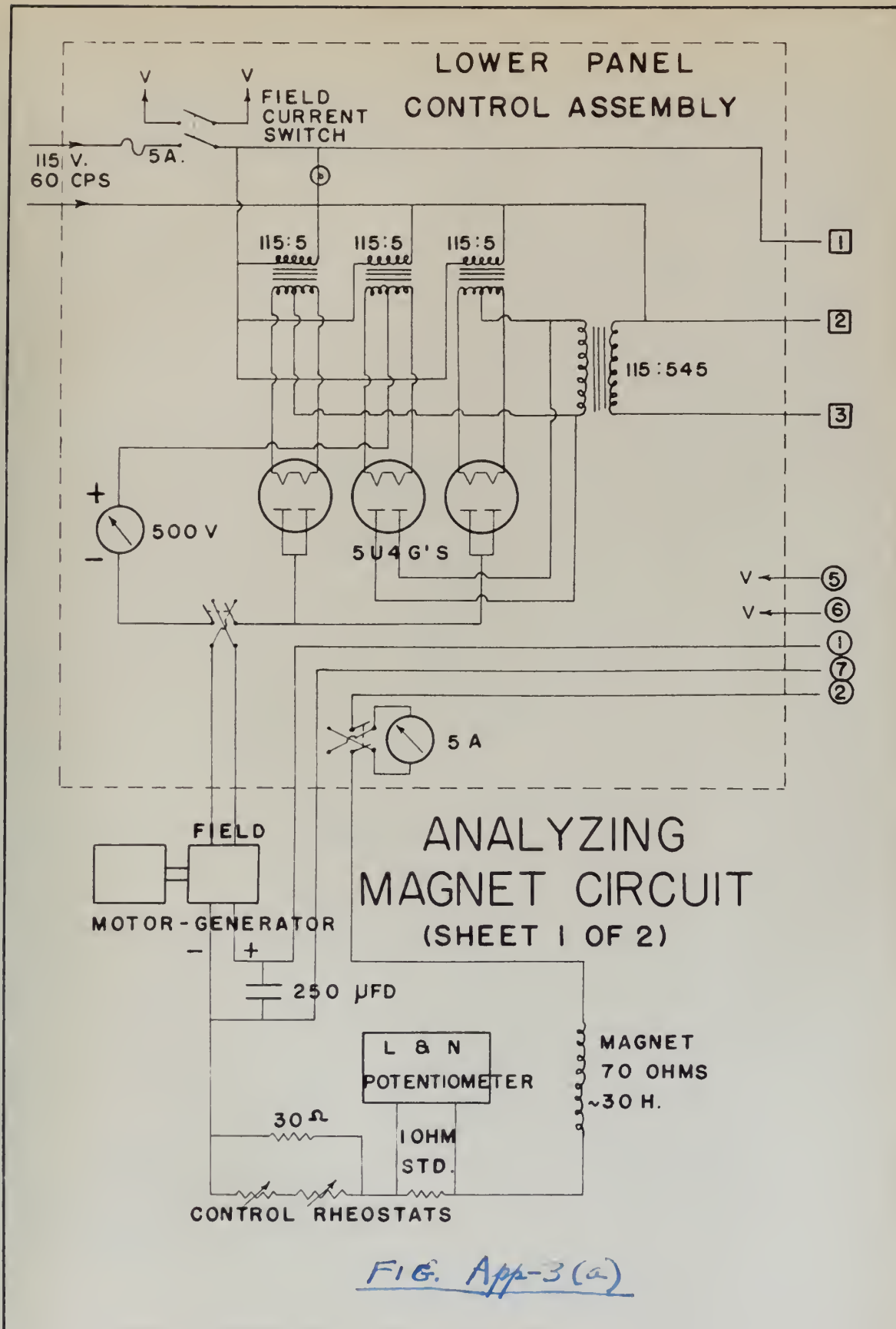
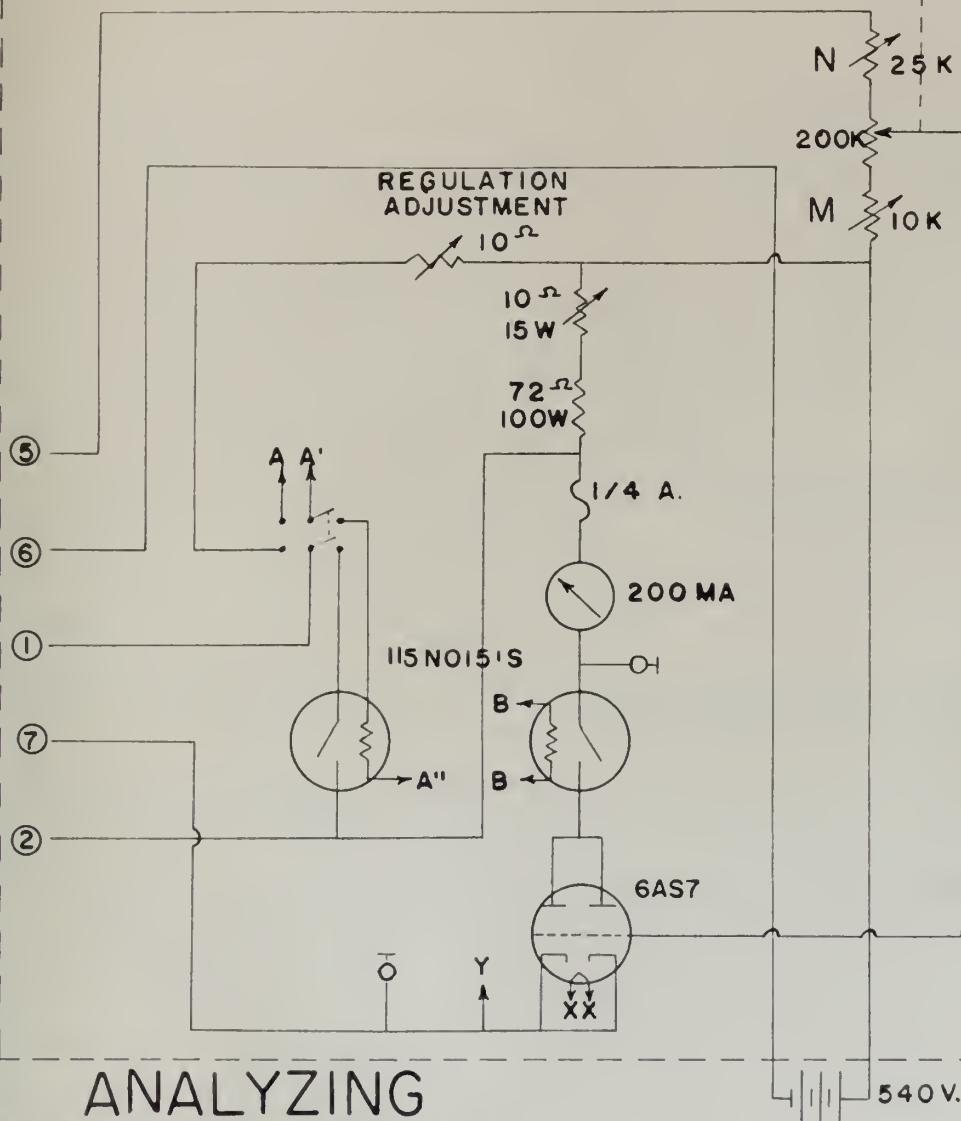
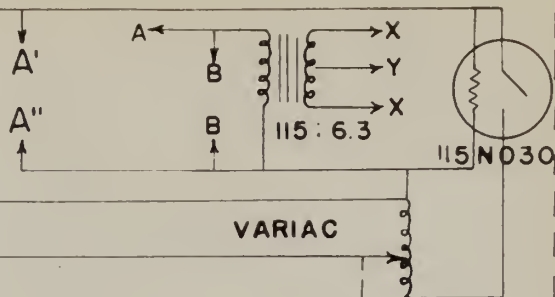


FIG. App-3(a)



# UPPER PANEL CONTROL ASSEMBLY

- 1
- 2
- 3



## ANALYZING MAGNET CIRCUIT (SHEET 2 OF 2)

FIG. App-3(6)



## REFERENCES

- Ajzenberg, F. and Lauritsen, T.: Rev. Mod. Phys. 24, 321 (1952)
- Bakker, C. J. and Segré, E.: Phys. Rev. 81, 489 (1951)
- Bethe, H. A.: Ann. d. Phys. 5, 325 (1930)
- Bethe, H. A.: Handbuch der Physik, 24, 273 (1933)
- Bethe, H. A.: Rev. Mod. Phys. 9, 69 (1937)
- Bloch, F.: Ann. d. Phys. 16, 285 (1933)
- Bloembergen, N. and van Heerden, P. J.: Phys. Rev. 83, 561 (1951)
- Bohr, A.: Kgl. Danske Vid. Sels. Math.-fys. Medd. 24, 19 (1948)
- Bohr, N.: Phil. Mag. 25, 10 (1913)
- Bohr, N.: Kgl. Danske Vid. Sels. Math.-fys. Medd. 18, 8 (1948)
- Breit, G. and Wigner, E. P.: Phys. Rev. 49, 519 (1936)
- Briggs, G. H.: Proc. Roy. Soc. 114, 341 (1927)
- Bröström, K. J., Huus, T., and Tangen, R.: Phys. Rev. 71, 661 (1947)
- Brown, L. M.: Phys. Rev. 79, 297 (1950)
- Compton, A. H.: Phys. Rev. 14, 249 (1919)
- Compton, A. H. and Allison, S. K.: X-Rays in Theory and Experiment  
(D. Van Nostrand Co., Inc., New York, 1935)
- Cooper, J. N.: Tech. Rpt. No.1, ONR Cont. N6onr-225, T.O. XI,  
NR 022 047 (1949)
- Dunbar, D. N. F., Reynolds, H. K., Wenzel, W. A., and Whaling, W.:  
Bull. Am. Phys. Soc. 27 (6), 6 (1952)
- Fermi, E.: Zeits. f. Phys. 45, 307 (1924)
- Fermi, E.: Zeits. f. Phys. 48, 73 (1928)
- Fermi, E.: Phys. Rev. 57, 485 (1940)
- Fowler, R. H.: Proc. Cambr. Phil. Soc. 21, 521 (1923)





Geiger, H.: Handbuch der Physik 24, 137 (1927)

Gerritsen, A. N.: Physica 12, 311 (1946)

Grove, G. R.; M.Sc. thesis, Ohio State University (1947)

Grove, G. R.: Ph.D. thesis, Ohio State University (1950)

Halpern, O. and Hall, H.: Phys. Rev. 73, 477 (1948)

Heller, Z. H. and Tendam, D. J.: Phys. Rev. 84, 905 (1951)

Henderson, G. H.: Phil. Mag. 44, 680 (1922a)

Henderson, G. H.: Proc. Roy. Soc. A102, 496 (1922b)

Henneberg, W.: Zeits. f. Phys. 86, 592 (1933)

Hirschfelder, J. O. and Magee, J. L.: Phys. Rev. 73, 207 (1948)

Hoel, P. G.: Introduction to Mathematical Statistics (John Wiley & Sons, Inc., New York, 1947)

Hönl, H.: Zeits. f. Phys. 84, 1 (1933)

Hunt, F. V. and Hickman, R. W.: Rev. Sci. Inst. 10, 6 (1939)

Huus, T. and Madsen, C. B.: Phys. Rev. 76, 323 (1949)

Kahn, D.: to be published Phys. Rev. (personal communications, S. K. Allison and D. Kahn, 1953)

Kramers, H. A.: Physica 13, 401 (1947)

Kuhn, W.: Zeits. f. Phys. 33, 409 (1925)

Landé, A.: Quantum Mechanics (Pitman Publishing Corp., New York, 1951)

Livingston, M. S. and Bethe, H.: Rev. Mod. Phys. 9, 245 (1937)

Madsen, C. B. and Venkateswarlu, P.: Phys. Rev. 74, 648 (1948a)

Madsen, C. B. and Venkateswarlu, P.: Phys. Rev. 74, 1782 (1948b)

Madsen, C. B., et al. (personal communications, S. K. Allison and C. B. Madsen, 1953)

Mano, G.: J. de Phys. et Rad. 5, 628 (1934)

Mather, R. and Segrè, E.: Phys. Rev. 84, 191 (1951)



Mott, N. F.: Proc. Camb. Phil. Soc. 27, 553 (1931)

Mott, N. F. and Massey, H. S. W.: The Theory of Atomic Collisions,  
Second Edition (Oxford University Press, 1949)

Neufeld, J.: ORNL Report, ORNL-884 (1950)

Pines, D.: Phys. Rev. 85, 931 (1952)

Russell, L. N.: Ph.D. thesis, Ohio State University (1952)

Schiff, L. I.: Quantum Mechanics (McGraw-Hill Book, Co., Inc., New  
York, 1949)

Siegbahn, M.: Spektroskopie der Röntgenstrahlen, Second Edition  
(Julius Springer, Berlin, 1931)

Slater, J.: Phys. Rev. 36, 57 (1930)

Smith, J. A.: M.Sc. thesis, Ohio State University (1952)

Strong, J.: Procedures in Experimental Physics (Prentice-Hall, Inc.,  
New York, 1945)

Taylor, A. E.: Rep. Prog. Phys. 15, 49 (1952)

Taylor, W.: Ph.D. thesis, Ohio State University (1952)

Thomas, L. H.: Proc. Roy. Soc. A114, 561 (1927)

Thomas, W.: Naturw. 13, 627 (1925)

von Weizsäcker, C. F.: Ann. Phys. Lpz. 5, 17, 869 (1933)

Walske, M. C.: Phys. Rev. 88, 1283 (1952)

Warshaw, S. D.: Phys. Rev. 76, 1759 (1949)

Weyl, P. K.: Bull. Am. Phys. Soc. 28 (1), 49 (1952)

Wilcox, H.: Phys. Rev. 74, 1947 (1948)













JUL 2

BINDERY

Thesis

20145

C44

c.1

Chilton

The stopping power of various  
elements for protons of mo-  
derately low energies.



BINDERY

Thesis

20145

C44

c.1

Chilton

The stopping power of various  
elements for protons of moder-  
ately low energies.

LIBRARY

U. S. Naval Postgraduate School  
Monterey, California

ARTS  
GOLD LETTERING  
AND  
SMITH BINDERY  
OAKLAND, CALIF.

thesC44

The stopping power of various elements f



3 2768 002 09772 7

DUDLEY KNOX LIBRARY